UNIVERSITÀ DEGLI STUDI DI PADOVA

CORSO DI LAUREA MAGISTRALE IN INGEGNERIA CIVILE

TESI DI LAUREA

CONCRETE BEHAVIOUR AT HIGH TEMPERATURE: BIBLIOGRAPHIC STUDY, THERMO-HYGRAL MODELING AND STATISTICAL PARAMETRIC ANALYSIS

RELATORE: CH.MO PROF. ING. RENATO VITALIANI

RELATORE ESTERO: PROF. FEKRI MEFTAH

LAUREANDO: DANIELE MONGIAT

ANNO ACCADEMICO: 2011-2012

INDICE

INDICE 1

INTRODUZIONE 5

CAPITOLO I : RICERCA BIBLIOGRAFICA 11

I.1 - GLI EFFETTI DELL'ALTA TEMPERATURA SULLA MICROSTRUTTURA DEL CALCESTRUZZO 11

I.1.1 - Evoluzione della struttura dei pori con la temperatura 14

I.1.2 - Processi di disidratazione 18

I.1.3 - Equilibrio liquido - vapore 21

I.1.4 - Isoterme di assorbimento e desorbimento 26

I.1.5 - Conclusione 31

I.2 - GLI EFFETTI DELL'ALTA TEMPERATURA SULLE PROPRIETA' TERMICHE DEL CALCESTRUZZO 32

I.2.1 - Conducibilità termica 33

I.2.2 - Capacità termica 36

I.2.2.1 - Entalpia di evaporazione ed entalpia di disidratazione 39

I.2.2.2 - Densità 40

I.2.2.3 - Capacità termica volumetrica 40

I.2.3 - Conclusione 42

I.3 - GLI EFFETTI DELL'ALTA TEMPERATURA SULLE PROPRIETA' IGROMETRICHE DEL CALCESTRUZZO 43

I.3.1 - Permeabilità 44

I.3.1.1 - Permeabilità geometrica 45

I.3.1.2 - Permeabilità relativa dei fluidi 50

I.3.1.3 - Viscosità dei fluidi 53

I.3.2 - Diffusività 55

I.3.3 - Conclusione 57

CAPITOLO II : MODELLAZIONE TERMO-IGROMETRICA (TH) 59

II.1 - MODELLO IGRO-TERMICO 60
II.1.1 - Equazioni di bilancio 60
II.1.2 - Equazioni costitutive 63
II.1.2.1 - Equazioni di stato 63
II.1.2.2 - Equilibrio liquido - vapore 63
II.1.2.3 - Flussi di massa 64
II.1.2.4 - Flusso termico di conduzione 65
II.1.2.5 - Isoterme di assorbimento e desorbimento 65
II.1.3 - Condizioni al contorno (B.C.) 66
II.2 - MODELLAZIONE AD ELEMENTI FINITI 68

CAPITOLO III : ANALISI PROBABILISTICA E SIMULAZIONI PARAMETRICHE 71

III.1 - FUNZIONI DI DENSITA' DI PROBABILITA' (PDF) 71
III.1.1 - PDF per varie realizzazioni stocastiche 75
III.2 - LUNGHEZZA DI CORRELAZIONE 78
III.2.1 - Mesh 2D 80
III.2.2 - Convergenza dei volumi elementari statistici VES verso i volumi VER per varie lunghezze di correlazione 82
III.3 - CURVE DI PERDITA DI MASSA 86
III.3.1 - Analisi della dispersione dei dati per Lc/Lcorr = 1 89
III.3.2 - Analisi della dispersione dei dati per Lc/Lcorr = 2 91
III.3.3 - Analisi della dispersione dei dati per Lc/Lcorr = 5 93
III.3.4 - Analisi della dispersione dei dati per Lc/Lcorr = 8 95
III.3.5 - Analisi della dispersione dei dati per Lc/Lcorr = 10 97
III.4 - Conclusione 100

CONCLUSIONI E PROSPETTIVE 101
APPENDICE CAPITOLO II 103
BIBLIOGRAFIA 107

TABLE OF CONTENTS

TABLE OF CONTENTS 3

INTRODUCTION 7

CHAPTER I : BIBLIOGRAPHIC STUDY 11

I.1 - THE EFFECT OF HIGH TEMPERATURES ON CONCRETE MICROSTRUCTURE 11

I.1.1 - Evolution of pore structure during heating 14

I.1.2 - Dehydration processes - chemical reaction 18

I.1.3 - Liquid - Vapour equilibrium 21

I.1.4 - The sorption and desorption isotherms 26

I.1.5 - Conclusion 31

I.2 - THE EFFECT OF HIGH TEMPERATURES ON THE THERMAL PROPERTIES OF CONCRETE 32

I.2.1 - Thermal conductivity 33

I.2.2 - Heat capacity 36

I.2.2.1 - Enthalpy of evaporation and Enthalpy of dehydration 39

I.2.2.2 - Density 40

I.2.2.3 - Volumetric heat capacity 40

I.2.3 - Conclusion 42

I.3 - THE EFFECT OF HIGH TEMPERATURES ON THE HYGRAL PROPERTIES OF CONCRETE 43

I.3.1 - Permeability 44

I.3.1.1 - Intrinsic permeability 45

I.3.1.2 - Relative permeability of fluids 50

I.3.1.3 - Viscosity of fluids 53

I.3.2 - Diffusivity 55

I.3.3 - Conclusion 57

CHAPTER II : THERMO-HYGRAL MODEL 59

II.1 - T-H MODEL 60
II.1.1 - Balance equations 60
II.1.2 - Constitutive equations 63
II.1.2.1 - Fluid state equations 63
II.1.2.2 - Liquid - Vapour equilibrium 63
II.1.2.3 - Mass fluxes 64
II.1.2.4 - Conductive heat flux 65
II.1.2.5 - Sorption-desorption isotherm 65
II.1.3 - Boundary conditions 66
II.2 - STAGGERED FINITE ELEMENT MODEL 68

CHAPTER III : PROBABILISTIC ANALYSIS AND PARAMETRIC SIMULATIONS 71

III.1 - PROBABILITY DISTRIBUTION FUNCTION 71
III.1.1 - Probability distribution functions for different sizes of SEV 75
III.2 - CORRELATION LENGTH 78
III.2.1 - 2D mesh 80
III.2.2 - Convergence of the SEV towards the REV for different correlation lengths 82
III.3 - WEIGHT LOSS CURVES 86
III.3.1 - Dispersion Analysis for the case Lc/Lcorr = 1 89
III.3.2 - Dispersion Analysis for the case Lc/Lcorr = 2 91
III.3.3 - Dispersion Analysis for the case Lc/Lcorr = 5 93
III.3.4 - Dispersion Analysis for the case Lc/Lcorr = 8 95
III.3.5 - Dispersion Analysis for the case Lc/Lcorr = 10 97
III.4 - Conclusion 100

CONCLUSION AND PERSPECTIVES 101
ANNEX CHAPTER II 103
REFERENCES 107

INTRODUZIONE

La modellazione dei processi di trasporto di massa ed energia nei mezzi porosi aperti parzialmente saturi è un argomento di ricerca che trova molte applicazioni nel campo dell'ingegneria civile. In particolare permette di ottenere strumenti di valutazione della patologia e durabilità dei materiali e delle strutture in condizioni di servizio (invecchiamento) o in situazioni accidentali (incendio).

Le modellazioni multi-scala e multi-fisiche sviluppate al L2MGC (Laboratoire de Mécanique et Matériaux du Génie Civil, Cergy-Pontoise) in collaborazione con IFSTTAR (ex LCPC, Laboratoire Central des Ponts et Chaussées, Paris) e l'Università degli Studi di Padova sono essenzialmente basate su approcci deterministici. Tuttavia, la natura eterogenea ed aleatoria della microstruttura dei materiali porosi studiati (geo-materiali) e delle loro proprietà di trasporto rende praticamente indispensabile il ricorso ad approcci probabilistici.

Un primo passo in questa direzione è stato quello di estendere la modellazione in modo da considerare la variabilità statistica e spaziale non correlata dei parametri fisici che governano i processi di trasporto studiati. Questo argomento è già stato oggetto di molte pubblicazioni ed articoli.

Partendo da questa base si è ampliato il modello esistente; si sono condotte delle analisi probabilistiche che tenessero conto dell'influenza della correlazione spaziale dei parametri in merito alla convergenza dei volumi elementari statistici (VES, ottenuti con realizzazioni stocastiche) verso i volumi elementari rappresentativi (VER, statisticamente invarianti). L'effetto della correlazione spaziale è stata studiata considerando il rapporto esistente tra la lunghezza di correlazione e la dimensione del volume elementare statistico.

La tesi è divisa e presentata in tre parti.

La prima parte è dedicata ad una ricerca bibliografica riguardante i principali parametri fisici (termici e igrometrici) che governano il comportamento igro-termico (T-H) del calcestruzzo in temperatura.

La seconda parte sintetizza il modello termo-igrometrico adottato, realizzato con il programma di calcolo francese Cast3m (CEA) e basato su un approccio a tre fluidi (acqua liquida, vapore acqueo e aria secca) in un mezzo poroso parzialmente saturo.

La terza parte è riservata all'analisi probabilistica. Vengono presentate le leggi di variazione statistica della permeabilità geometrica (parametro oggetto di questo studio) e la sua fluttuazione spaziale.

INTRODUCTION

Mass and energy transfers processes in partially saturated open porous media is a research topic that finds many applications in structures field. In particular, this subject of research permit to obtain tools to evaluate the pathology and durability of materials and structures in service situation (aging) or in accidental situation (fire).

The multi-scales and multi-physics modelings developed at L2MGC in partnership with IFSTTAR (ex LCPC) and the University of Padua to allow this evaluation are primarily based on deterministic approaches (mean models). However, the heterogeneous and random nature of the microstructure of studied porous materials (geo-materials) and their transfer properties make essential the recourse to probabilistic approaches.

A first step in this direction was to extend these modelings to take into account the not correlated statistical and spacial variability for physical parameters governing the studied processes of transfer. This work was the object of many publications and articles.

With the work carried out within the framework of this stage, the L2MGC wishes to consolidate the research in progress on the stochastic approaches of the transfers in the porous media. Its purpose is to implement model tools that allow to better take into account the random structural risk impacting the lifespan of the works.

The following part of the work consists in carrying out probabilistic analyses. We will then focus on the influence of the space correlation of the parameters on the convergence of statistic elementary volumes (SEV: achievements obtained by random realizations) towards representative elementary volumes (REV) which are statistically invariant. The effect of the space correlation is studied by considering the length of correlation of the probabilistic parameter with regard to the size of the SEV (smaller than that of the REV).

The work is carried out and presented in three parts followed by a general conclusion.

The first part is dedicated to a bibliographical study related to the principal physical parameters (hydrous and thermal) that govern the thermo-hygral behavior (TH) of concrete in temperature.

The second part gives in a synthetic way the framework of the adopted TH model, based on an approach with three fluids (liquid water, vapor and dry air) in partially saturated porous medium. The presentation of the model relates to the conservation equations and their discretization with finite elements.

The third and last part is devoted to the probabilistic part of the analysis. The laws of statistical variation of the geometrical permeability (main parameter of this study) and its spacial fluctuation are here presented. Then, a parametric study related to different realization of SEV is carried out.

The report ends with a general conclusion and some perspectives.

INTRODUCTION

La modélisation des processus de transferts (de masse et d'énergie) dans les milieux poreux partiellement saturés est un sujet de recherche amont qui trouve de nombreuses applications dans le domaine de la construction. En particulier, ce sujet de recherche permet de disposer d'outils d'évaluation de la pathologie/durabilité des matériaux et des structures en situation de service (vieillissement) ou en situation accidentelle (incendie).

Les modélisations multi-échelles et multi-physiques développées au L2MGC en partenariat avec IFSTTAR (ex LCPC) et l'Université de Padoue pour permettre une telle évaluation sont essentiellement basées sur des approches déterministes (modèles moyens). Cependant, la nature hétérogène et aléatoire de la microstructure des matériaux poreux étudiés (géo-matériaux) et de leurs propriétés de transfert rend indispensable le recours à des approches probabilistes.

Une première extension dans ce sens a été d'étendre ces modélisations pour prendre en compte la variabilité statistique et spatiale non corrélée des paramètres physiques régissant les processus de transfert étudiés. Ce travail a fait l'objet de nombreuses publications et communications.

Par le travail effectué dans le cadre de ce stage, le L2MGC souhaite consolider les actions de recherches en cours sur les approches stochastiques des transferts dans les milieux poreux. In fine, il s'agit de mettre en œuvre des outils modèles permettant une meilleure prise en compte de l'aléa structurel impactant la durée de vie des ouvrages.

La poursuite du travail consiste à mener des analyses probabilistes et focalisant sur l'influence de la corrélation spatiale des paramètres sur la convergence de volumes élémentaires statistiques (VES: réalisations obtenues par des tirages aléatoires) vers des volumes élémentaires représentatifs (VER) qui sont statistiquement invariants. L'effet de la corrélation spatiale est notamment étudié en considérant le rapport de la longueur de corrélation du paramètre probabiliste à la taille du VES (plus petite que celle du VER).

Le travail réalisé est présenté en trois parties suivies d'une conclusion générale.

La première partie est dédiée à une étude bibliographique portant sur les principaux paramètres physiques (hydriques et thermiques) qui régissent le comportement thermo-hydrique (TH) du béton en température.

La deuxième partie donne de façon synthétique le cadre de modélisation TH adopté, basé sur une approche à trois fluides (eau liquide, vapeur d'eau et air sec) en milieu poreux partiellement saturé. La présentation du modèle porte sur les équations de conservation ainsi que leur discrétisation élément fini.

La troisième et dernière partie est consacrée à la partie probabiliste de l'analyse. Les lois de variation statistique de la perméabilité géométrique (paramètre faisant l'objet de cette étude) et sa fluctuation spatiale y sont présentées. Puis, une étude paramétrique portant sur différentes réalisation de VES est menée.

Le rapport se termine par des conclusions et des perspectives.

CHAPTER I

* * *

BIBLIOGRAPHIC STUDY

This chapter will deal with the evolution of concrete microstructure and its material properties that govern heat and mass transport mechanism when it is subjected to high temperatures. The evolution of microstructure and material properties will be presented from the experimental point of view as well as from the related theoretical models proposed in the literature.

I.1 - THE EFFECT OF HIGH TEMPERATURES ON CONCRETE MICROSTRUCTURE

Concrete is essentially a mixture of two components: aggregates and paste. The aggregate component is usually sand, gravel or crushed stone. It is mainly responsible for the unit weight, the elastic modulus, and the dimensional stability of concrete. Therefore, it has a very important effect on the volume changes of concrete exposed to high temperatures. The paste component is typically used to bind aggregates in concrete and mortar. It is a porous medium which is composed of a solid skeleton, produced from the hydration of Portland cement, and pores, which are filled by different fluid phases. The principal solid phases generally present in the hydrated cement paste (*hcp*), that can be resolved by an electron microscope, are: the calcium silicate hydrates C-S-H which are very important in determining the properties of the paste such as strength and permeability, and the calcium hydroxide $Ca(OH)_2$ (also called portlandite). The pores structure is relevant for concrete. It contributes to fix the mechanical strength of concrete, but it allows too the interaction with the external environment which takes place through the connected pores. Besides, it is the container of the liquid water and gas phases (vapour and dry air). **Figure 1** gives a schematic representation of cement paste seen as a partially saturated medium.

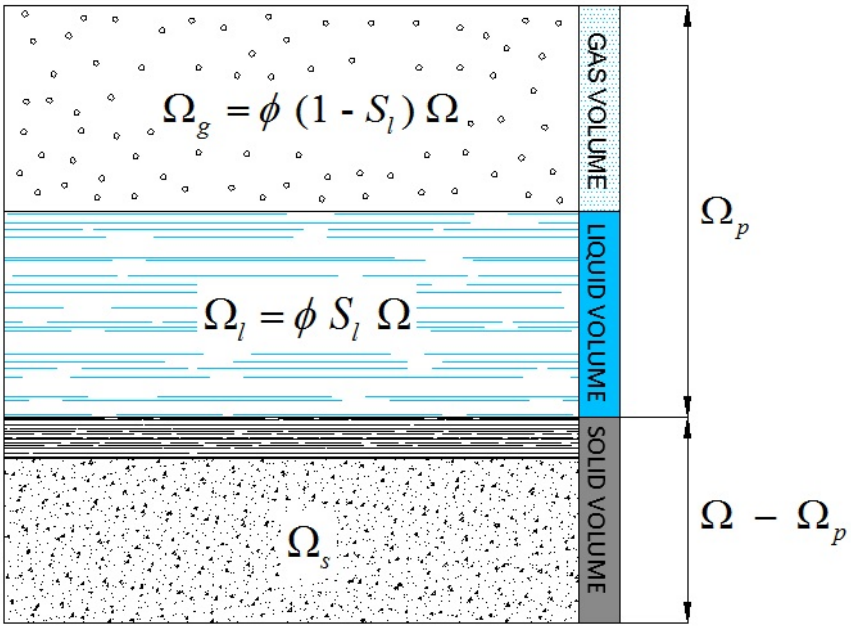

Figure 1 - Schematic representation of a non-saturated porous material

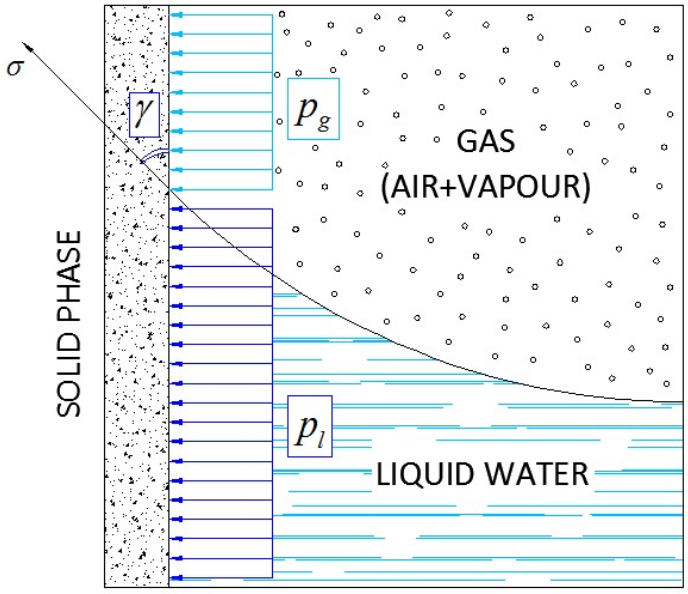

Figure 2 - Schematic representation of a capillary pore

Indeed, for a given Representative Elementary Volume (REV) Ω, the volume of pores Ω^p allows to define the porosity ratio $\phi = \Omega^p / \Omega$. Furthermore, we introduce the degree of saturation of pores with liquid water $S^l = \Omega^l / \Omega^p$. It is an experimentally determined

function of the relative humidity *RH* (obtained through the sorption isotherms). The remaining volume of pore is filled by a gaseous mixture $S^g = \left(1 - S^l\right) = \Omega^g / \Omega^p$.

The interfacial surface tension of water in a capillary pore leads to a concave meniscus between liquid water and gas phase. This may give rise to a discontinuity in fluid pressure. The difference between the liquid water pressure p^l and the gas (dry air p^a + vapour p^v) is called the capillary pressure p^c which is a function of the liquid water saturation S^l.

$$p^c\left(S^l\right) = p^v + p^a - p^l \tag{1}$$

Assuming null contact angle between liquid phase and solid matrix, the capillary pressure of water p^c can be related to the pore radius *r* with the Laplace equation:

$$p^c = \frac{2\sigma(T)}{r} = 2\sigma(T)\chi \tag{2}$$

where $\sigma(T)$ is the surface tension of water which depends upon temperature, and χ is the curvature of meniscus. Any change in the curvature of meniscus will change the equilibrium between liquid-vapour phases. A relation, between the liquid water and the vapour, can be obtained by means of Kelvin equation considering that liquid is incompressible and the vapour is as a perfect gas.

Water can exist in the hydrated cement paste in many forms:

- capillary and physically adsorbed water; their loss are mainly responsible for the shrinkage of the *hcp* while drying
- interlayer water; it can be lost only during strong drying and leads to the C-S-H structure to shrink considerably

All these type of water can evaporate up to 105°C (at atmospheric pressure and slow rate of heating). Another type of water which is non-evaporable water is chemically combined. It is considered to be an integral part of the structure of various cement hydration products and it is evolved when the hydrates decompose on heating. Based on

the Feldman-Sereda model, the different types of water associated with the C-S-H are illustrated **in figure 3.**

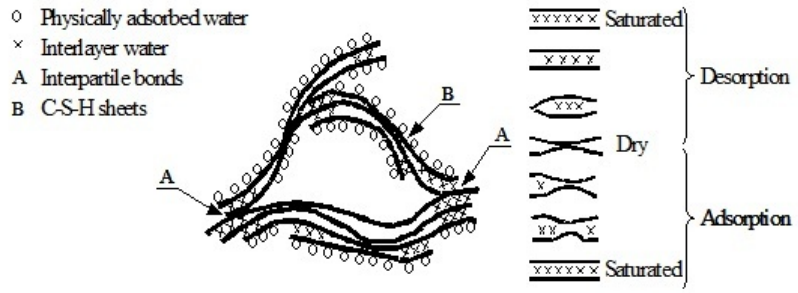

Figure 3 - Probable structure of hydrated silicates (Feldman & Sereda, 1968)

In facts there is a third phase in concrete microstructure, known as transition zone, which represents the interfacial region between the particles of coarse aggregate and the *hcp*. Concrete has micro-cracks in the transition zone even before a structure is loaded. It has a great influence on the stiffness of concrete. In the composite material, the transition zone serves as a bridge between the two components: the mortar matrix and the coarse aggregate particles. Therefore the Broken bridges (i.e. voids and micro-cracks in this zone) would not permit stresses transfer (Mehta & Monterio, 2001).

I.1.1 - Evolution of pore structure during heating

The loss of stability of solid phases in concrete, paste and aggregates, when exposed to high temperatures, affects its pore structure. The physical and chemical changes occurring in solid phases induces changes in pore size distribution and total porosity. Noumowe (1995) has given the distributions of pores with different levels of temperatures for an ordinary concrete heated up to 600°C **(figure 4).**

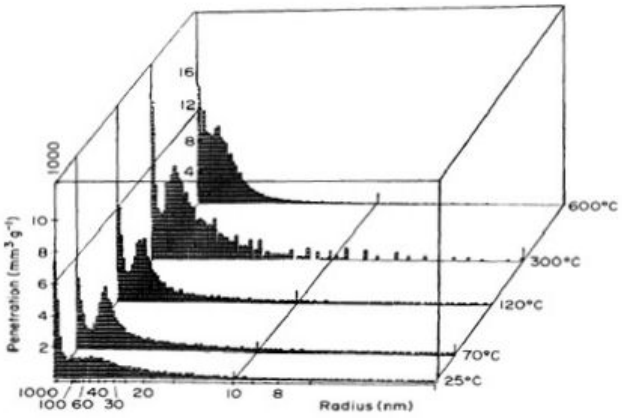

Figure 4 - Pore size distribution of a normal concrete (Noumowe, 1995)

It can be seen that the total pore volume of a heated concrete increases not linearly with the increase of temperature **(see figure 5).** On heating up to 300°C, a relatively small increase in pore volume is observed in comparison to the weight losses. It was considered to be due to structural changes resulting from the desiccation and dehydration processes occurring mainly in pores of radii less than 40 Å (Andrade et al., 2003). Heating up to 600°C will increase the total pore volume. This increase is higher than it would be expect in comparison with weight losses. On the other hand Bažant & Thonguthai (1978, 1979) observed an upward jump in concrete permeability of two orders of magnitude. Therefore, this was related to the fact that the pore volume available for capillary water must increase significantly when temperature and pore pressure increase. Then, it may therefore suspected that either an expansion of pores has occurred by break down of partition walls or micro-cracks are formed (Andrade et al., 2003).

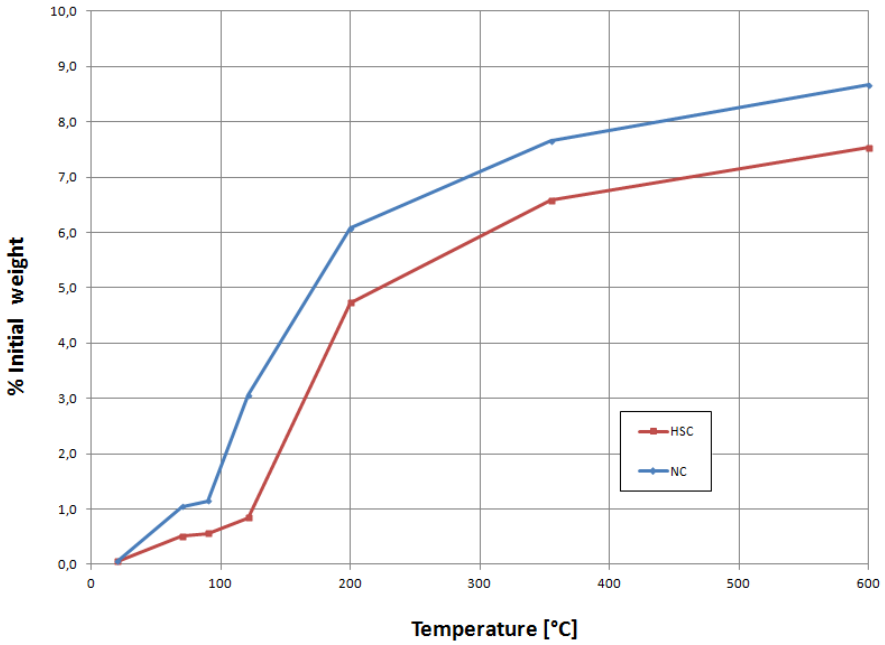

Figure 5 - Weight variations (Noumowe, 1995)

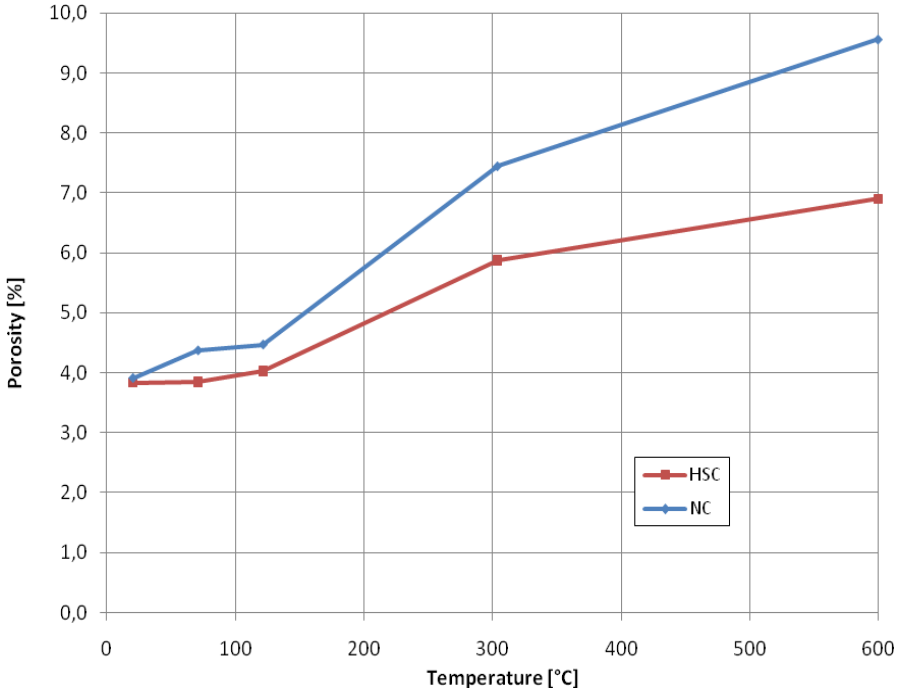

Figure 6 - Mercury porosity of NC and HSC (Noumowe, 1995)

Many authors investigated about micro-cracking (Dougill, 1968, Blundell et al., 1976). They have been indicated that the differential strain between the aggregate (which expand) and the cement paste (which shrink) at different temperatures will initially

induced a small compressive stress in the paste. As the temperature increases, compressive stress is reduced and changes to a larger tensile stress. Khoury et al. (1985) have suggested that the incompatibilities in strains between aggregates and cement paste in concrete under load at elevated temperatures could, to a large extent, are reduced by the load induced thermal strain (LITS). The changes of porosity with the increase of temperature were measured for several types of concrete by (Schneider & Herbst, 1989). Their results showed that the dependence of porosity on temperature can be approximated for concrete by a linear relationship:

$$\phi_T = \phi_0 + A_\phi \left(T - T_0\right) \tag{3}$$

where A_ϕ is a constant dependent on the type of concrete. For the experimental data for three types of the B35-concrete, the following coefficients in (3) have been found by using the least-squares method (Gawin et al., 1999):

	Silicate concrete	Limestone concrete	Basalt concrete
ϕ_0	0,060	0,087	0,0802
A_ϕ [K^{-1}]	0,000195	0,000163	0,00017

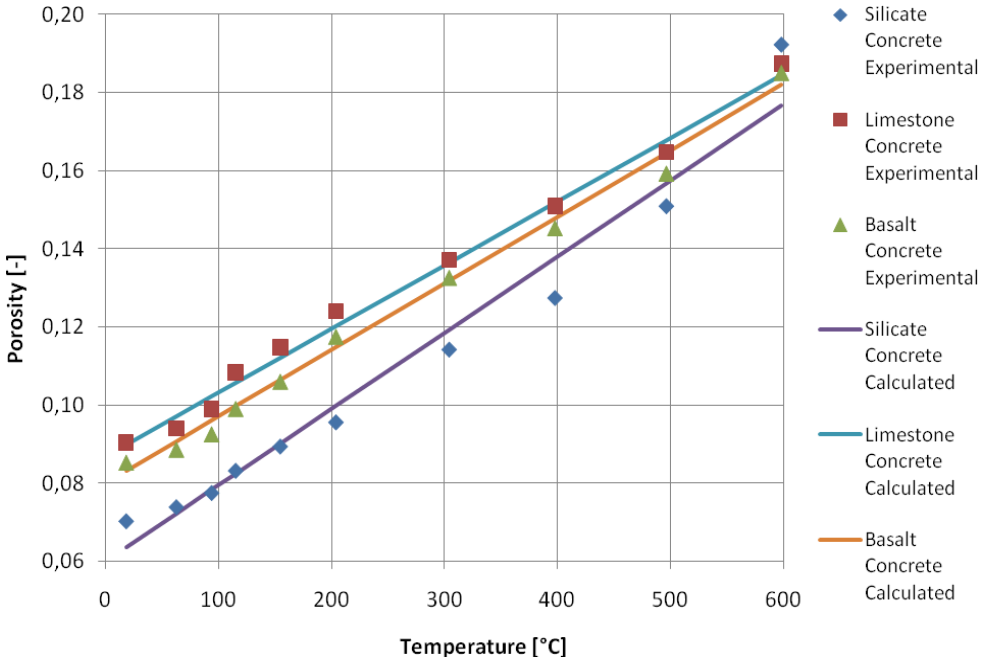

Figure 7 - Porosity from experimental data (Gawin et al., 1999)

and approximated ones using (3)

Another relationship for the evolution of porosity due to the dehydration process has been proposed by (Feraille, 2000) as follows:

$$\phi_T = \phi_0 + 0,72 \cdot 10^{-3} m_{dehydr} \tag{4}$$

where ϕ_0 is the initial porosity and m_{dehydr} is the mass of water which is proposed to be experimentally determined from the dehydration processes, as we will see in detail in the following section. It should be noted also that the above equation takes into account the Le Chatelier contraction.

I.1.2 - Dehydration processes - Chemical reaction

The combined reaction in cement paste and aggregate in concrete, which are initiated when concrete is subjected to elevated temperature, have been examined by many authors (Harmathy & Allen, 1973, Schneider 1982) with the aid of differential thermal analysis investigations. Dehydration (i.e. release of chemically bound water) from the C-S-H becomes significant above 105°C, while the dehydration of the calcium hydroxide $Ca(OH)_2$ takes place at about 500°C producing CaO and H_2O. Both will produce a reduction in the mass of the cement paste of the solid skeleton. However, the strength of concrete is more related to the C-S-H than the $Ca(OH)_2$.

The amount of water that is released upon heating due to dehydration into the pores of concrete depends on the amount of hydrated water m_{hydr} (consumed by the hydration process) before heating. Therefore, it is a function of the degree of hydration. The degree of hydration before heating depends on the age of concrete as well as its temperature and humidity history. The degree of hydration may conveniently be referred to the equivalent hydration period (maturity) t_e. It represents the period of hydration, in the water and at 25°C, needed to give the same degree of hydration as the actual time period gives at variable *RH* and *T*. By fitting the results of Powers & Brownyard (1948) at 25°C, it has found (Bažant & Kaplan, 1996) that:

$$m_{hydr}\left(t_e\right) \approx 0.21c\left(\frac{t_e}{\tau_e + t_e}\right)^{1/3} \tag{5}$$

where the characteristic period $\tau_e = 23\text{days}$ for a concrete with w/c = 0.43 (see figure 8)

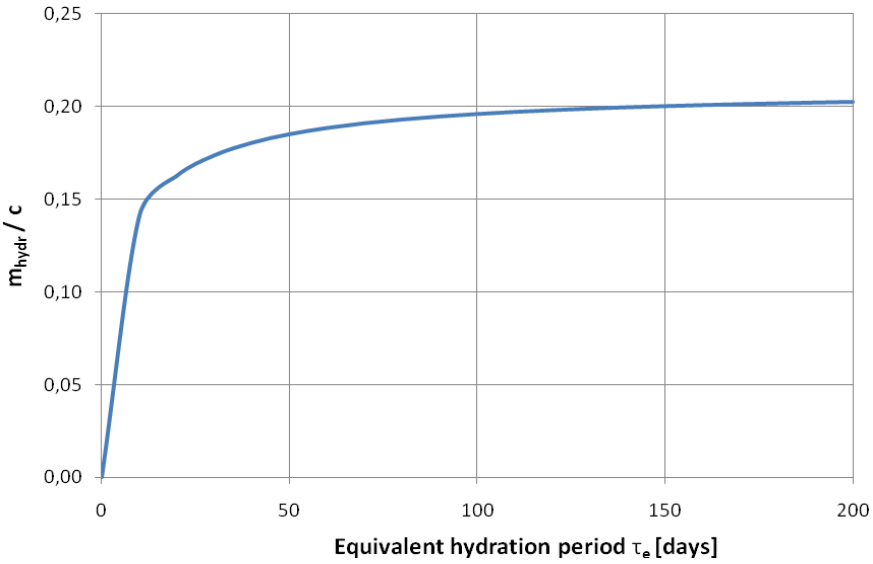

Figure 8 - Fit of Powers & Brownyard's data (Bažant & Kaplan, 1996)

The amount of water that is released by the dehydration m_{dehydr} (kg per m^3 of concrete), when reaching various temperatures is experimentally obtained by weight loss measurements on heated specimens and can be expressed according to Bažant & Kaplan (1996) as:

$$m_{dehydr}(T) = m_{hydr}^{105°C} \cdot f(T) \tag{6}$$

in which $m_{hydr}^{105°C}$ is the hydrated water content at 105°C. $f(T)$ is a function of dehydration. Moreover Gawin et al. (2001) have calculated the dehydrated water content $m_{dehydr}(T)$, when temperature increases, by using a step function showing a sharp change between 200°C and 500°C. The following law can represent this kind of behaviour:

$$m_{dehydr}(T) = c \cdot f_{aging} \cdot f_{stechio} \cdot f(T) \tag{7}$$

Where c is the cement content, f_{aging} is aging degree of concrete (between 0 and 1), $f_{stechio}$ is stechiometric factor and $f(T)$ is a function of dehydration given **in figure 9**

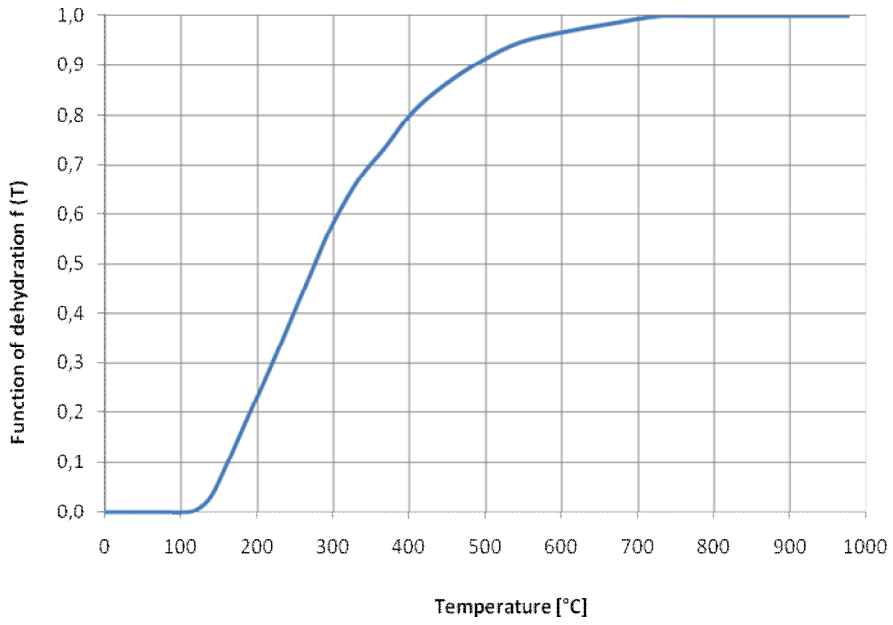

Fig 9 - Function of dehydration f(T) for an ordinary concrete (Gawin et al., 2001)

Based on an experimental work on the cement paste, Feraille (2000) has noted the evolution of dehydration. According to the author, the dehydration is not an instantaneous process and it needs some time to take place. The author has proposed the following formula, which takes into account the asymptotic evolution of dehydration $\dot{m}_{dehydr}$ through the characteristic time τ of mass loss:

$$\dot{m}_{dehydr} = -\frac{1}{\tau}\left(m_{dehydr}(T) - m_{eq}(T)\right) \tag{8}$$

where $m_{eq}(T)$ is the water mass at the equilibrium measured during the thermo-gravimetric tests. It is expressed as:

$$\begin{aligned} m_{eq}(T) = {} & \frac{7.5}{100} m_{eq}^{105°C}\left[1 - exp\left(-\frac{\mathrm{T}-105}{200}\right)\right] H(T-105) \\ & + \frac{2}{100} m_{eq}^{105°C}\left[1 - exp\left(-\frac{\mathrm{T}-400}{10}\right)\right] H(T-400) \\ & + \frac{1.5}{100} m_{eq}^{105°C}\left[1 - exp\left(-\frac{\mathrm{T}-540}{5}\right)\right] H(T-540) \end{aligned} \tag{9}$$

where H is the Heaviside function and $m_{eq}^{105°C} = c\left(1+0.2\ f_{aging}\right)$ in [kg/m^3]. We will use in this study **equation 9** to calculate the dehydrated water content $m_{dehydr}\left(T\right)$, and the evolution of dehydration as follows:

$$\dot{m}_{dehydr} = \frac{\partial}{\partial T}\left(m_{dehydr}\left(T\right)\right)\frac{\partial T}{\partial t} \tag{10}$$

I.1.3 - Liquid-Vapour equilibrium

Let us now assume that there is no dissipation occurring during the phase change. This turns to assume that the liquid water (both capillary and adsorbed) and the vapour remain in a local thermodynamic equilibrium. Therefore, this local equilibrium gives rise to a set of restrictions in the equilibrium configuration that must be satisfied at all times. However, it can be considered that the specific Gibbs functions of the two phases, considered at the same temperature, are equal at each time.

In the work of Feraille (2000) we can see the following steps to establish a relation between pure liquid water and vapour phases; starting considering that the enthalpies of both liquid water $g_l\left(p^l,T\right)$ and vapour $g_v\left(p^v,T\right)$ are functions of temperature and pressure, the partial derivatives of these two functions with respect to their pressures can be written as follows:

$$\frac{\partial}{\partial p^l} g_l\left(p^l,T\right) = \frac{1}{\rho^l\left(T\right)} \tag{11}$$

$$\frac{\partial}{\partial p^v} g_v\left(p^v,T\right) = \frac{1}{\rho^v\left(p^v,T\right)} \tag{12}$$

and considering that the liquid water is incompressible (ρ^l is independent of p^l) and the vapour is an ideal gas ($\rho^v = \frac{p^v M^l}{RT}$). After integrating the two equations above we obtain:

$$g_l\left(p^l, T\right) = \frac{p^l}{\rho^l\left(T\right)} + C_1\left(T\right) \tag{13}$$

$$g_v\left(p^v, T\right) = \frac{RT}{M^l}\ln\left(p^v\right) + C_2\left(T\right) \tag{14}$$

from the equality of enthalpies of the two phase we can get:

$$\frac{p^l}{\rho^l\left(T\right)} + \frac{RT}{M^l}\ln\left(p^v\right) + C_1\left(T\right) + C_2\left(T\right) = 0 \tag{15}$$

To determine $C_1\left(T\right) + C_2\left(T\right)$ the author considered the case in which the liquid water and the vapour coexist in a big and closed container. The separation surface between the two phases is flat (no capillary effect). In this case and at the equilibrium conditions, the pressure of both liquid and vapour is the same (no body force is considered) and will be equal to the saturation pressure of pure vapour $p^{vs}\left(T\right)$. This state can be taken as a reference state and should verified (15). So we can find $C_1\left(T\right) + C_2\left(T\right)$. Finally, the relation between the liquid and the vapour, which is known as generalised Clapeyron relation, would be expressed as follows (Feraille, 2000):

$$p^l = p^{vs}\left(T\right) + \frac{\rho^l\left(T\right)RT}{M^l}\ln\left(\frac{p^v}{p^{vs}\left(T\right)}\right) \tag{16}$$

Now if we are in the case in which three phases (i.e. liquid water, vapour and dry air) can coexist at the same time, like in the case of a partially saturated concrete **(see figure 10)**, then we will need to change the condition of equilibrium over the separation surface as that ($p^v = p^{vs}$ and $p^l = p^{vs} + p^a$) and we can get the following relationship:

$$p^l = p^{vs}(T) + p^a + \frac{\rho^l(T)RT}{M^l}\ln\left(\frac{p^v}{p^{vs}(T)}\right) \tag{17}$$

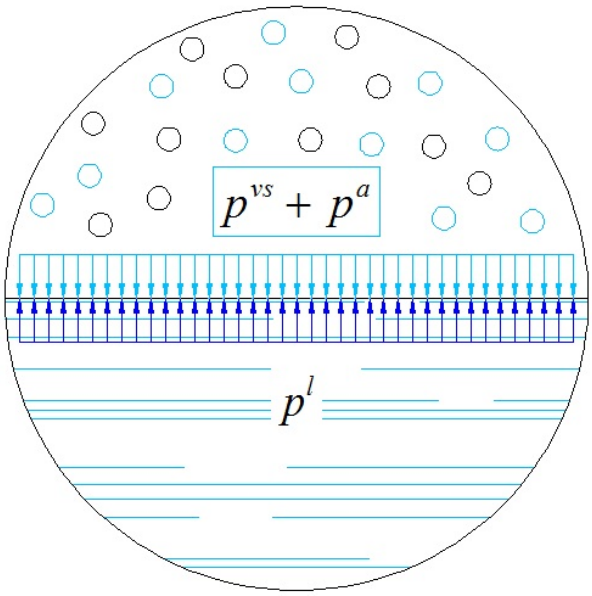

Figure 10 - Reference state when there are three different phases (liquid, vapour and air) co-existing at the same time at equilibrium conditions

If we know that at 20°C the saturation vapour pressure is $p^{vs} = 2350\,\text{Pa}$ and the dry air pressure is $p^a = 99000\,\text{Pa}$, then $p^g = p^{atm} = 101325$ Pa. This can be a particular case of **(17)** which can give the known relationship of Kelvin as follows:

$$p^l = p^{atm} + \frac{\rho^l(T)RT}{M^l}\ln\left(\frac{p^v}{p^{vs}(T)}\right) \tag{18}$$

The saturation pressure of pure vapour $p^{vs}(T)$, which depends only upon temperature, could be obtained from empirical correlation. Tabulated results (Raznjevic, 1970), which link the water vapour saturation pressure p^{vs} with temperature T could be approximated by the following formula (Monteith & Unsworth, 1990):

$$p^{vs}(T) = 610,7 \cdot 10^{\,[7,5\,T/(237,3\,+\,T)]} \tag{19}$$

It should be noted that this equation is taken until the critical point of water 647,15 K, after which it is not possible to distinguish between the liquid and vapour. Another

equation can be taken for p^{vs} after the critical temperatures following the *L*-function given in (Ju & Zhang, 1998) for the superheated steam:

$$p^{vs}(T) = p^{vs}(647{,}15)\left[L_0 + L_1\frac{T}{647{,}15} + L_2\left(\frac{T}{647{,}5}\right)^2\right] \qquad (20)$$

where L_0 = 15,8568, L_1 = -34,1706 and L_2 = 15,7437

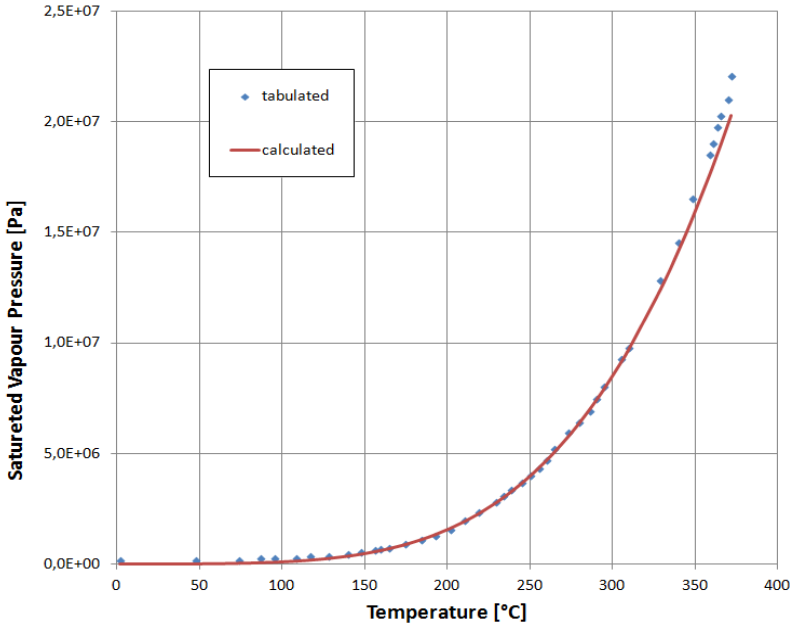

Figure 11 - Saturated vapour pressure

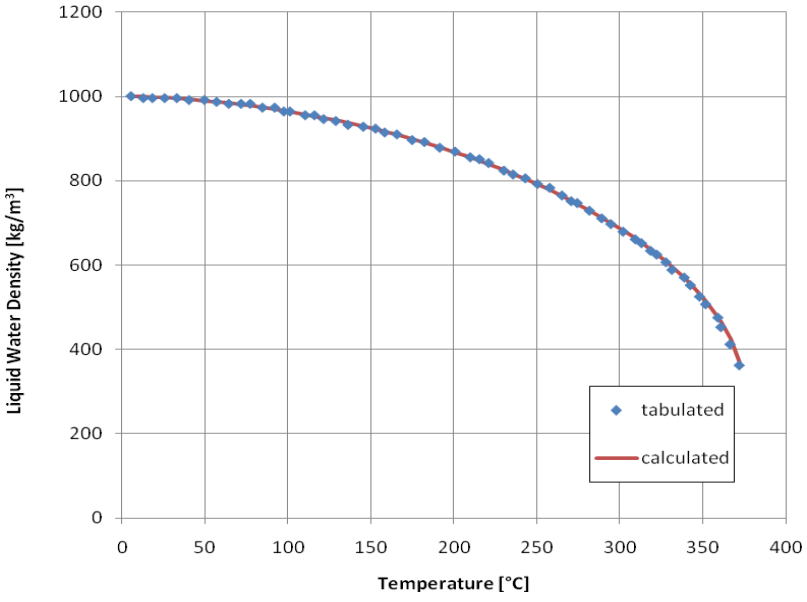

Figure 12 - Density of liquid water function of temperature

In **(17)**, the saturation vapour pressure p^{vs} should be the pressure that takes into account the coexistence of air. In fact, it is different from that one given in **(16)**, which is the saturation pressure of pure vapour. However, Feraille (2000) showed that below the critical temperature of water, the tow saturation vapour pressures coincide. In this work, we introduce a boiling-point temperature which, when reached, gives an additional evaporation in the pore until the full drying of material. This boiling temperature is the temperature for which the saturation vapour pressure is equal to the gas pore pressure. When this situation is met, the temperature remains constant while the water saturation degree decreases. Note that beyond the boiling-point temperature, no liquid water exist. Therefore, there is no need to define specific liquid water properties (density, viscosity, heat capacity…) after the critical temperature.

The state equation of liquid water is rather complex, and usually creates numerical problems. As a sufficient approximation of the dependence of the bulk density of liquid water upon its temperature and pressure, the following formula may be used (Gawin et al., 1999),

$$\rho^l = \rho_0^l \left[1 - \beta^l \left(T - T_0 \right) + \alpha^l \left(p^l - p_0^l \right) \right] \tag{21}$$

where ρ_0^l = 999,84 kg/m^3 is the water density at the reference temperature T_0 and pressure p_0^l, $\beta^l = \left(1/v^l\right)\left(\partial v^l/\partial T\right)_{p^l}$ is volume thermal expansion coefficient of the water, $\alpha^l = \left(1/v^l\right)\left(\partial v^l/\partial p^l\right)_T$ is the isothermal compression modulus of water (β^l = 4,3×10^{-9} Pa^{-1}), and $v^l = 1/\rho^l$ is the water specific volume. The coefficient β^l change in a non-linear manner with temperature (e.g. β^l = 0,68×10^{-4} K^{-1} at T = 273.15 K and β^l = 10,1×10^{-4} K^{-1} at T = 420 K), thus average value for the temperature range under interest should be used in calculations. The state equation **(21)**, basically valid for the bulk (free) liquid water, is often used also for the description of the capillary and bound water, e.g. (Gawin et al., 1999). However, due to a very complex nature of interaction between the water and skeleton, its applicability is questionable, especially as far as pressure dependence is concerned (although capillary water is in traction, but its density is not expected to be lower than that for bulk water). Nevertheless, because of lack of any reliable data, equation **(21)** may be used, but assuming water incompressibility, i.e.

α^l = 0 (Gawin et al., 1999). We can use the experimental results given by (Raznjevic, 1970) for the density of liquid water as a function of temperature, which could be approximated by the following formula given in (Deseur, 1999) and will be adopted here **(see figure 12)**:

$$\rho^l = 314,4 + 685,6\left[1 - \left(\frac{T - 273,15}{374,14}\right)^{\frac{1}{0,55}}\right]^{0,55} \tag{22}$$

I.1.4 - The sorption and desorption isotherms

The sorption and desorption isotherms are useful for calculations of pores water vapour pressures. These isotherms are the equilibrium curves of pore relative vapour pressure versus specific water content at constant temperatures. In another word relative humidity *RH* is controlled while the moisture content within the sample is measured. Since the degree of saturation S^l is fundamental for realistic modelling of thermo-hygral behaviour of the specific concrete, thus it must be determined during sorption tests at several temperatures (Bažant & Thonguthai, 1978).

The isotherms are available only for moderate temperature. Theorically, it should be possible to determine these isotherms also above 100°C, but this would require measurements at very high ambient pressure. Such data are not available (Bažant & Kaplan, 1996).

At elevated temperature Bažant & Thonguthai (1978) assumed that a local thermodynamic equilibrium always exists between the phases of pore water (vapour and liquid) within a very small element of concrete. An approximate, but rational, constitutive relation which relates pore pressure p^v, water content *w* and temperature *T* is presented as follows:

$$w/c = \left[\left(w_{s0}/c\right)\cdot RH\right]^{1/m}$$
$$\text{with} \quad RH = \frac{p^v}{p^{vs}(T)} \tag{23}$$

where c = mass of (anhydrous) cement per m^3 of concrete; w_{s0} = saturation water content at 25°C. The value of w_{s0}/c can be determined if the concrete mix is specified (Neville, 1973; Powers & Brownyard, 1948). The same value for concrete that was mentioned in Bažant & Thonguthai (1978), w_{s0}/c = 100/300 has been taken. The function $m(T)$ in equation **(23)** has been empirically corrected by fitting with test data given by (England & Ross, 1970). It has been found that the following semi-empirical expression **(24)** is acceptable (Bažant & Thonguthai, 1978):

$$m(T) = 1,04 - \frac{T'}{22,34 + T'} \qquad (24)$$

$$with \quad T' = \left(\frac{T + 10}{T_0 + 10} \right)^2$$

where T is the temperature in °C; T_0 = 25°C;

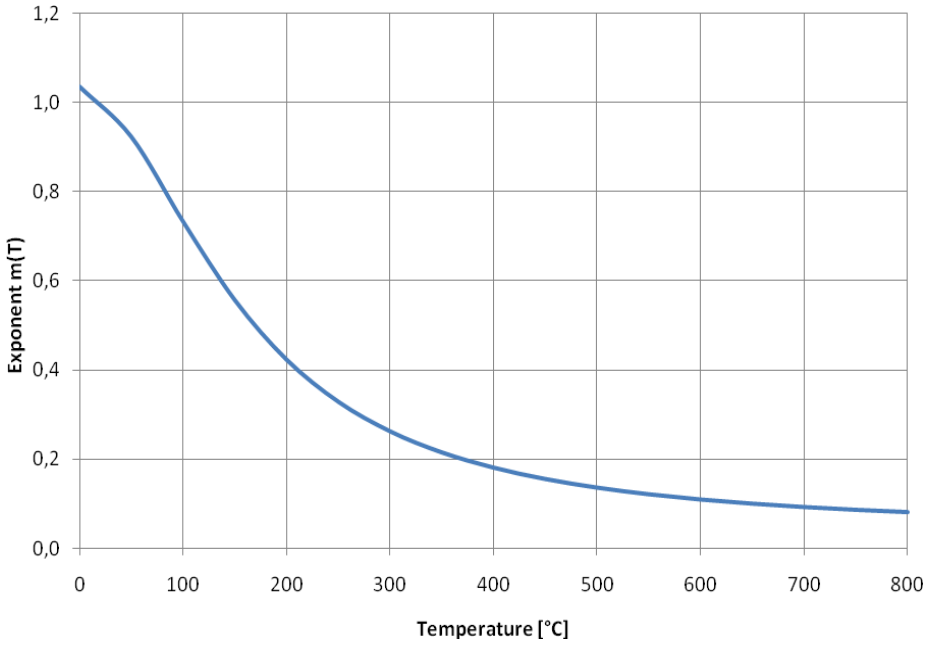

Figure 13 - Exponent m(T) for temperature dependence of sorption isotherms (Bažant & Thonguthai, 1978)

From **(23)** we can write the degree of saturation $S^l = S^l(RH,T)$ as a function of relative humidity and temperature as follows:

$$S^l\left(RH,T\right) = \frac{\left(w/c\right)_{RH,\,T}}{\left(w/c\right)_{RH_0,\,T_0}} \tag{25}$$

where $\left(w/c\right)_{RH_0,\,T_0}$ is calculated at the initial state. According to this equation which is shown in **figure 14** we could note that at a higher temperature the saturated state is reached with lower water content. The degree of liquid saturation S^l can also be related to the capillary pressure p^c. Since a direct experimental determination is difficult, an indirect determination of the $S^l - p^c$ relation by using the desorption isotherm is generally employed. Applying Kelvin's law which relate the relative humidity to the capillary pressure, yield to an expression for the missing capillary pressure curve and the degree of saturation $S^l = S^l(p^c,T)$ as follows:

$$S^l\left(p^c,T\right) = \frac{1}{\left(w/c\right)_{RH_0,\,T_0}}\left[\left(w_{s0}/c\right)\cdot\exp\left(\frac{M^l}{\rho^l RT}\,p^c\right)\right]^{1/m(T)} \tag{26}$$

An example of such dependence, obtained using the concrete data from (Bažant & Thonguthai, 1978) is shown in **figure 15:**

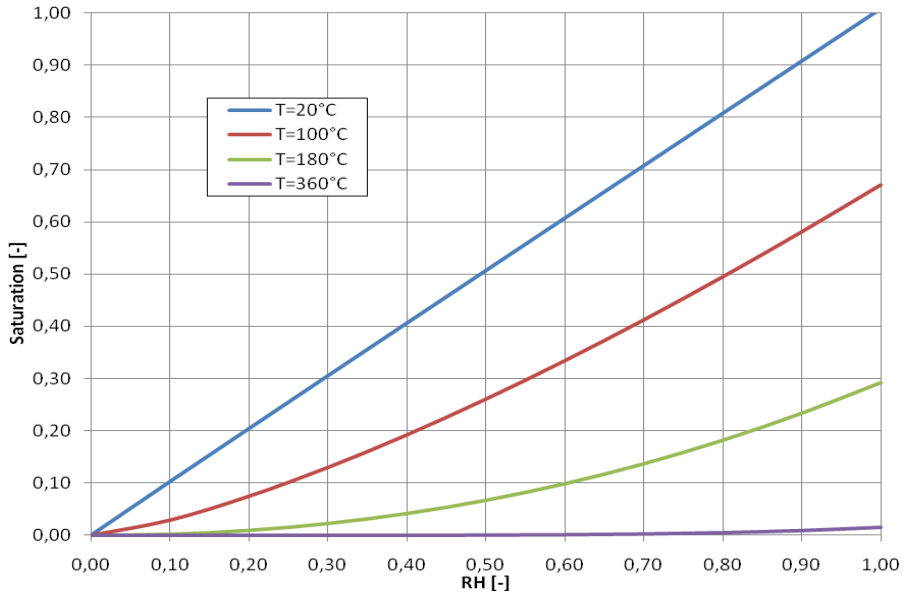

Figure 14 - desorption isotherms S(RH, T)

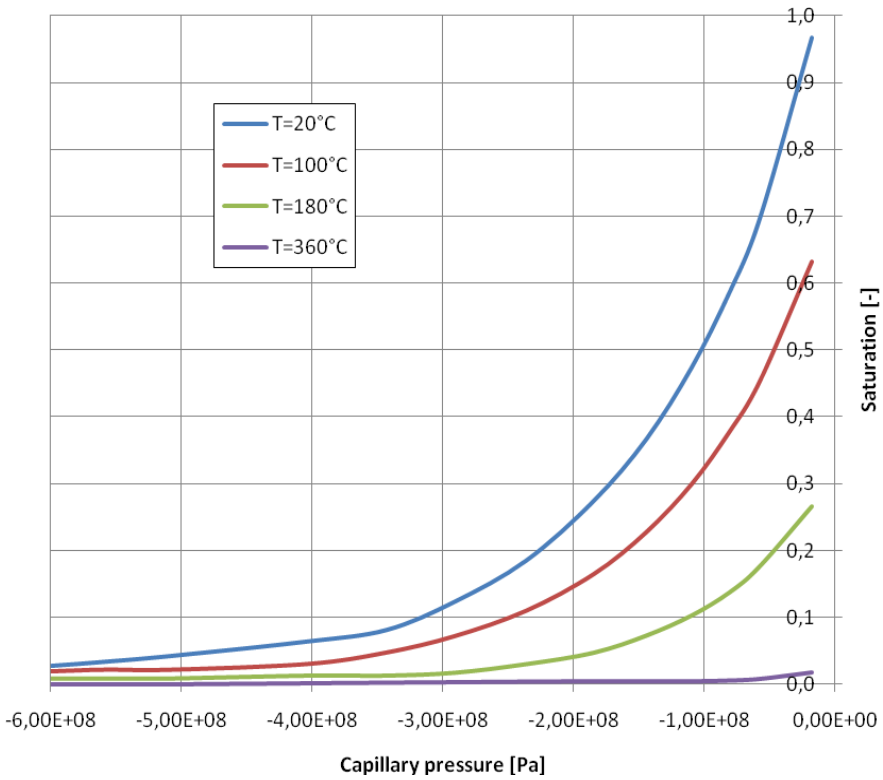

Figure 15 - desorption isotherms S(p^c, T)

The following equation between capillary pressure, temperature and saturation is developed here based on the work of (Bendar, 2002):

$$S^l\left(p^c,T\right)=S^l\left(p^c\right)\frac{\sigma\left(T\right)}{\sigma\left(T_0\right)} \tag{27}$$

where $\sigma\left(T\right)$ is the surface tension of water which depend upon temperature, and can be given by (Le Neindre, 1993) as follows :

$$\sigma\left(T\right)=\sigma_0\left(1-\frac{T}{T_{cr}}\right)^n \tag{28}$$

where σ_0 = 0,155 [N/m^2] and n = 1,26. Based upon the pore network model of (Mualem, 1976), a relation between the capillary pressure and the liquid saturation is proposed in (van Genuchten, 1980) in the form:

$$S^l\left(p^c\right)=\left[1+\left(\frac{\left|p^c\right|}{B}\right)^{1/(1-A)}\right]^{-A} \tag{29}$$

where A, B are parameters of the material, evaluated with a least-square fit in comparison with the experimental results of the retention curve. **Figure 16 and 17** show the evolution of S^l with regard to both relative humidity RH and capillary pressure p^c using **(27)** and **(29)**. We can relate the capillary pressure p_c to the saturation degree S_l by the following relationship (Baggio, Bonacina, & Strada, 1993):

$$p_c\left(S_l\right) = a\left(S_l^{-b} - 1\right)^{\left(1-\frac{1}{b}\right)} \tag{30}$$

where a and b are material parameters identified for each studied case.

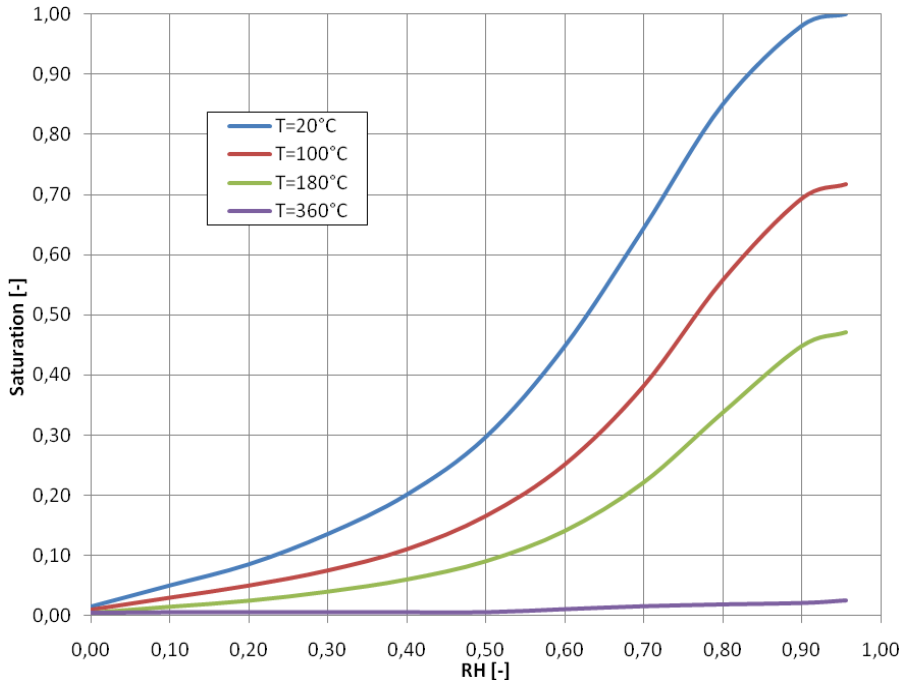

Figure 16 - desorption isotherms S(RH, T)

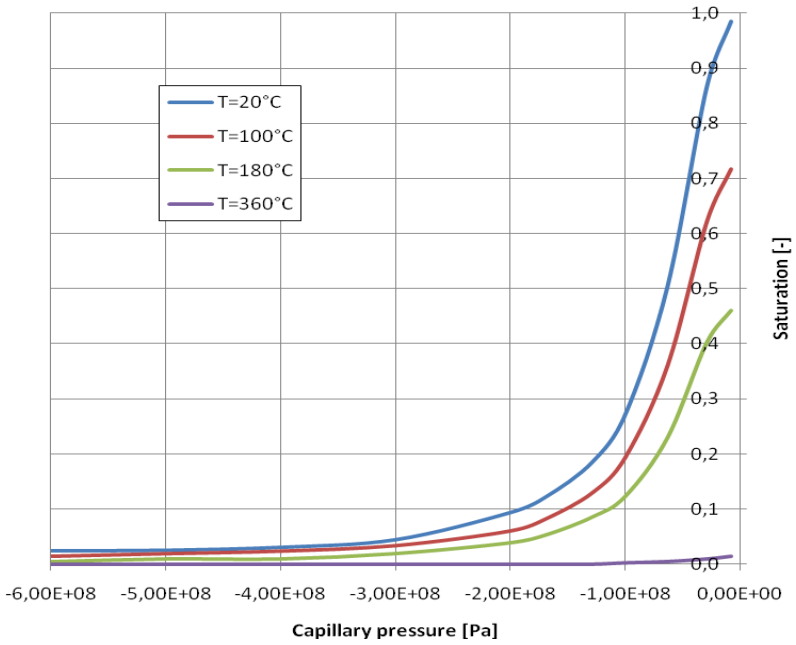

Figure 17 - desorption isotherms $S(p^c, T)$

I.1.5 - Conclusion

The pore structure of concrete at high temperatures and its physical properties too are strongly influenced by the thermo-hygral state of concrete and actual loading, as well as their time histories. During dehydration process considerable amounts of heat are adsorbed as well as a considerable amount of mass are released. Physical properties of fluids (liquid water and moist air) filling up the pores of the material are strongly temperature dependent too. The thermo-hygral behaviour of concrete at high temperature is therefore significantly influenced by the changes in the microstructure and the fluids phases.

I.2 - THE EFFECT OF HIGH TEMPERATURES

ON THE THERMAL PROPERTIES OF CONCRETE

Starting with thermal phenomena, it can be stated that in most cases the main mechanism for heat transport is heat conduction. Heat conduction responds to gradients of temperature *T*. However, additional heat transfer will also be accomplished by advection due to the movement of the three phases: solid, liquid and gas. The latent heat inherent to phase changes may also have significant thermal effects (Gens, 2001).

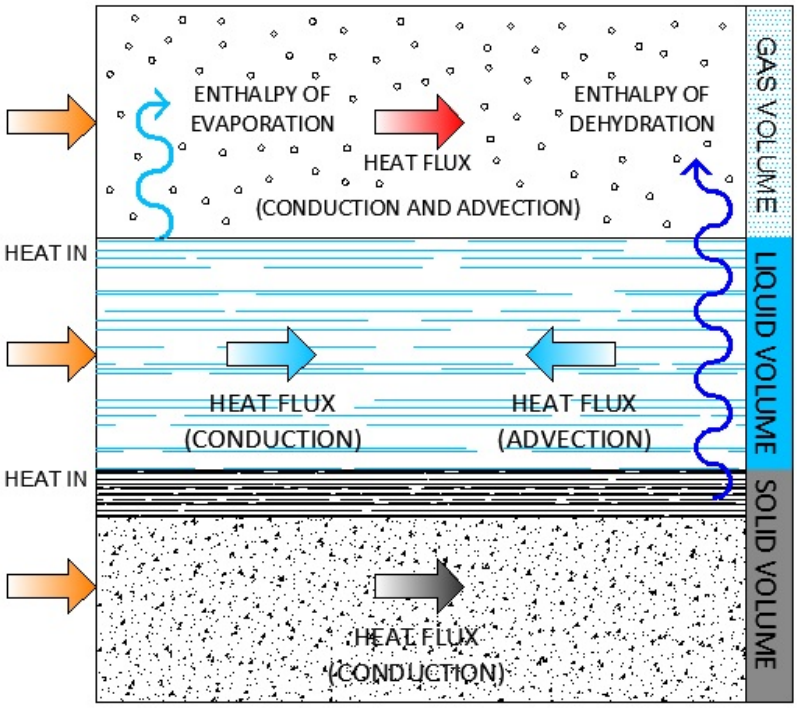

Figure 18 - Heat transport mechanism in a porous medium

(Gens, 2001)

The evolution of the temperature distribution in any structure is governed by the thermal properties of the material, particularly heat capacity and heat conductivity. In the case of concrete, it is hard to determine these properties because of the numerous phenomena that occur simultaneously within the microstructures of concrete and they cannot be separated easily. These effects include in particular the evolution of the porosity, moisture content, type and amount of aggregate, changes in the chemical composition

and the latent heat consumption generated by certain chemical phenomena. Because of these effects, unique relation cannot rigorously describe the dependence of concrete properties on temperature (Harmathy, 1970). Therefore, in this section, we will study these effects on the thermal properties of concrete subjected to a high temperature from the experimental and theoretical point of view.

I.2.1 - Thermal conductivity

For an ordinary concrete thermal conductivity will decrease when the temperature rises. Thermal conductivity as function of high temperature is very difficult to measure due to the influence of many parameters as porosity, moisture content, type and amount of aggregate. The thermal conductivity reduction due to the temperature is marked clearly for a concrete with siliceous aggregate, weak for a calcareous aggregate, and little meaningful for the lightweight aggregate (Collet, 1977).

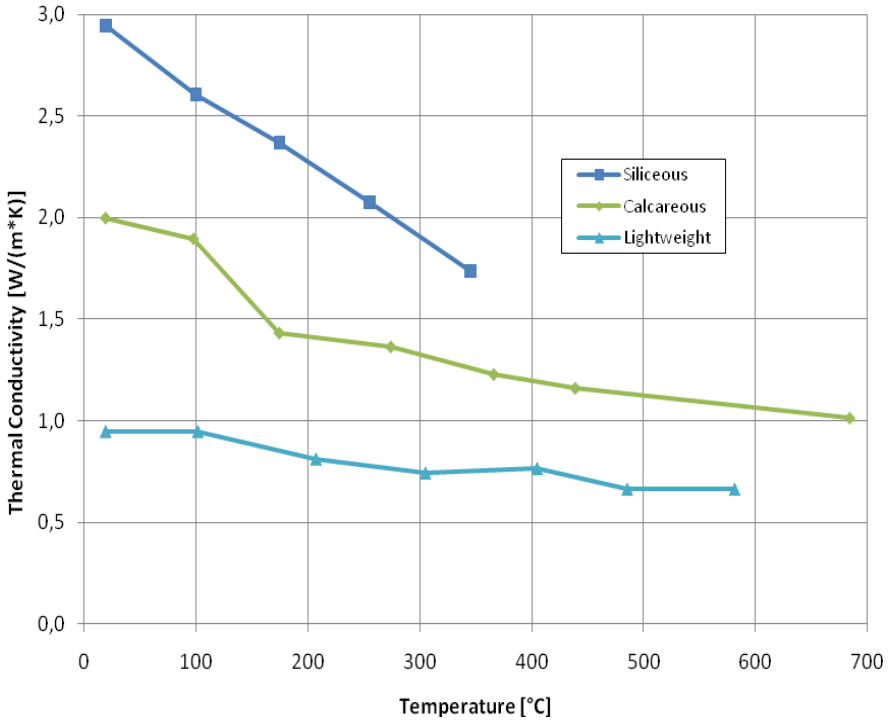

Figure 19 - Thermal conductivity of different structural concretes

(Collet, 1977)

The thermal conductivity of siliceous concrete presented in (Anderberg, 2003) and used in Swedish fire engineering design is shown in **figure 20** In Eurocode 2 (2002) and Eurocode 4 (2003) a compromise has been made in order to permit the thermal

conductivity to be chosen between an upper and a lower limit as shown in **figure 20.** The upper and the lower limit of thermal conductivity of normal weight concrete may be determined successively from the following relations in the range of temperature $20°C \le T \le 1200°C$:

$$\lambda = 2 - 0,2451(T/100) + 0,0107(T/100)^2 \quad (\text{Upper Limit})$$

$$\lambda = 1,36 - 0,136(T/100) + 0,0057(T/100)^2 \quad (\text{Lower Limit}) \tag{31}$$

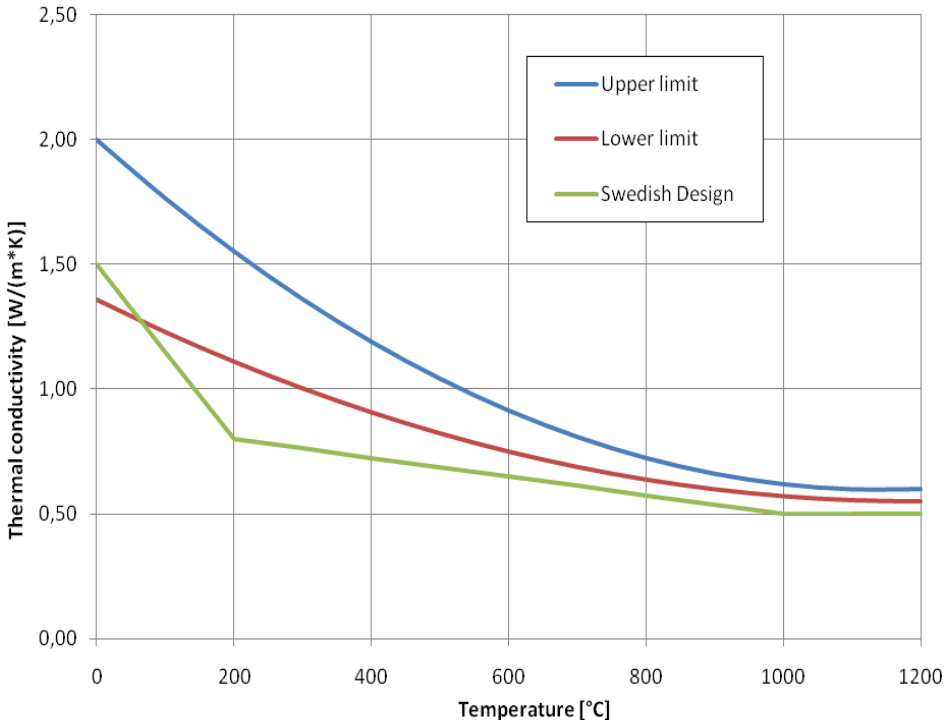

Figure 20 - Thermal conductivity of siliceous aggregate concrete

(Anderberg, 2003)

The effective thermal conductivity of a partially saturated concrete depends upon the degree of saturation and the temperature (Gawin, Majorana & Schrefler, 1999).

$$\lambda(S_l, T) = \lambda_d(T)\left(1 + \frac{4\ \phi\ \rho_l\ S_l}{(1-\phi)\ \rho_s}\right) \tag{32}$$

where ρ_l is the liquid water density and $\lambda_d(T)$ is thermal conductivity of the dry material, whose temperature dependence can be expressed by means of the following relationship (Harmathy, 1970):

$$\lambda_d(T) = \lambda_{d0}[1 + A_\lambda (T - T_0)] \tag{33}$$

λ_{d0} being the dry conductivity at reference temperature T_0, A_λ is a coefficient which takes the effect of the thermal damage on the dry thermal conductivity. An example of the thermal conductivity for concrete using **(32),** with the following data will be presented in **figure 21**.

The state equation of liquid water is rather complex and usually creates numerical problems. The following formula, function of the bulk density of liquid water as well as of temperature and gas pressure, may be used (Reid, Praunsnitz & Bruce, 1987; Forsyth & Simspon, 1991):

$$\rho_l = \rho_{l0}[1 - \beta_l (T - T_0) + \alpha_l (p_l - p_{l0})] \tag{34}$$

where ρ_{l0} = 999,84 kg/m^3 is water density at reference temperature T_0 and pressure p_{l0}, $\beta_l = (1 / v_l)(\partial v_l / \partial T)_{pl}$ is volume thermal expansion coefficient for water, α_l is the isothermal compression modulus of water and $v_l = \rho_l^{-1}$ is water specific volume. The state equation is valid for free liquid water and is generally assumed that it is valid also for the description of capillary water. Its applicability is therefore questionable, equation (34) is nevertheless used assuming water as incompressible i.e. $\alpha_l = 0$.

λ_{d0}	1,39 [W/(m K)]
A_λ	0,0006 [K^{-1}]
ρ^s	2590 [kg/m^3]
ρ^l	999,84 [kg/m^3]
T_0	293,15 [K]

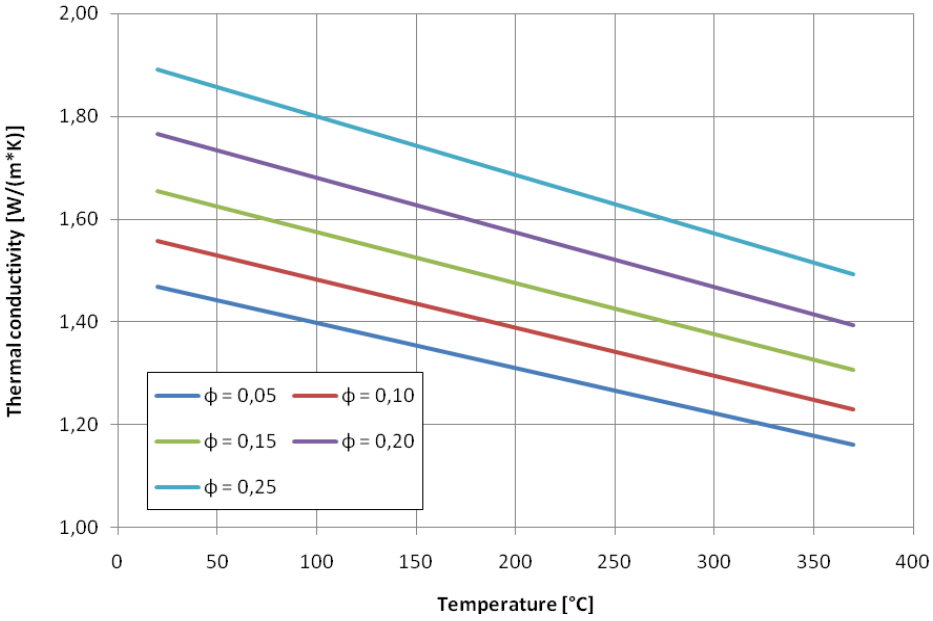

Figure 21 - Dependence of thermal conductivity from temperature according to (32)

Therefore, concerned to this thermal property, it will be used for our study **equation 32**. This equation can be considered the more realistic in a partially saturated concrete since it takes into account the effect of temperature as well as the effect of moisture by the intermediate of the degree of saturation.

I.2.2 - Heat capacity

It is the heat amount per mass unit required to change the temperature of the material by one degree. At a constant pressure *p*, the heat capacity, designated by C_p, may be expressed as follows (Harmathy, 1970; Harmathy & Allen, 1973):

$$C_p = \left(\frac{\partial H}{\partial T_p} \right) \tag{35}$$

where *H* is enthalpy and *T* is temperature.

At elevated temperatures the changes in the heat capacity with different concretes types may be caused by the latent heat of the different reactions involved during heating (water release, dehydration, decarbonization, $\alpha \rightarrow \beta$ quarts inversion). From the reported test results in fig 17, Schneider (1988) has concluded that:

- The type of aggregate has little influence on the heat capacity if temperatures below 800°C are considered.

- The water content is important for temperatures below 200°C. Wet concrete show an apparent heat capacity nearly twice higher than oven-dried concretes.

Also according to Franssen (1987), the wet concretes present an obvious calorific capacity that is nearly two times higher than the one of the dry concretes. For concretes, that are initially wet, heating up to 90°C can cause a rapid but temporary increase in heat capacity between two and three times the magnitude of the initial value (Blundell et al., 1976; Ohigishi et al., 1972). This is due to a rapid vaporization of free or evaporable water. At about 150°C, the heat capacity is the same of the initially pre-dried concrete and it increases linearly with temperature (Blundell et al., 1976).

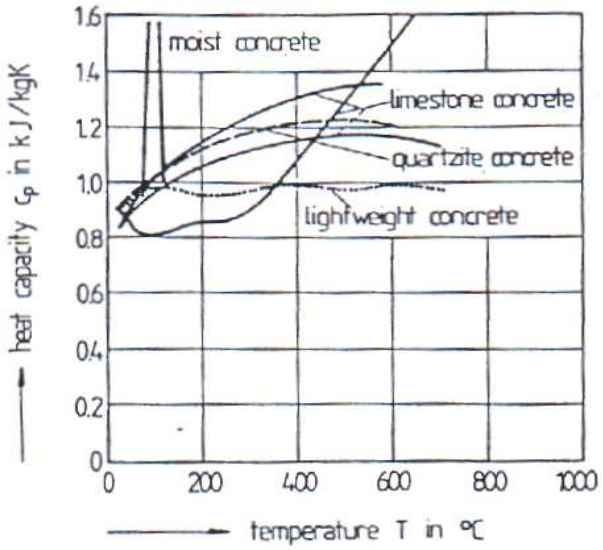

Figure 22 - Heat capacity of different concretes

(Schneider, 1988)

Harmathy (1970) estimated the heat capacity of idealized Portland cement pastes from theoretical considerations coupled with experimental data. The most important considered reactions were the dehydration of both C-S-H gel and calcium hydroxide $Ca(OH)_2$. Note that, this later gives the most conspicuous peak of the curve at about 500°C **(see figure 23).** The two reactions indicate that at the temperature while dehydration occurs, i.e. from 100 to 850°C, the latent heat contribution to the heat capacity C_p is very significant. Its value may be several times higher than the "sensible

heat capacity $\bar{C}_p$" due to the absorption of heat in the dehydration reaction. If heating is accompanied by chemical reactions or phase transitions that take place at a given temperature, the enthalpy is a function of both the temperature T and the degree of conversion ξ of the reactants into the products. According to Harmathy (1970), and Harmathy & Allen (1973) the C_p is usually referred to "apparent heat capacity " at a constant pressure and it may be expressed as follows:

$$C_p = \left(\frac{\partial H}{\partial T}\right)_{p,\xi} + \left(\frac{\partial H}{\partial \xi}\right)_{p,T} \frac{\partial \xi}{\partial T} = \bar{C}_p + \Delta H_p \frac{\partial \xi}{\partial T} \tag{36}$$

where $\bar{C}_p$ is the sensible heat contribution to the heat capacity at a given degree of conversion ξ, and ΔH_p is the enthalpy of the reaction that occurs (evaporation, dehydration).

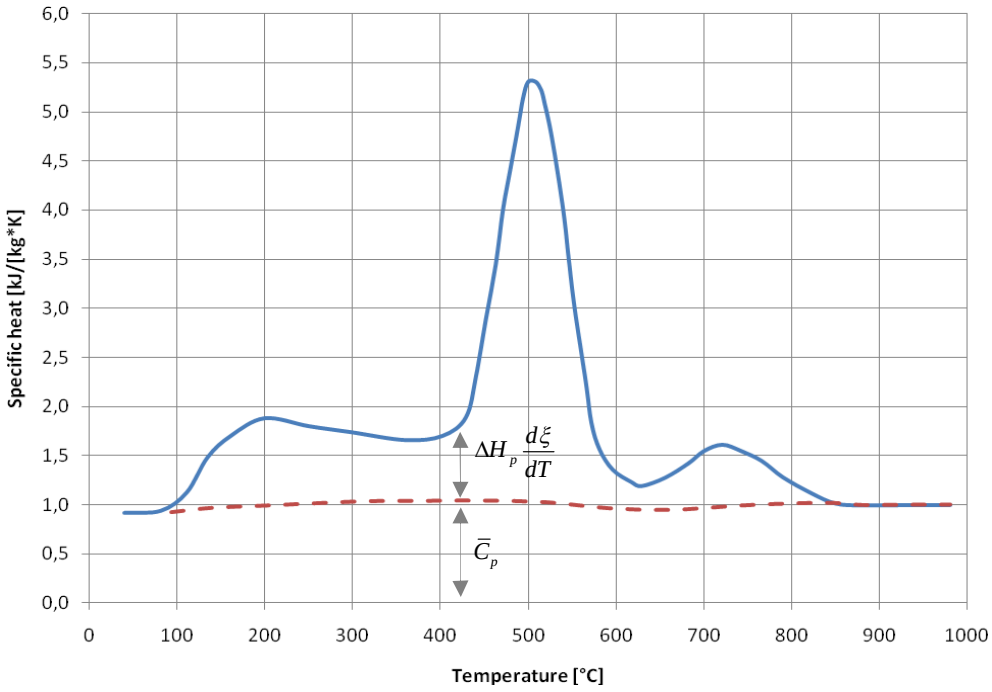

Figure 23 - Heat capacity of a cement paste with different water-cement ratio (Harmathy, 1970)

I.2.2.1 - Enthalpy of evaporation and Enthalpy of dehydration

The enthalpy of evaporation depends upon the temperature and may be approximated by the Watson formula (Forsyth & Simpson, 1991) :

$$\Delta H_{vap} = 2,672 \times 10^5 \left(T_{cr} - T\right)^{0,38} \tag{37}$$

where T_{cr} = 647,15 K is the critical temperature of water. A comparison with the experimental data from (Incropera & de Witt, 1990) is shown in **figure 24**.

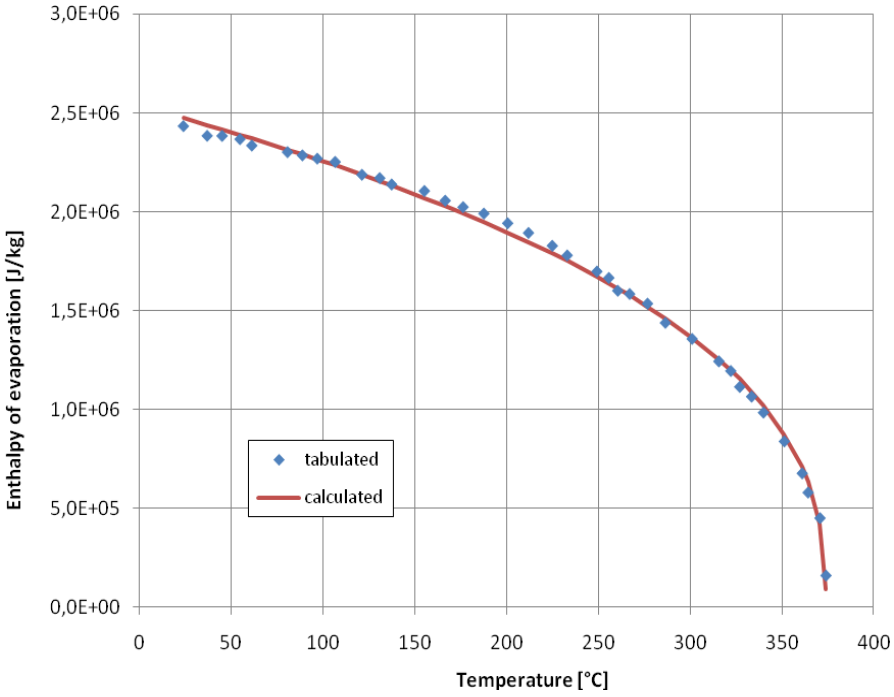

Figure 24 - Comparison of experimental data for enthalpy of evaporation with calculated data using (37)

Concerning to enthalpy of dehydration, it's firstly needed to discuss about the non-evaporable water. It is the water driven from the cement paste when it's heated to temperatures above 105°C and generally it contains nearly all chemically combined water in the C-S-H, all the water in the $Ca(OH)_2$, and also some water not held by chemical bonds. It takes 1670 J/kg to establish a bond of non-evaporable water in the C-S-H while the energy of the water of crystallization of $Ca(OH)_2$ is 3560 J/kg (Khoury & Majorana, 2003).

I.2.2.2 - Density

According to (Anderberg, 2003) the density of concrete changes with temperature. Due to a first loss of free water up to about 200°C and then to a second loss of chemically bound water, the density is decreasing by increasing temperature. The relative decrease of density up to 1000°C is between 11-13 %.

These results of water loss are reflected in the definition of concrete density ρ in the Eurocode 2 and presented in the table below (Anderberg, 2003):

$\rho = \rho_{20°C}$	For $20°C \le T \le 115°C$
$\rho = \rho_{20°C}\left(1-0.02\left(T-115\right)/85\right)$	For $115°C \le T \le 200°C$
$\rho = \rho_{20°C}\left(0.98-0.03\left(T-200\right)/200\right)$	For $200°C \le T \le 400°C$
$\rho = \rho_{20°C}\left(0.95-0.07\left(T-400\right)/800\right)$	For $400°C \le T \le 1200°C$

Variation of density with temperature influenced by water loss (Anderberg, 2003)

I.2.2.3 - Volumetric heat capacity

In order to assess the volumetric heat capacity ρC_p which is used normally in the energy conservation equation, taking into account the effect of latent heat, therefore, equation **(36)** and the table above can be used for that. In a partially saturated concrete the volumetric heat capacity ρC_p [J/(m^3 K)] can be expressed as a combination of the volumetric capacities of its constituents, as well as the effect of the evaporation and dehydration processes (Gawin et al., 1999).

$$\rho C_p \frac{\partial T}{\partial t} = \left(\rho C_p\right)_{eff} \frac{\partial T}{\partial t} + \left(\Delta H \dot{m}\right)_{vap} + \left(\Delta H \dot{m}\right)_{dehydr} \tag{38}$$

where $\left(\rho C_p\right)_{eff}$ is the effective volumetric heat capacity, ΔH_{vap}, ΔH_{dehydr} are the enthalpy of evaporation and dehydration respectively and $\dot{m}_{vap}$, $\dot{m}_{dehydr}$ are the rate of

evaporation and dehydration respectively. The effective volumetric heat capacity in equation (**38)** reads:

$$\left(\rho C_p\right)_{eff} = \left(1-\phi\right)\rho^s C_{ps} + \phi\left[S^l \rho^l C_{pl} + \left(1-S^l\right)\left(\rho^a C_{pa} + \rho^v C_{pv}\right)\right] \tag{39}$$

where the thermal capacities C_{pi} [J/(kg K)] depend upon the temperature of the material; ρ^i is a density, *i = s, l, v, a*.

The dependence of temperature on the volumetric heat capacity for the solid skeleton may be approximated by a linear relationship (Harmathy & Allen, 1973):

$$\left(1-\phi\right)\rho^s C_{ps} = \left(1-\phi_0\right)\rho_0^s C_{ps0}\left[1 + A_c\left(T - T_0\right)\right] \tag{40}$$

where $\left(1-\phi_0\right)\rho_0^s C_{ps0}$ is the volumetric heat capacity of the solid skeleton at the reference temperature $T_{0,}$ and A_c is a coefficient which considers the effect of temperature on the dry volumetric heat capacity. The thermal capacity for the gaseous constituents, in the case of a perfect gas and at a constant pressure, would be chosen independent from temperature changes for both air and vapour. Their heat capacities will be $C_{pa} = 1003,5$ and $C_{pv} = 1880,0$ (Feraille, 2000). Based on the results for the thermal capacity of the liquid water given by Raznjevic (1970), an approximated formula has been given by Feraille (2000) as follows:

$$C_{pl} = 4180 + 300 \cdot \left(\frac{T-273}{T-715}\right)^2 \tag{41}$$

An example of the volumetric heat capacity for a partially saturated concrete using equation **(39),** using the data in the table are shown in **figure 25.** Here densities and porosity are considered independent from the temperature to show only the effect of moisture, influenced by $S^l(RH,T)$, on the volumetric heat capacity of concrete.

C_{ps0}	810 [J/(kg K)]
A_c	0,000186 [K^{-1}]
ϕ	0,1 [-]
ρ^s	2590 [kg/m^3]
ρ^l	999,84 [kg/m^3]
T_0	293,15 [K]

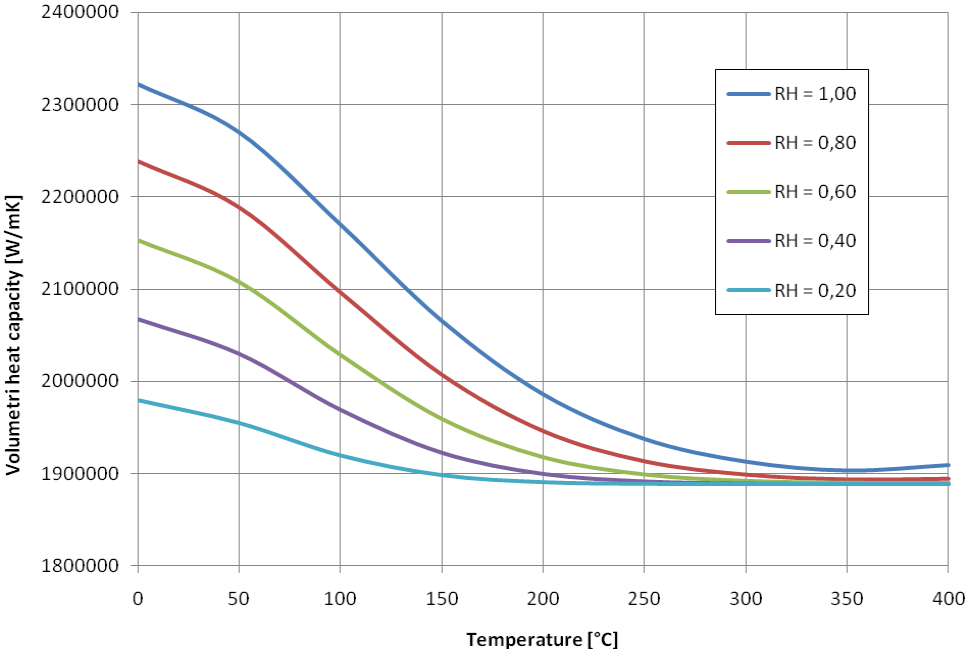

Figure 25 - Dependence of the volumetric heat capacity of concrete upon temperature and capillary pressure according to 32

Here, equation **(38)** given by Gawin et al., (1999) will be adopted in order to express the volumetric heat capacity ρC_p in a partially saturated concrete subjected to high temperatures.

I.2.3 - Conclusion

With regard to thermal conductivity, the degree of saturation and the degradation of concrete were the principal factors affecting its evolution. As previously mentioned, chemical and physical reactions take place in heated concrete. These changes are generally endothermic and they contribute for the apparent increase in heat capacity at elevated temperatures. Unique relations cannot rigorously describe the heat capacity of concrete at different temperatures, and the latent heat effects must be taken into account.

I.3 - THE EFFECT OF HIGH TEMPERATURES

ON THE HYGRAL PROPERTIES OF CONCRETE

When temperature increases in a concrete structure (e.g. in a wall), water vapour pressure is continuously forming in a zone close to the heated surface. This derives principally from the rapid evaporation of water inside the wall, when it reaches and passes the boiling point of water. Vapour pressure are also due to the water that is liberated during the dehydration of cement paste. This increase in the water vapour pressure in the hot region will create a thermodynamic imbalance between the hot and the cold regions. This will entail a diffusion process of the water vapour and of the dry air through the wall and towards the external atmosphere in order to maintain the equilibrium between liquid and vapour **(see figure 26)**

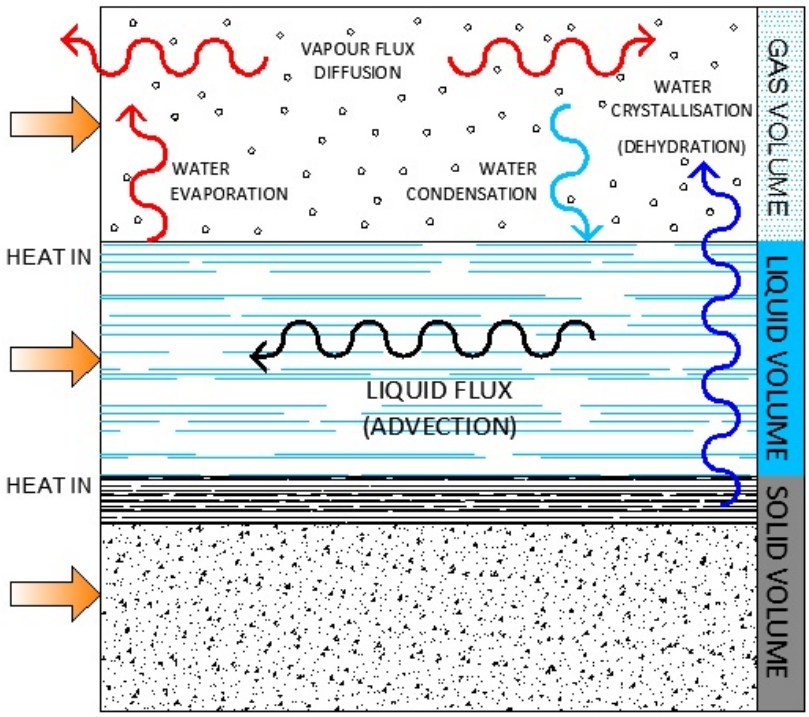

Figure 26 - Mass transport mechanism in a non-saturated porous medium subjected to heating

An appropriate prediction of the moisture distribution in a concrete structure subjected to high temperatures needs to know the material properties that control the movement of the fluids inside the porous medium. Permeability and diffusivity are the most important properties of the cementitious materials. These are very sensitive to porosity changes or micro-cracking phenomena. In facts, the increases in permeability and porosity of such materials are currently accepted as providing a reliable indication of their degradation whether if it has thermal, mechanical or physic-chemical origin. Therefore, in this chapter these properties and their evolutions will be studied when the concrete will be subjected to high temperatures.

I.3.1 - Permeability

In a partially saturated porous medium like concrete the liquid and gas transport will be governed by the absolute permeability of the material which can be defined as:

$$K' = -\frac{K\, k_{ri}}{\mu_i} \tag{42}$$

where:

- K' in [m^3/kg s] is the conventional permeability (apparent permeability) of the material
- K in [m^2] defined as (intrinsic permeability) which is a material property independent of the fluid
- k_{ri} [-] is the relative permeability of fluid and it depends on the degree of saturation of the liquid phase
- μ_f in [Pa s] is the dynamic viscosity of fluid and $i = l, g$.

In the following sections we will carry out a detailed study of each one of the above properties and their evolutions with high temperatures.

I.3.1.1 - Intrinsic permeability

Intrinsic permeability is a characteristic of the geometrical connectivity of the porous network, irrespective of the filling fluid. Therefore, the relative permeability is the additional variable that must take into consideration the penetration of gas and liquid and their coexistence within the porous network. In their investigations on pore pressures in heated concrete, (Bažant & Thonguthai, 1978, 1979) found an upward jump in the permeability of concrete by two orders of magnitude (about 200 times) as the temperature rises above 100°C. It was concluded that the pore volume available to capillary water must increase significantly as temperature and pore pressure increase. That means porosity changes from a system of closed, isolated pores to an open interconnected network **(see figure 27).**

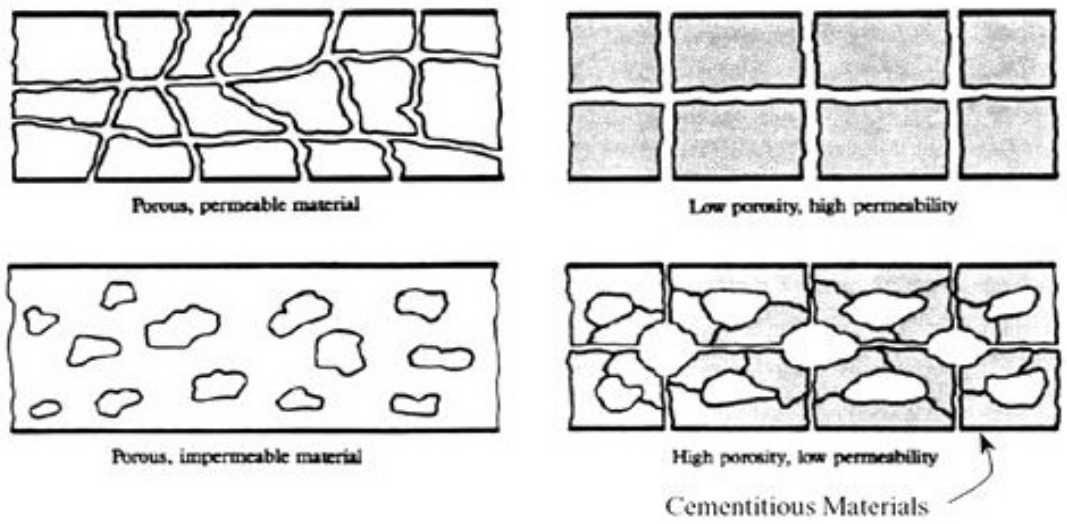

Figure 27 - Illustration of permeability and porosity (after Bakker)

Kalifa & Tsimbrovska (1998) studied the influence of high temperature on the intrinsic permeability K [m^2] of concrete. The main features of this work could be seen in **figure 28**. At 105°C, the permeability of the high performance concrete (HPC) ($\approx 10^{-17}$ m^2) is 10 times inferior to the one of a normal concrete (NC) ($\approx 10^{-16}$ m^2). Between 105°C and 400°C, the permeability of the HPC increases more quickly than the one of the NC; At 400°C, the permeability of the HPC ($\approx 3x10^{-15}$ m^2) is slightly superior to that one of the NC ($\approx 10^{-15}$ m^2). According to the authors, before 300°C the augmentation of

permeability is due to the increase in the capillary pore, while after 300°C the micro-cracking plays a very important role in permeability augmentation.

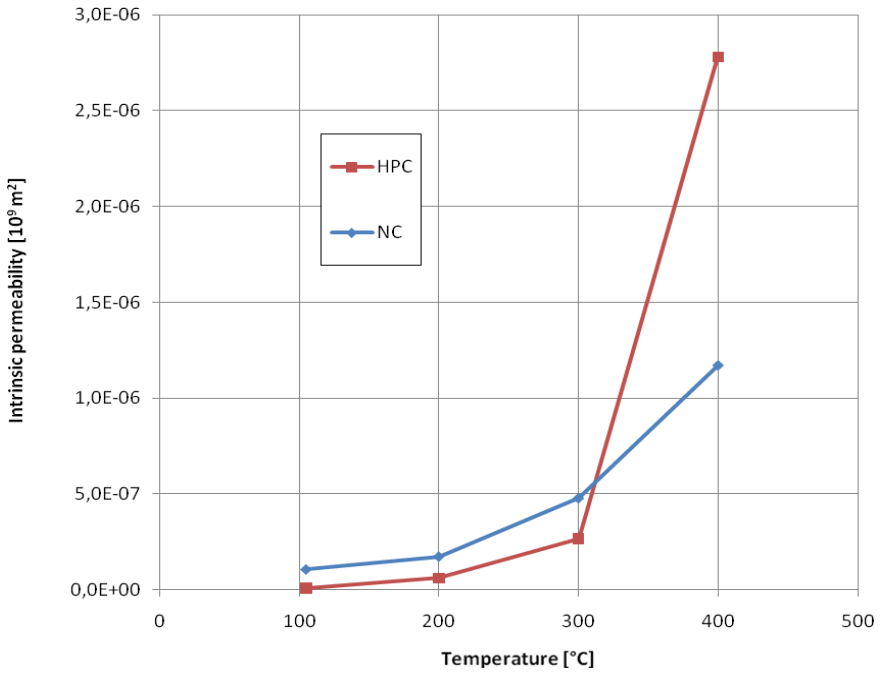

Figure 28 - The intrinsic permeability vs temperature for an ordinary concrete and for a HPC (Kalifa & Tsimbrovska, 1998)

Besides the temperature effect, the mechanical load also influences the evolution of intrinsic permeability. Indeed, a load applied up to the ultimate strength is assumed to involve an extensive damage in the specimen generating macroscopic cracking and, therefore, a sharp increase in permeability (Gérard et al., 1996; Wang et al., 1997 and Torrenti et al., 1999).

An experimental study was conducted by Picandet et al. (2001) to characterize the effect of external load-induced cracking on the permeability of concrete after unloading. Compared to the undamaged sample, a uniaxial compressive load at 90% of the ultimate strength can increase the axial permeability by about one order of magnitude after unloading. This increase in permeability is directly related to the maximum applied strain during loading and is due to the formation of a connected network of micro-cracks, which does not close down completely after the samples are unloaded **(see**

figure 29). An expression has been proposed by the author in order to reproduce the experimental results as follows:

$$K\left(\phi_M\right) = K_0 \cdot exp\left(A \cdot \phi_M\right)^B \tag{43}$$

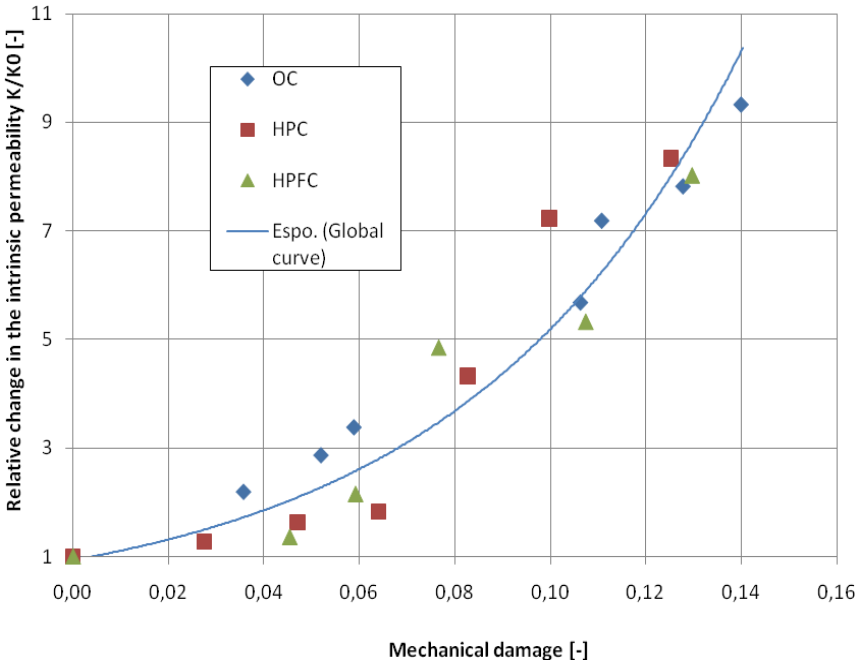

Figure 29 - Relation between increase in permeability and damage value from 'Grindosonic' evaluation and that one fitted by using (43)

(Picandet et al., 2001)

A generic relationship by (Gawin, Majorana & Schrefler, 1999) gives the intrinsic permeability as a function of temperature and gas pressure:

$$K(T, p_g) = K_0 \cdot 10^{A_T (T - T_0)} \cdot \left(\frac{p_g}{p_{g0}}\right)^{A_p} \tag{44}$$

where K_0 is the intrinsic permeability at reference temperature T_0 and gas pressure p_{g0}. As example we will take the data of B35-silicate concrete from (Gawin et al., 1999 after Schneider & Herbst, 1989) with K_0 = 1,5x10^{-16} m^2, A_T =0,005, A_p =0,368, to show the behaviour of the intrinsic permeability with temperature and pressure, without taking into account the damage effect **(see figure 30).**

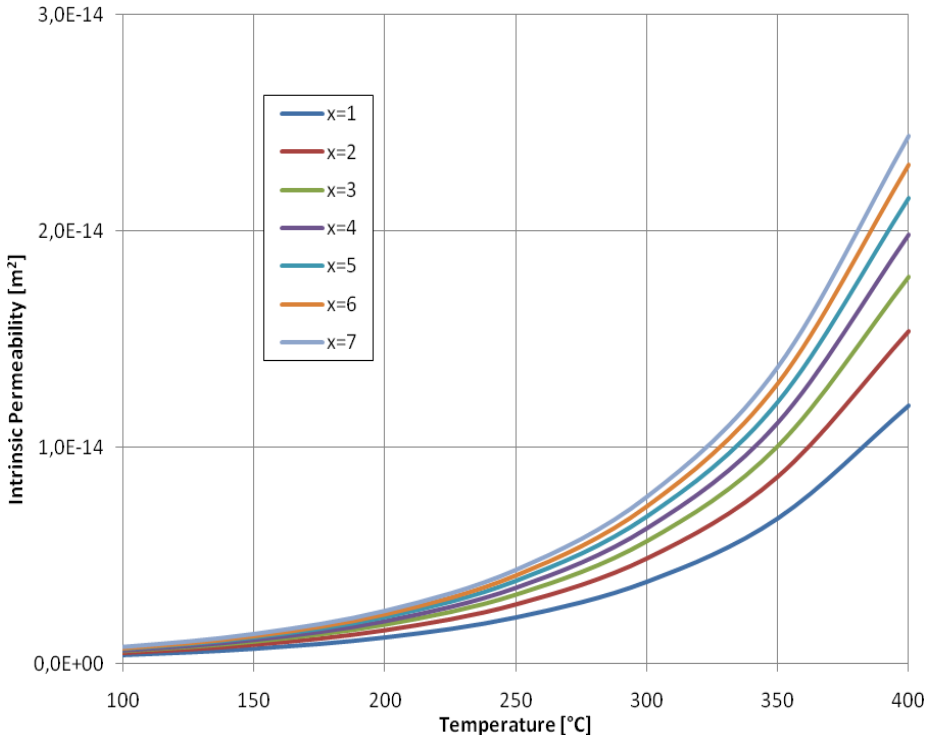

Figure 30 - Dependence of the intrinsic permeability upon temperature and pressure calculated from (44) with $x = p^g / p_0^g$

An approach was developed by Meschke & Grasberger (2003) based on an additive decomposition of the permeability into two portions: the first related to the moisture transport through the partially saturated pore space k_ϕ multiplied by the initial intrinsic permeability K_0 and the second one related to the moisture flux within a crack K_d.

$$K = K_0 k_\phi(\phi) + K_d \tag{45}$$

The relationship between permeability and pore structure of hardening cement paste at early ages was investigated experimentally by (Nyame & Illston, 1981). According to this work a relationship between permeability and the pore structure can be expressed as follows (Meschke & Grasberger, 2003):

$$k_\phi(\phi) = 10^\delta \qquad \text{with} \quad \delta = \frac{6(\phi - \phi_0)}{0.3 - 0.4\phi_0} \tag{46}$$

where ϕ_0 denotes the initial porosity and $\phi - \phi_0$ is the change of porosity.

When is necessary to consider cracking of concrete, the increase of permeability due to the change of porosity is insufficient. The effect of cracks on moisture transport is significantly larger compared to the effect of elastic and inelastic change of porosity. In a smeared crack approach, isotropic damage permeability K_d is introduced as a function of the width w_c [μm] of a discrete crack smeared over an equivalent strain localisation zone with a characteristic length l_c (Meschke & Grasberger, 2003). The authors proposed the following relationship:

$$K_d = \frac{w_h^3}{12 l_c}$$
$$with \quad w_h = \frac{w_c^2}{R^{2.5}} \quad for \; w_c \geq w_h \tag{47}$$

where w_h in [μm] is the equivalent hydraulic width, *R* is a parameter describes the crack roughness. A calibration of the crack parameter *R* with the experimental data given by (Aldea et al., 2000, Oshita & Tanabe, 2000) could be seen in **figure 31**

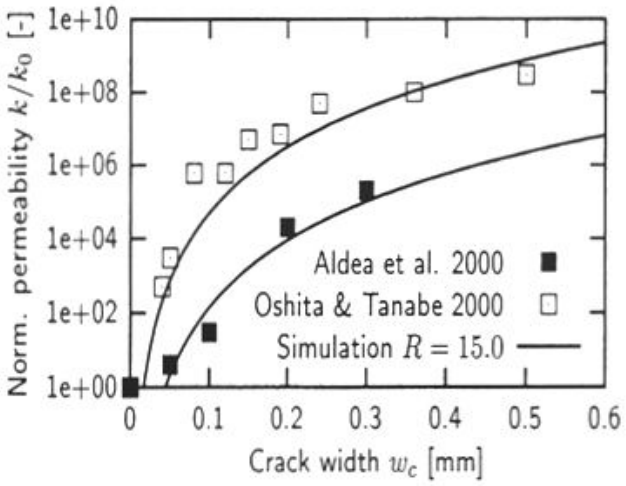

Figure 31 - Calibration of the crack parameter R

(Meschke & Grasberger, 2003)

In this study it will be used equation **(44)** proposed by Gawin et al., (1999) which takes into account the compound effects of temperature, pressure and mechanical damage for the intrinsic permeability. In this equation the effect of mechanical damage can be replaced by **(43)** proposed by (Picandet et al., 2001).

I.3.1.2 - Relative permeability of fluids

Few experimental results exist concerning the relative permeability of cement-based materials to gas and even less concerning the relative permeability to liquid. To overcome this difficulty, analytic expressions have been derived by (van Genuchten, 1980), based on the model of Mualem, which predicts the hydraulic conductivity from the statistical pore size distribution **(see figure 32)**

$$k_{rl}(S) = \sqrt{S}\left(1-\left(1-S^{1/A}\right)^{A}\right)^{2} \tag{48}$$

In addition, the author proposed a methodology to estimate the parameters of this equation, by using the fitted expression. Thus the parameter *A* is the exponent appearing in the capillary pressure curve of equation **(29).**

In the particular case of cement-based materials, (Savage & Janssen, 1997) have shown the relevancy of **(48)** to consider the liquid-water movement in a non-saturated Portland cement concrete.

According to Couture et al. (1996) and Nasrallah & Perre (1988), the water relative permeability for concrete depends upon the saturation with liquid phase and can be usually expressed as the following **(see figure 32)**

$$k_{rl} = \left(\frac{S - S_{ir}}{1 - S_{ir}}\right)^{A_l} \text{ for } S > S_{ir} \tag{49}$$

where S_{ir} is the irreducible saturation (sometimes assumed as S_{ir} = 0), and A_l is a constant, with the value from the range < 1 , 3 >.

When the relative humidity *RH* reaches a value higher than 75%, is observed a rapid increase of the capillary water flux (Bažant & Najjar, 1972). Such kind of behaviour can be described by the following relationship (Gawin et al., 1999) see **figure 32**.

$$k_{rl} = \left[1+\left(\frac{1-RH}{0.25}\right)^{B_l}\right]^{-1} \cdot S^{A_l} \tag{50}$$

where A_l, B_l are constant with value from the range < 1 , 3 >. It should be noted that the term in square brackets has a form originally proposed in (Bažant & Najjar, 1972).

According to Gawin et al. (1999) this equation has good numerical properties and allows avoiding a use of irreducible saturation concept. This concept creates serious theoretical and numerical problems (Couture et al., 1996). Therefore, equation **(50)** will be adopted in this study.

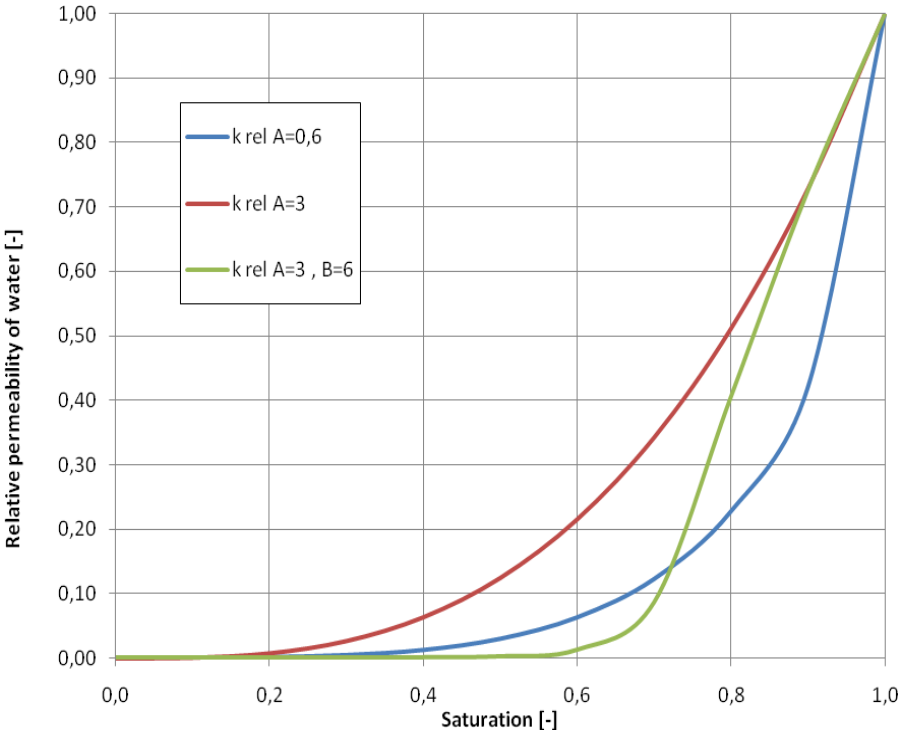

Figure 32 - Relative permeability of water calculated with different models, expressed by equations 48, 49 and 50 respectively

The gas relative permeability of concrete, similarly to most capillary porous materials, may be described from the analytic expressions given by Luckner et al. (1989), based on the model of Mualem (1976):

$$k_{rg}(S) = \sqrt{1-S}\left(1-S^{1/A}\right)^{2A} \tag{51}$$

Moreover it can be also described by the formula given by (Couture et al., 1996; Nasrallah & Perre, 1988):

$$k_{rg} = 1-\left(\frac{S}{S_{cr}}\right)^{A_g} \text{ for } S < S_{cr} \tag{52}$$

where S_{cr} is the critical saturation value, above which there is no gas flow in the medium, A_g is a constant, which usually has value from the range <1 , 3>. We can see from **figure 33** that there is no big difference between the two models proposed. Therefore we will use that one given by (50).

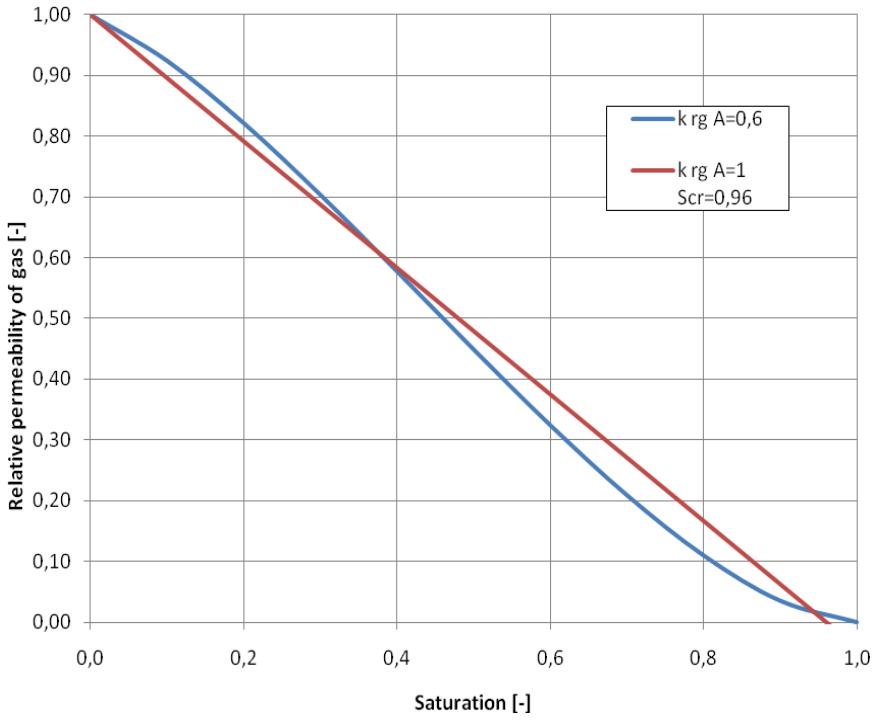

Figure 33 - Relative permeability of gas,

calculated from models expressed by equations (51), (52)

I.3.1.3 - Viscosity of fluids

The dynamic viscosity of liquid water μ_l [Pa s] depends strongly upon temperature and can be evaluated, with a sufficient accuracy, in a wide temperature range, using the approximate formula (Thomas & Sansom, 1995):

$$\mu_l = 0,6612\left(T - 229\right)^{-1,562} \tag{53}$$

the results are compared with the related experimental data (Incropera & de Witt, 1990) in **figure 34**.

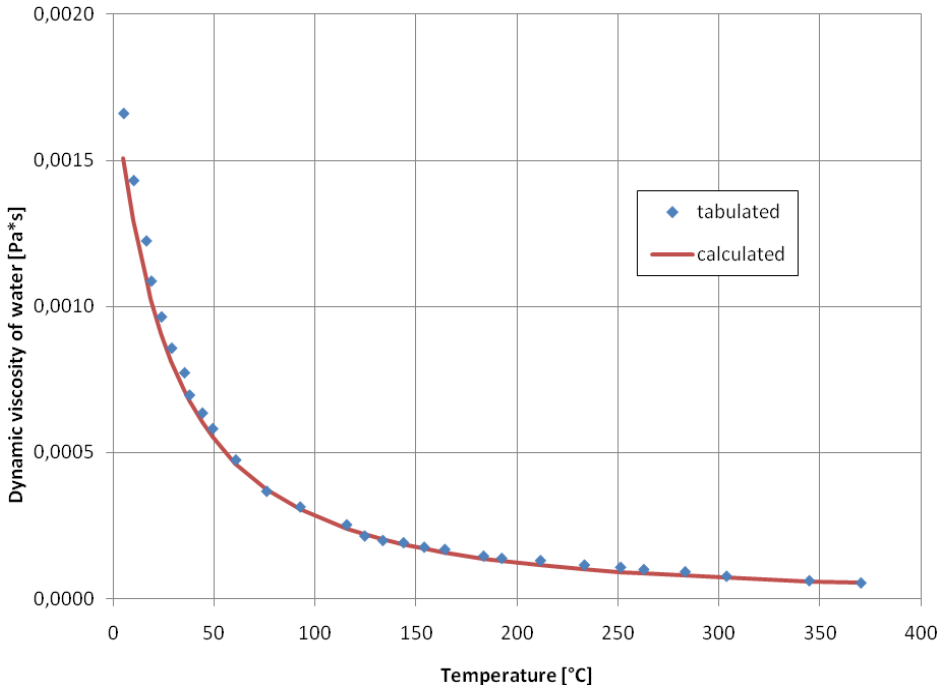

Figure 34 - Comparison of the experimental data for the dynamic viscosity of water with those calculated using approximated formula (53)

The dynamic viscosity of moist air μ_g [Pa s], which depends upon the temperature and the ratio of the vapour and gas pressure, using the data from (Mason & Monchik, 1965), can be approximated using the following formula (Forsyth & Simpson, 1991):

$$\mu_g = \mu_v + \left(\mu_a - \mu_v\right)\left(\frac{p^a}{p^g}\right)^{0,608} \tag{54}$$

where the ratio p^a/p^g is the mole fraction of dry air in the gas phase, and μ_v is the water vapour dynamic viscosity:

$$\mu_v = \mu_{v0} + \alpha_v \left(T - T_0\right) \tag{55}$$

with μ_{v0} = 8,85 × 10^{-6} [Pa s], α_v = 3,53 × 10^{-8} [Pa s K^{-1}]. Further, the dry air dynamic viscosity μ_a is given by:

$$\mu_a = \mu_{a0} + \alpha_a \left(T - T_0\right) + \beta_a \left(T - T_0\right)^2 \tag{56}$$

with μ_{a0} = 17,17 × 10^{-6} [Pa s], α_a = 4,73 × 10^{-8} [Pa s K^{-1}], β_a = 2,22 × 10^{-11} [Pa s K^{-2}]. Another formula exists in the literature (Pezzani, 1988) which is simpler since it is function of temperature only:

$$\mu_g = 3{,}85 \times 10^{-8} T \tag{57}$$

A comparison of the experimental data of moist air with the ones calculated using the approximated formulas is shown in **figure 35**. From this figure we can see that the results obtained from **(54)** fit quit well with the tabulated results compared to that obtained by **(57).** Therefore we will use equation **(54)** in our study.

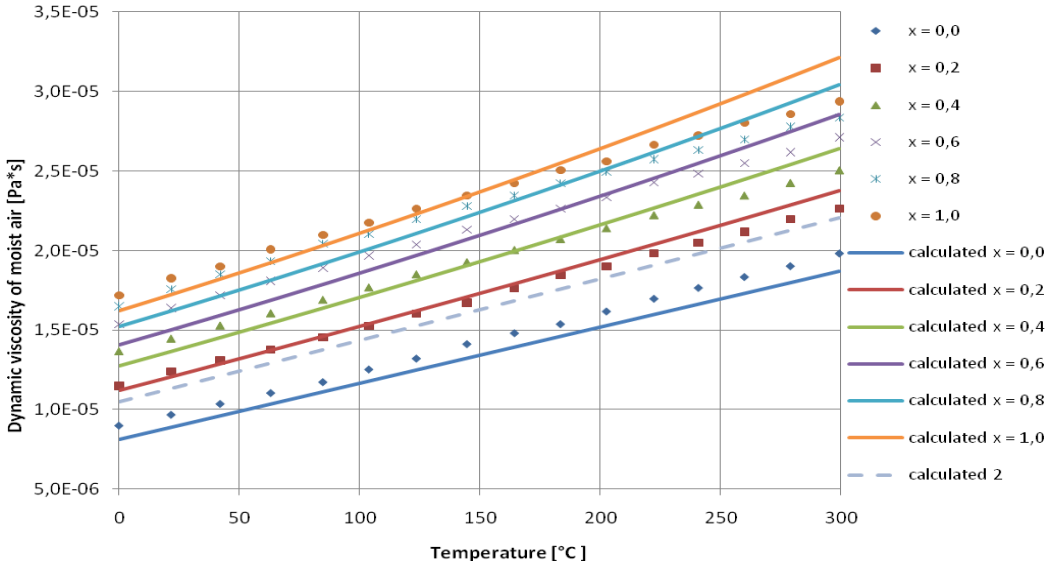

Figure 35 - Comparison between experimental data for the dynamic viscosity of moist air and the calculated data using approximated formula (54) and (57) where x = p^a/p^g

I.3.2 - Diffusivity

The diffusivity of vapour in the air at temperature T and pressure p^g is given in (Daian, 1989):

$$D_{va}\left(T, p^g\right) = D_{v0}\left(\frac{T}{T_0}\right)^{A_v} \frac{p_0^g}{p^g} \tag{58}$$

where D_{v0} = 2,58 × 10^{-5} [m^2 s^{-1}] is the diffusion coefficient of vapour species in the air at the reference temperature T_0 = 273,15 K and pressure p_0^g = 101325 Pa (Forsyth & Simpson, 1991). A_v is a constant, and for the value A_v = 1,667 there is a good correlation with the experimental data concerning vapour diffusion at different temperature (Mason & Monchik, 1965). **Figure 36** show an example for the behaviour of the above equation **(58).**

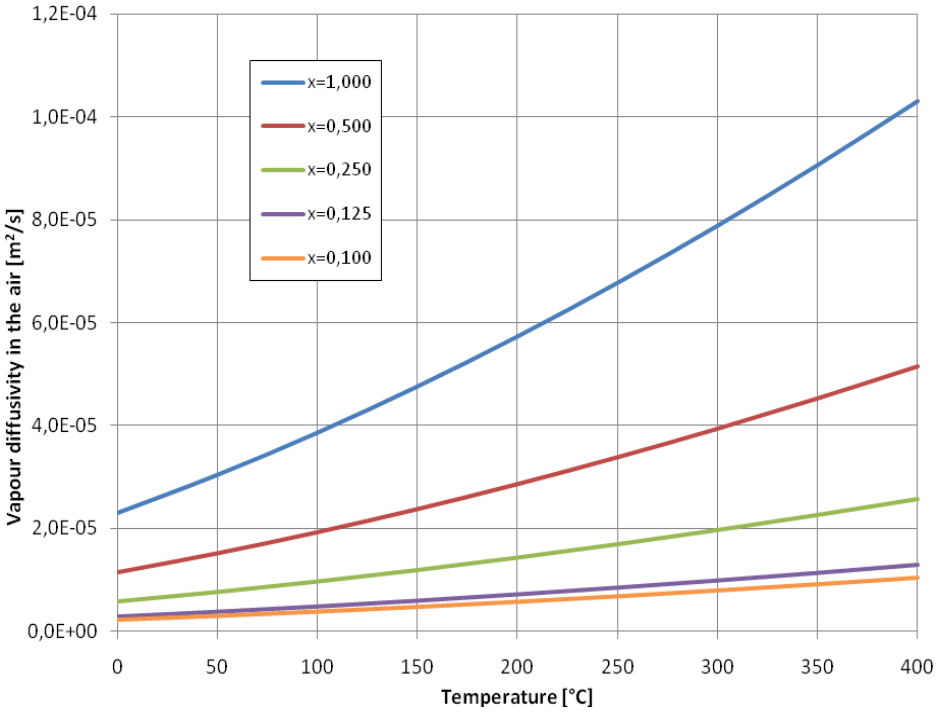

Figure 36 - Dependence of vapour diffusivity in the air

with calculated temperature and pressure using (58) with $x = p_0^g / p^g$

The pore space in concrete has a very complex inner structure, that influences the vapour diffusion process. Therefore and because of the lack of experimental results the simplest way of taking it into account is the introduction of tortuosity factor, as it has

been suggested by (Bažant & Najjar, 1972; Perre, 1987), which considers the tortuous nature of the pathway in the porous media. The tortuosity factor is usually assumed to be constant in the whole range of moisture content. For concrete the range is $\tau \cong 0{,}4$-$0{,}6$, used by several authors (e.g. Daian, 1989). Moreover it could be approximated by the following formula (Millington, 1959).

$$\tau\left(\phi,\, S^l\right) = \phi^{1/3}\left(1 - S^l\right)^{7/3} \tag{59}$$

Several authors (e.g. Perre, 1987) have defined the effective diffusion coefficient, taking into account the reduction of space offered to the diffusion of gaseous constituents, as:

$$D_{eff}\left(S^l\right) = \phi\left(1 - S^l\right)^{B_v} \tau D_{va}\left(T,\, p^g\right) \tag{60}$$

where B_v is a constant, usually from the range <1 , 3> (Daian, 1988).

Now it should be introduced the resistance factor (structure factor) f_s which considers both the tortuosity effect τ and the reduction of space offered to the diffusion of gaseous constituents.

$$D_{eff}\left(S^l\right) = f_s\left(\phi,\, S^l\right) D_{va}\left(T,\, p^g\right) \tag{61}$$

where $\phi_g = \left(1 - S^l\right)\phi$.

This structure factor f_s could be also approached through the expression derived by (Millington, 1959) for variably saturated porous media and used by several authors (e.g. Adenekan et al., 1993; Sleep & Sykes, 1993; Mainguy et al., 2001),

$$f_s\left(\phi,\, S^l\right) = \phi_g^{4/3}\left(1 - S^l\right)^2 = \phi^{4/3}\left(1 - S^l\right)^{10/3} \tag{62}$$

During diffusion of vapour in a porous material with very narrow pores (e.g. in concrete), the number of collisions of water molecules with the solid matrix is non-negligible compared with the number of collisions with air molecules. This is known as Knudsen effect, but we didn't take it into account in our model.

Now it follows an example to show the temperature dependence of the effective vapour diffusion coefficient, evaluated according to **(58), (59), (60)** and $\phi(T)$ which has been given in **(3) (see figure 37)**

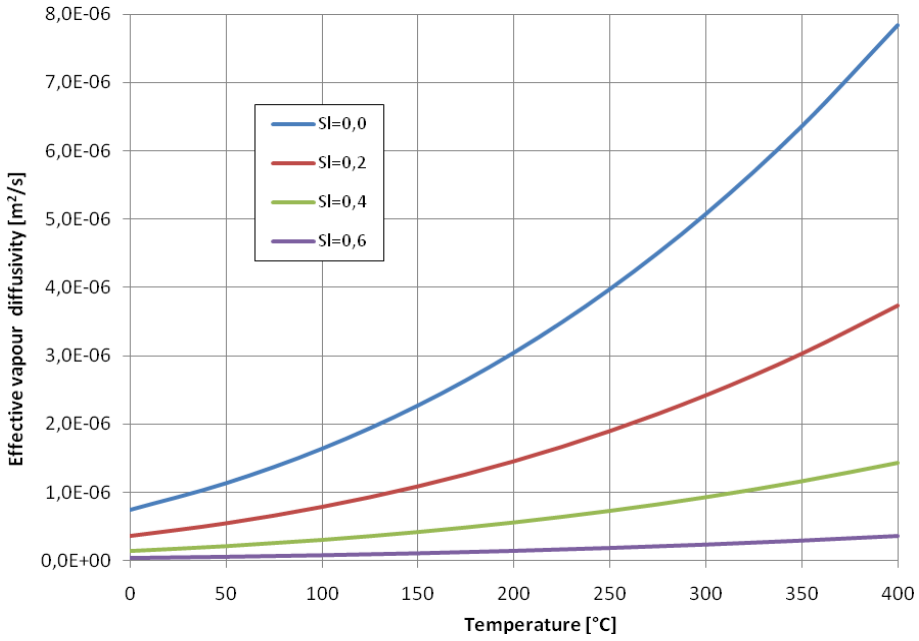

Figure 37 - The effective vapour diffusion coefficient for B-35 basalt concrete at different levels of saturation degree with $x = p_0^g / p^g = 1$ in 58 and $B_v = 1$ in 60

I.3.3 - Conclusion

The significant increase in concrete permeability and diffusivity characteristics at high temperatures is mainly generated by arising of micro-cracks and by changes of material inner structure as well as by crack opening due to high gas pressure values. As a result, it depends not only upon temperature, moisture content and gas pressure, but also upon a degree of cracks development, which may be described by the use of damage parameter ϕ_M .

CHAPTER II

* * *

THERMO-HYGRAL MODEL

When subjected to drying and or to heating, heterogeneous porous media such as aged cementitious materials or soils exhibit coupled mass and heat transfer processes that may control their mechanical behavior. The modeling of the thermo-hygral (TH) behavior of open porous media (saturated or unsaturated) is then of great interest in civil engineering applications. This modeling may be performed by taking into account the heterogeneity of the porous medium either by using homogenization techniques to derive a macroscopic behavior from the properties at the microstructure scale, or by random statistical analysis of these properties. The three-fluid model constitutes a general modeling framework of the TH behavior of partially saturated open porous media. The mathematical model has been developed by writing the relevant balance equations for the constituents at the pore scale and by up-scaling these equations to the macroscopic scale, taking into account thermodynamic constraints. The final model after introduction of the constitutive equations, consists of a mass balance equation for the dry air, a mass balance equation for the water phases (liquid and vapour), a mass balance equation for the solid phase, an energy balance and a linear momentum balance equation for the mixture fluids plus solid phase. The three-fluid model is the basis of several numerical tools which can now be found in general purpose finite element codes such as Cast3M of CEA. The aim of this section is then to develop a numerical tool able to analyze the effect of random distributions of some key parameters on the TH behavior of a partially saturated medium. As a first step in this direction, attention is paid to the intrinsic (geometrical) permeability. A staggered solution strategy permits to solve the equations sequentially. This appropriate partitioning reduces the size of the discretized problem to be solved at each time step. It is based on a specific iterative algorithm to account for the interaction between all the transfer processes to conserve their full coupling. Staggered procedures show a superior flexibility as compared to monolithic ones if successive fields have to be introduced. They may have however also problems linked to convergence which did however not appear in the present case.

II.1 - T-H MODEL

The general approach to modeling non-equilibrium mass and heat transfer processes in a partially saturated open porous medium is to start from a set of balance equations governing the time evolution of mass and heat of solid matrix and fluids filling the porous network, the exchange between the phases and with the surrounding medium. These balance equations are supplemented with an appropriate set of constitutive relationships which permit to reduce the number of independent state variables that control the physical process under investigation.

In the following, the full set of balance equations will be presented. The governing equations of the model are given in terms of the chosen state variables, the capillary pressure p_c the gas pressure p_g and the temperature T. This choice is of particular importance: the chosen quantities must describe a well posed initial-boundary value problem, should guarantee a good numerical performance of the solution algorithm, and should make easy their experimental identification.

II.1.1 - Balance equations

The balance equations can be obtained by using the procedure of space averaging of the microscopic balance equations, written for the individual constituents of the medium. The theoretical framework is based on the works of Bear (1991), Hassanizadeh & Gray (1980), Gray & Schrefler (2001) and Lewis & Schrefler (1998).

For sake of brevity only the final form of the macroscopic conservation equations is given. Hence, mass balance equations write, for the solid matrix:

$$\frac{\partial m_s}{\partial t} = \dot{m}_{dehyd} \tag{63}$$

for the liquid water:

$$\frac{\partial m_l}{\partial t} + \nabla \cdot \left(m_l \mathbf{v}_l \right) = -\dot{m}_{vap} - \dot{m}_{dehyd} \tag{64}$$

for the vapour:

$$\frac{\partial m_v}{\partial t} + \nabla \cdot \left(m_v \mathbf{v}_v \right) = \dot{m}_{vap} \tag{65}$$

and for the dry air:

$$\frac{\partial m_a}{\partial t} + \nabla \cdot \left(m_a \boldsymbol{v}_a \right) = 0 \tag{66}$$

where m_π is the mass per unit volume of porous medium of each constituent:

$$\begin{gathered} m_s = (1-\phi)\ \rho_s \quad , \quad m_l = \phi\ S_l\ \rho_l \\ m_v = \phi\ (1-S_l)\ \rho_v \quad , \quad m_a = \phi\ (1-S_l)\ \rho_a \end{gathered} \tag{67}$$

in which ρ_π is the corresponding density, ϕ the porosity and S_l the degree of saturation of pores with liquid water, the complementary part of the pore volume being filled with the gas mixture. These equations take into account phase changes due to dehydration (i.e. loss of chemically bound water of solid skeleton constituents of the porous medium), evaporation and condensation phenomena. A source term, corresponding to dehydration mass rate m_{dehyd} and to evaporation / condensation mass rate m_{vap}, are therefore considered.

Moreover, fluid velocities $\boldsymbol{v}_\pi$ are split into relative components in order to describe mass transport, within the porous network, by both permeation and diffusion phenomena due, respectively, to pressure and concentration gradients. They read:

$$\begin{aligned} \boldsymbol{v}_l &= \boldsymbol{v}_s + \boldsymbol{v}_{l-s} \\ \boldsymbol{v}_v &= \boldsymbol{v}_s + \boldsymbol{v}_{g-s} + \boldsymbol{v}_{v-g} \\ \boldsymbol{v}_a &= \boldsymbol{v}_s + \boldsymbol{v}_{g-s} + \boldsymbol{v}_{a-g} \end{aligned} \tag{68}$$

where $\boldsymbol{v}_s$ (which is neglected) is the velocity of the solid phase, $\boldsymbol{v}_{\pi-s}$ is the velocity of the liquid water ($\pi = l$) and gas mixture ($\pi = g$) with respect to the solid phase and $\boldsymbol{v}_{\pi-g}$ is the velocity of the vapour ($\pi = v$) and dry air ($\pi = a$) with respect to the gas mixture (moist air). In what follows, the solid mass balance equation **(63)** will not explicitly appear since it will be used only to determine the evolution of porosity in mass balance equations of fluids according to:

$$\frac{\partial \phi}{\partial t} = -\frac{\dot{m}_{dehyd}}{\rho_s} \tag{69}$$

where the solid phase density ρ_s is assumed to be constant. It is worth noting that equation **(69)** is strictly local since the effect of the deformation of the solid skeleton on the porosity has been neglected in the adopted context of small-strain deformations. With regard to the energy conservation equation, the space averaging procedure gives:

$$\rho C_p \frac{\partial T}{\partial t} + \left(m_l C_l \boldsymbol{v}_{l-s} + m_g C_g \boldsymbol{v}_{g-s} \right) \cdot \nabla T + \nabla \cdot \boldsymbol{q} = -H_{vap} \dot{m}_{vap} + H_{dehyd} \dot{m}_{dehyd} \tag{70}$$

with the heat capacity of the whole porous medium given by:

$$\rho C_p = \sum_{\pi = s,l,v,a} \left(m_\pi C_\pi \right) \tag{71}$$

where C_π is the specific heat capacity of each constituent, H_{vap} is the enthalpy of evaporation, H_{dehyd} the enthalpy of dehydration and q the flux vector of heat conduction. Note that the second term of the left-hand side of equation **(70)** gives the heat convection process which encompasses both advective and diffusive heat transfers within the porous network. Moreover, the right-hand side corresponds to the latent heat due to phase changes (evaporation, condensation, dehydration).

II.1.2 - CONSTITUTIVE EQUATIONS

II.1.2.1 - Fluid state equations

The liquid water is considered to be incompressible such that its density depends on the temperature only. The vapour, dry air and the gas mixture are considered to behave as ideal gases, which gives ($\pi = v, a, g$):

$$\rho_\pi = \frac{M_\pi}{RT} p_\pi \tag{72}$$

where p is the pressure, M_π the molar mass and R the universal gas constant. Furthermore, the pressure and density of the gas mixture can be related to the partial pressures and densities of the constituents by:

$$\rho_g = \rho_v + \rho_a \quad , \quad p_g = p_v + p_a \tag{73}$$

which gives:

$$M_g = M_a + \left(M_v - M_a\right)\frac{p_v}{p_g} \tag{74}$$

II.1.2.2 - Liquid - Vapour equilibrium

By assuming that the evaporation process occurs without energy dissipation, that is, liquid and vapour water have equal free enthalpies, one can derive generalized Clausius-Clapeyron equation which is a relationship between liquid and vapour pressure:

$$p_v = p_{vs} \exp\left(\frac{M_v}{\rho_l RT}\left(p_g - p_c - p_{vs}\right)\right) \tag{75}$$

where the capillary pressure:

$$p_c = p_g - p_l \tag{76}$$

has been introduced for the porous medium and p_{vs} is the saturating vapour pressure.

II.1.2.3 - Mass fluxes

According to the velocity decomposition **(68)**, the mass fluxes can be made explicit:

$$\boldsymbol{J}_{l-s} = m_l \boldsymbol{v}_{l-s} = -K \frac{\rho_l k_{rl}}{\mu_l} \nabla p_l \tag{77}$$

$$\boldsymbol{J}_{v-s} = m_v \boldsymbol{v}_{g-s} + m_v \boldsymbol{v}_{v-g} = -K \frac{\rho_v k_{rg}}{\mu_g} \nabla p_g - D \rho_g \frac{M_v M_a}{M_g^2} \nabla \left(\frac{p_v}{p_g} \right) \tag{78}$$

$$\boldsymbol{J}_{a-s} = m_a \boldsymbol{v}_{g-s} + m_a \boldsymbol{v}_{a-g} = -K \frac{\rho_a k_{rg}}{\mu_g} \nabla p_g - D \rho_g \frac{M_v M_a}{M_g^2} \nabla \left(\frac{p_a}{p_g} \right) \tag{79}$$

In the above equations, where Darcy's and Fick's laws are introduced, K is the intrinsic permeability, $k_{r\pi}$ is the relative one, μ_π is the dynamic viscosity, D is the diffusivity and M_π is the molar mass. For the gas mixture, the Darcy's part of the mass flux $J_{\pi\text{-}s}$ with $\pi = v, a$ is controlled by the barycentric velocity of the gas $v_{g\text{-}s}$ while the Fick's part ($m_\pi v_{\pi\text{-}g}$), which is controlled by the concentration gradient, gives the diffusion of each component within the gas mixture (Kuiken, 1994). Furthermore, the concentration gradient writes:

$$\nabla \left(\frac{p_v}{p_g} \right) = \frac{1}{p_g} \left(\left(\frac{\rho_v}{\rho_l} - \frac{p_v}{p_g} \right) \nabla p_g - \frac{\rho_v}{\rho_l} \nabla p_c \right) = -\nabla \left(\frac{p_a}{p_g} \right) \tag{80}$$

Thus, the vapour and dry air fluxes recast in the following generic form:

$$\boldsymbol{J}_{\pi-s} = -K \frac{\rho_\pi k_{rg}}{\mu_g} \nabla p_g \mp D \frac{M_v M_a}{RTM_g} \left(\frac{\rho_v}{\rho_l} - \frac{p_v}{p_g} \right) \nabla p_g \pm D \frac{M_v M_a}{RTM_g} \frac{\rho_v}{\rho_l} \nabla p_c \tag{81}$$

where the upper signs correspond to vapour case ($\pi = v$) while the lower signs give the dry air flux ($\pi = a$).

II.1.2.4 - Conductive heat flux

In the energy balance equation **(70)**, the heat conduction process in the porous medium can be described by Fourier's law which relates the temperature to the heat flux as follows:

$$\boldsymbol{q} = -\lambda\left(S_l, T\right)\nabla T \tag{82}$$

Where $\lambda\left(S_l, T\right)$ is the effective thermal conductivity which is a function of the temperature and of the degree of saturation with liquid water of the pores.

II.1.2.5 - Sorption-desorption isotherm

Solving the presented equations aims at determining the spatial and temporal distribution of temperature, masses of constituents and corresponding pressures within the porous medium. By introducing the previous constitutive equations, the problem involves, at this stage, as main unknowns $(S_l, p_c, p_g, T, \dot{m}_{vap})$ or alternatively $(S_l, p_v, p_a, T, \dot{m}_{vap})$. This set is reduced by introducing an additional explicit relationship (Baroghel-Bouny, 1994; Al Najim, Meftah, & Mebarki. 2003; Dal Pont, 2004; Meftah & Sabeur 2006):

$$S_l = S_l\left(p_c, T\right) \tag{83}$$

which is the sorption-desorption isotherm, characterizing phenomenologically the microstructure of the porous medium (pore size distribution). Using this additional relationship, the reduced set of unknowns is then $(p_c, p_g, T, \dot{m}_{vap})$ where a choice is made here to retain the state variables (p_c, p_g) instead of (p_v, p_a) or (p_l, p_a). Moreover, the set of unknowns can be further reduced. For this purpose (Lewis & Schrefler, 1998), conservation equations of liquid **(64)** and vapour **(65)** are summed in order to eliminate the evaporation source term m_{vap} and thus obtain the balance equation for total water mass m_w:

$$\frac{\partial m_w}{\partial t} + \nabla \cdot \boldsymbol{J}_{w-s} = -\dot{m}_{dehyd} \tag{84}$$

with:

$$m_w = m_l + m_v \tag{85}$$

$$\boldsymbol{J}_{w-s} = \boldsymbol{J}_{l-s} + \boldsymbol{J}_{v-s} \tag{86}$$

Hence, this equation is supplied by mass conservation equation of dry air **(66)** and energy **(70)** in order to determine the state variables (p_c, p_g, T), which are the main unknowns of the problem.

II.1.3 - BOUNDARY CONDITIONS

The hygro-thermal problem consists in determining the temperature T and the pressure p_g and p_c fields, satisfying the conservation equations **(66)**, **(70)** and **(84)** within the domain - with the following boundary conditions at the domain frontier Σ:

$$p_g = \bar{p}_g \quad \text{on} \quad \Sigma_p \tag{87}$$

$$p_c = \bar{p}_c \quad \text{on} \quad \Sigma_p \tag{88}$$

$$T = \bar{T} \quad \text{on} \quad \Sigma_T \tag{89}$$

$$-\boldsymbol{J}_{v-s} \cdot \boldsymbol{n} = \bar{q}_v - h_g \left(\rho_v - \rho_v^{\infty} \right) \quad \text{on} \quad \bar{\Sigma}_p \tag{90}$$

$$-\boldsymbol{J}_{a-s} \cdot \boldsymbol{n} = \bar{q}_a - h_g \left(\rho_a - \rho_a^{\infty} \right) \quad \text{on} \quad \bar{\Sigma}_p \tag{91}$$

$$-\boldsymbol{J}_{l-s} \cdot \boldsymbol{n} = \bar{q}_l \quad \text{on} \quad \bar{\Sigma}_p \tag{92}$$

$$-\left(\boldsymbol{q} - H_{vap} \boldsymbol{J}_{l-s} \right) \cdot \boldsymbol{n} = \bar{q}_T - h_T \left(T - T_{\infty} \right) - \varepsilon \sigma \left(T^4 - T_{\infty}^4 \right) \quad \text{on} \quad \bar{\Sigma}_T \tag{93}$$

Where $\Sigma_{\bullet}$ is part of the boundary at which the pressures and the temperature are known (Dirichlet type boundary conditions) while $\bar{\Sigma}_{\bullet}$ is the complementary part (with unit outward normal ***n***) at which the mass fluxes of fluids and heat flux are imposed, q_π are the prescribed fluxes, ρ_π^∞ with $\pi = v,a$, respectively, T_∞ are the densities of vapour and dry air, respectively, the temperature in the far field surrounding gas, h_g, respectively h_T, is the convective mass, respectively energy, exchange coefficient, ε is the emissivity and σ is the Stefan-Boltzmann constant. Moreover, the initial conditions $p_g\left(x,t=0\right)$, $p_c\left(x,t=0\right)$ and $T\left(x,t=0\right)$ are also to be specified, where ***x*** is the vector of spatial coordinates. Note that the convective term on the right-hand-side of equation **(93)** corresponds to Newton's law of cooling and describes the conditions occurring in most practical situations at the interface between a porous medium and the surrounding fluid (moist air in this case). The second left-hand-side term gives the energy exchange at the external surface due to vaporization process.

The introduction of mass convective boundary conditions **(90)** and **(91)** requires to express the mass densities ρ_π ($\pi = v, a$) in terms of the retained variables of the problem (p_c, p_g, T). Nevertheless, the relationships relating the densities to the state variables are strongly nonlinear which does not permit to obtain a straightforward algebraic form of these boundary conditions, suitable for the discretized problem.

Indeed, the variables at the boundary $\bar{\Sigma}_p$ should be factorized such that additional terms, associated to these boundary conditions, arise in the operators of the discretized formulation in order to make them well conditioned. In order to overcome this difficulty, it is proposed here to linearize, for a given time stage t, the relationships relating the densities to the state variables at the neighborhood of a reference time stage t_{ref}:

$$\rho_\pi \approx \rho_\pi^{ref} + \frac{\partial \rho_\pi}{\partial p_g}\left(p_g - p_g^{ref}\right) + \frac{\partial \rho_\pi}{\partial p_c}\left(p_c - p_c^{ref}\right) + \frac{\partial \rho_\pi}{\partial T}\left(T - T^{ref}\right) \tag{94}$$

where $(p_c, p_g, T)_{ref}$ are the values of the variables at t_{ref}. The choice of the reference time will depend on the adopted iterative algorithm presented in the following.

II.2 - STAGGERED FINITE ELEMENT MODEL

Starting from the weak form of the previous initial-boundary value problem which writes, respectively, for total water, dry air and energy:

$$\int_\Omega p^* \frac{\partial m_w}{\partial t} d\Omega - \int_\Omega \nabla p^* \cdot J_{w-s} d\Omega = \int_{\bar{\Sigma}_p} p^* \left(\bar{q}_l + \bar{q}_v - h_g \left(\rho_v - \rho_v^\infty \right) \right) d\Sigma - \int_\Omega p^* \dot{m}_{dehyd} d\Omega \tag{95}$$

$$\int_\Omega p^* \frac{\partial m_a}{\partial t} d\Omega - \int_\Omega \nabla p^* \cdot J_{a-s} d\Omega = \int_{\bar{\Sigma}_p} p^* \left(\bar{q}_a - h_g \left(\rho_a - \rho_a^\infty \right) \right) d\Sigma \tag{96}$$

$$\begin{aligned} \int_\Omega T^* \left(\rho C_p \frac{\partial T}{\partial t} + \left(m_l C_l v_{l-s} + m_g C_g v_{g-s} \right) \cdot \nabla T \right) d\Omega - \int_\Omega T^* \cdot H_{vap} \cdot \frac{\partial m_l}{\partial t} d\Omega \\ + \int_\Omega T^* \nabla H_{vap} \cdot m_l v_{l-s} d\Omega + \int_\Omega \nabla T^* \cdot H_{vap} m_l v_{l-s} d\Omega \\ - \int_\Omega \nabla T^* \cdot q d\Omega - \int_\Omega T^* \left(H_{vap} + H_{dehyd} \right) \dot{m}_{dehyd} d\Omega \\ = \int_{\bar{\Sigma}_T} T^* \left(\bar{q}_T - h_T \left(T - T_\infty \right) - \varepsilon \sigma \left(T^4 - T_\infty^4 \right) \right) d\Sigma \end{aligned} \tag{97}$$

where p^* and T^* are weighting functions that respectively vanish at the boundary Σ_p and Σ_T, and in which essential boundary conditions **(91)-(93)** have been used, then the standard Galerking finite element method yields to the following set of nonlinear algebric equations:

$$\tilde{\mathbf{K}}_{cc} \Delta \mathbf{p}_c^{n+1} + \mathbf{K}_{cc} \mathbf{p}_c^n = \mathbf{f}_c^{n+\theta} - \tilde{\mathbf{K}}_{cg} \Delta \mathbf{p}_g^{n+1} - \mathbf{K}_{cg} \mathbf{p}_g^n - \tilde{\mathbf{K}}_{cT} \Delta \mathbf{T}^{n+1} - \mathbf{K}_{cT} \mathbf{T}^n \tag{98}$$

$$\tilde{\mathbf{K}}_{gg} \Delta \mathbf{p}_g^{n+1} + \mathbf{K}_{gg} \mathbf{p}_g^n = \mathbf{f}_g^{n+\theta} - \tilde{\mathbf{K}}_{gc} \Delta \mathbf{p}_c^{n+1} - \mathbf{K}_{gc} \mathbf{p}_c^n - \tilde{\mathbf{K}}_{gT} \Delta \mathbf{T}^{n+1} - \mathbf{K}_{gT} \mathbf{T}^n \tag{99}$$

$$\tilde{\mathbf{K}}_{TT} \Delta \mathbf{T}^{n+1} + \mathbf{K}_{TT} \mathbf{T}^n = \mathbf{f}_T^{n+\theta} - \tilde{\mathbf{K}}_{Tc} \Delta \mathbf{p}_c^{n+1} - \mathbf{K}_{Tc} \mathbf{p}_c^n - \tilde{\mathbf{K}}_{Tg} \Delta \mathbf{p}_g^{n+1} - \mathbf{K}_{Tg} \mathbf{p}_g^n \tag{100}$$

in which the time discretization scheme corresponding to the θ-method has been considered, with:

$$\Delta\mathbf{p}_c^{n+1} = \mathbf{p}_c^{n+1} - \mathbf{p}_c^n \quad ; \quad \Delta\mathbf{p}_g^{n+1} = \mathbf{p}_g^{n+1} - \mathbf{p}_g^n \quad ; \quad \Delta\mathbf{T}^{n+1} = \mathbf{T}^{n+1} - \mathbf{T}^n \tag{101}$$

$$\tilde{\mathbf{K}}_{\bullet\bullet} = \frac{\mathbf{C}_{\bullet\bullet}}{\Delta t} + \theta\mathbf{K}_{\bullet\bullet} \tag{102}$$

where Δt is the time step, the superscript n refers to the time stage t_n and $n+\theta$ the time stage $t_n + \theta\Delta t$. The matrices $\mathbf{C}^{22}$ and $\mathbf{K}^{22}$ are given in the annex to this chapter.

The set of nonlinear equations **(98)-(100)** is solved using a staggered iterative scheme with two nested levels of iterations. The first level (local iteration k) concerns the convergence process for each of the three equations when solved for one variable while the other variables are kept constant. The second level (global iteration j) concerns the convergence of the interaction between the three equations when considering simultaneously the three updated variables. Moreover, a quasi-Newton iterative algorithm is adopted; each equation is solved for the total increment $\Delta\mathrm{x}_{\bullet}^{(n+1)}\left(\text{with } \Delta\mathrm{x}_{\mathrm{c}} = \Delta\mathrm{p}_{\mathrm{c}},\ \Delta\mathrm{x}_{\mathrm{g}} = \Delta\mathrm{p}_{\mathrm{g}},\ \Delta\mathrm{x}_{\mathrm{T}} = \Delta\mathrm{T}\right)$ by keeping fixed the linearization point at the previous converged step (at time stage t_n) and by cumulating the residuals during the iterations. Accordingly, the set of equations **(98)-(100)** can be put in the following generic form:

$$\begin{aligned}&\tilde{\mathbf{K}}_{\alpha\alpha}^{n}\Delta\mathbf{x}_{\alpha}^{n+1,\,j+1,k+1} = \mathbf{f}_{\alpha}^{n+\theta} - \mathbf{K}_{\alpha\alpha}^{n}\mathbf{x}_{\alpha}^{n} - \tilde{\mathbf{K}}_{\alpha\beta}^{n}\Delta\mathbf{x}_{\beta}^{n+1,\,j} - \mathbf{K}_{\alpha\beta}^{n}\mathbf{x}_{\beta}^{n}\\ &-\tilde{\mathbf{K}}_{\alpha\gamma}^{n}\Delta\mathbf{x}_{\gamma}^{n+1,\,j} - \mathbf{K}_{\alpha\gamma}^{n}\mathbf{x}_{\gamma}^{n} + \bar{\mathbf{R}}_{\alpha}^{n+\theta,\,j+1,k}\end{aligned} \tag{103}$$

with $(\alpha = c, g, T), (\beta, \gamma \neq \alpha), (\beta \neq \gamma)$ and where $\bar{\mathbf{R}}_{\alpha}^{n+\theta,\,j+1,k}$ is the sum of the residuals of the k previous iterations. Solving of the above equation gives:

$$\begin{aligned}x_{\alpha}^{n+1,\,j+1,k+1} &= x_{\alpha}^{(n)} + \Delta x_{\alpha}^{n+1,\,j+1,k+1}\\ x_{\alpha}^{n+\theta,\,j+1,k+1} &= x_{\alpha}^{(n)} + \theta\Delta x_{\alpha}^{n+1,\,j+1,k+1}\end{aligned} \tag{104}$$

which allows to determine the updated residual $\mathbf{R}_\alpha^{n+\theta,\,j+1,k+1}$:

$$\mathbf{R}_\alpha^{n+\theta,\,j+1,k+1} = \mathbf{f}_\alpha^{n+\theta} - \mathbf{f}_\alpha^{n+\theta,\,j+1,k+1} \tag{105}$$

$$\begin{aligned}\mathbf{f}_\alpha^{n+\theta,\,j+1,k+1} &= \tilde{\mathbf{K}}_{\alpha\alpha}^{n+\theta,\,j+1,k+1}\Delta\mathbf{x}_\alpha^{n+1,\,j+1,k+1} + \mathbf{K}_{\alpha\alpha}^{n+\theta,\,j+1,k+1}\mathbf{x}_\alpha^n \\ &+\tilde{\mathbf{K}}_{\alpha\beta}^{n+\theta,\,j+1,k+1}\Delta\mathbf{x}_\beta^{n+1,\,j} + \mathbf{K}_{\alpha\beta}^{n+\theta,\,j+1,k+1}\mathbf{x}_\beta^n \\ &+\tilde{\mathbf{K}}_{\alpha\gamma}^{n+\theta,\,j+1,k+1}\Delta\mathbf{x}_\gamma^{n+1,\,j} + \mathbf{K}_{\alpha\gamma}^{n+\theta,\,j+1,k+1}\mathbf{x}_\gamma^n\end{aligned} \tag{106}$$

while equation **(103)** gives:

$$\begin{aligned}\mathbf{f}_\alpha^{n+\theta} &= \tilde{\mathbf{K}}_{\alpha\alpha}^{n}\Delta\mathbf{x}_\alpha^{n+1,\,j+1,k+1} + \mathbf{K}_{\alpha\alpha}^{n}\mathbf{x}_\alpha^n + \tilde{\mathbf{K}}_{\alpha\beta}^{n}\Delta\mathbf{x}_\beta^{n+1,\,j} + \mathbf{K}_{\alpha\beta}^{n}\mathbf{x}_\beta^n \\ &+\tilde{\mathbf{K}}_{\alpha\gamma}^{n}\Delta\mathbf{x}_\gamma^{n+1,\,j} + \mathbf{K}_{\alpha\gamma}^{n}\mathbf{x}_\gamma^n - \bar{\mathbf{R}}_\alpha^{n+\theta,\,j+1,k}\end{aligned} \tag{107}$$

Hence, the cumulated residual at iteration $k + 1$ can be obtained as:

$$\begin{aligned}\bar{R}_\alpha^{n+\theta,\,j+1,k+1} &= R_\alpha^{n+\theta,\,j+1,k+1} + \bar{R}_\alpha^{n+\theta,\,j+1,k} \\ &= \left(\tilde{K}_{\alpha\alpha}^{n} - \tilde{K}_{\alpha\alpha}^{n+\theta,\,j+1,k+1}\right)\Delta x_\alpha^{n+1,\,j+1,k+1} + \left(K_{\alpha\alpha}^{n} - K_{\alpha\alpha}^{n+\theta,\,j+1,k+1}\right)x_\alpha^{(n)} \\ &+\left(\tilde{K}_{\alpha\beta}^{n} - \tilde{K}_{\alpha\beta}^{n+\theta,\,j+1,k+1}\right)\Delta x_\beta^{n+1,\,j+1,k+1} + \left(K_{\alpha\beta}^{n} - K_{\alpha\beta}^{n+\theta,\,j+1,k+1}\right)x_\beta^{(n)} \\ &+\left(\tilde{K}_{\alpha\gamma}^{n} - \tilde{K}_{\alpha\gamma}^{n+\theta,\,j+1,k+1}\right)\Delta x_\gamma^{n+1,\,j+1,k+1} + \left(K_{\alpha\gamma}^{n} - K_{\alpha\gamma}^{n+\theta,\,j+1,k+1}\right)x_\gamma^{(n)}\end{aligned} \tag{108}$$

The final form of the set of equations **(103)**, to be solved at each local iteration $k + 1$, is then given by:

$$\tilde{\mathbf{K}}_{\alpha\alpha}^{n}\Delta\mathbf{x}_\alpha^{n+1,\,j+1,k+1} = \mathbf{Y}_\alpha^{n+\theta,\,j+1,k} \tag{109}$$

with:

$$\begin{aligned}Y_\alpha^{n+\theta,\,j+1,k} = f_\alpha^{n+\theta} &+\left(\tilde{K}_{\alpha\alpha}^{n} - \tilde{K}_{\alpha\alpha}^{n+\theta,\,j+1,k}\right)\Delta x_\alpha^{n+1,\,j+1,k} - K_{\alpha\alpha}^{n+\theta,\,j+1,k}x_\alpha^n \\ &-\tilde{K}_{\alpha\beta}^{n+\theta,\,j+1,k}\Delta x_\beta^{n+1,\,j} - K_{\alpha\beta}^{n+\theta,\,j+1,k}x_\beta^n \\ &-\tilde{K}_{\alpha\gamma}^{n+\theta,\,j+1,k}\Delta x_\gamma^{n+1,\,j} - K_{\alpha\gamma}^{n+\theta,\,j+1,k}x_\gamma^n\end{aligned} \tag{110}$$

CHAPTER III

* * *

PROBABILISTIC ANALYSIS AND PARAMETRIC SIMULATIONS

Porous media, such as concrete and soils, are heterogeneous materials which exhibit strong dispersion of their properties that control the thermo-hygral behavior. Furthermore, the heterogeneity effect is illustrated here by considering a random distribution of the intrinsic permeability within the specimen. Other material parameters can also be randomly generated, but restriction here to permeability is motivated by the fact that it is one major parameter when dealing with transport phenomena (Dal Pont, Schrefler & Ehrlacher, 2005).

III.1 - PROBABILITY DISTRIBUTION FUNCTION

Therefore, a two order of magnitude dispersion interval [K_{min} , K_{max}] is considered which is the commonly observed range of variation of experimentally measured values of permeability for similar material mixes. Furthermore, the probability distribution function (PDF) $\varphi(K)$ of the random intrinsic permeability K is considered to follow either a log-uniform or a log-normal law, given respectively by:

$$\varphi^{LU}(K) = \frac{1}{(\ln(K_{\max}) - \ln(K_{\min}))K} \tag{111}$$

$$\varphi^{LN}(K) = \frac{1}{\sqrt{2\pi}\sigma_n K} \exp\left(-\frac{(\ln(K) - \ln(\overline{K}_G))^2}{2\sigma_n^2} \right) \tag{112}$$

Where $\overline{K}_G = \sqrt{K_{\min} K_{\max}}$ is the geometric mean and σ_n is the standard deviation of the under-laying normal distribution of the permeability logarithm ln (K). The superscripts $\bullet^{LU}$ and $\bullet^{LN}$ refer, respectively, to log-uniform and log-normal cases. Accordingly, the probability $P\left(K \le K_p\right)$ at which all drawn values of K will be found less or equal to a fixed value K_p is then obtained by the standard cumulative distribution function (CDF) Φ, given by:

$$P\left(K \le K_p\right) = \Phi\left(K_p\right) = \int_0^{K_p} \varphi(K) dK \tag{113}$$

Moreover, the mean value (expectation) $\overline{K}_M$ and the standard deviation σ can be determined by the following relationships:

$$\overline{K}_M^{LU} = \frac{K_{\max} - K_{\min}}{\ln(K_{\max}) - \ln(K_{\min})} \tag{114}$$

$$\overline{K}_M^{LN} = \overline{K}_G \exp\left(\frac{\sigma_n^2}{2}\right) \tag{115}$$

$$\sigma = \overline{K}_M^{LN} \sqrt{\exp(\sigma_n^2) - 1} \tag{116}$$

Both log-distributions are centered at $\overline{K}_G$ in the log-scale. The standard deviation for the log-normal distribution is chosen such that 99,7% of drawn values (lying within three standard deviations ($3\sigma_n$) away from $\overline{K}_G$, in the log-scale) fall within the considered dispersion interval. Thus, the standard deviation is given by:

$$\sigma_n = \frac{\ln(K_{\max}) - \ln(K_{\min})}{6} \tag{117}$$

Figure 38 gives (in the decimal log-scale) the probability distribution profiles in the case of $K_{\min} = 10^{-19}$, $K_{\max} = 10^{-17}$ *and* $\overline{K}_G = 10^{-18} m^2$**,** corresponding to a cementitious material with a relatively low water-to-cement ratio (Bamforth, 1987; Lydon, 1995; Halamickova, 1995). The other numerical values are then:

$$\overline{K}_M^{LN} = 1,34 \cdot 10^{-18} \text{ and } \sigma = 1,20 \cdot 10^{-18} m^2 .$$

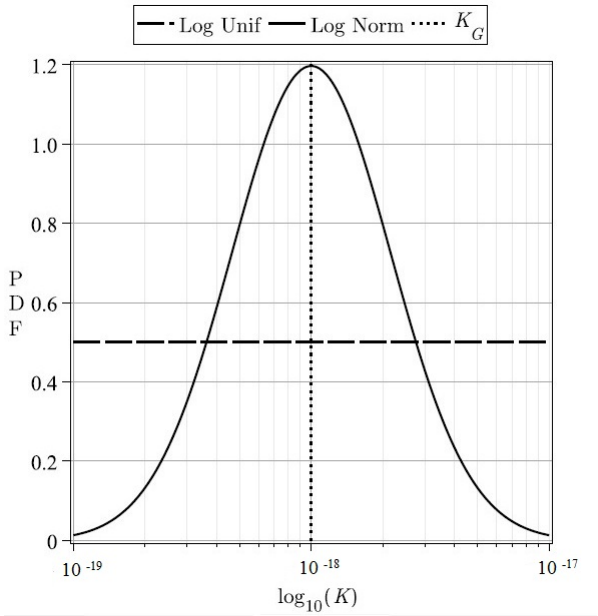

Figure 38 - Probability distribution function and cumulative distribution function

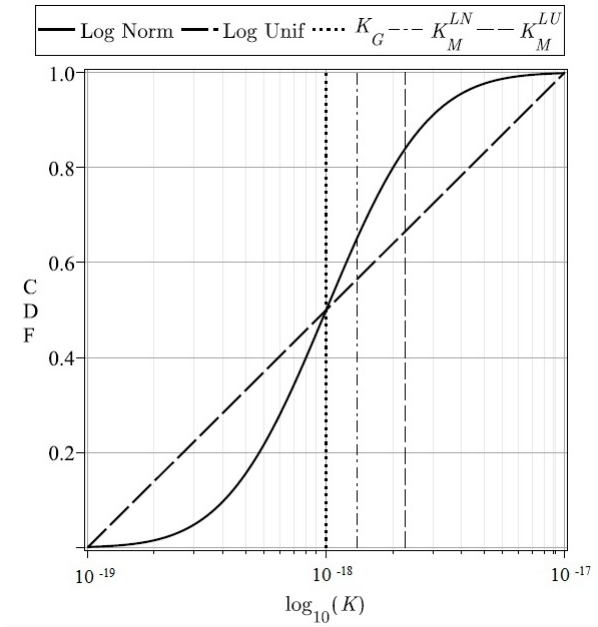

Figure 39 - Probability distribution function for log-uniform and log-normal case

Figure 39 presents CDFs obtained with above-mentioned numerical values. For both log-uniform and log-normal distributions, the mean value $\overline{K}_M$ of intrinsic permeability is greater than the geometric mean $\overline{K}_G$. This latter is the median value with regard which random values are equally distributed: $P\left(K \leq \overline{K}_G\right) = P\left(K \geq \overline{K}_G\right) = 0,5$

Hence, log-type distributions which are suitable for describing non negative random physical parameters (and generally considered for this purpose), inherently lead to a skewness: the mean value $\overline{K}_M$ shifts toward $K_{\max}$ with regard to the median value $\overline{K}_G$, i.e, a right-skewness. This makes determinant the choice of the probability distribution function for intrinsic permeability (or any other random material parameter). Indeed, the overall thermo-hygral behavior may be significantly affected by the deviation of the mean with respect to the median.

III.1.1 - Probability distribution functions (PDFs) for different sizes of SEV and different correlation lengths

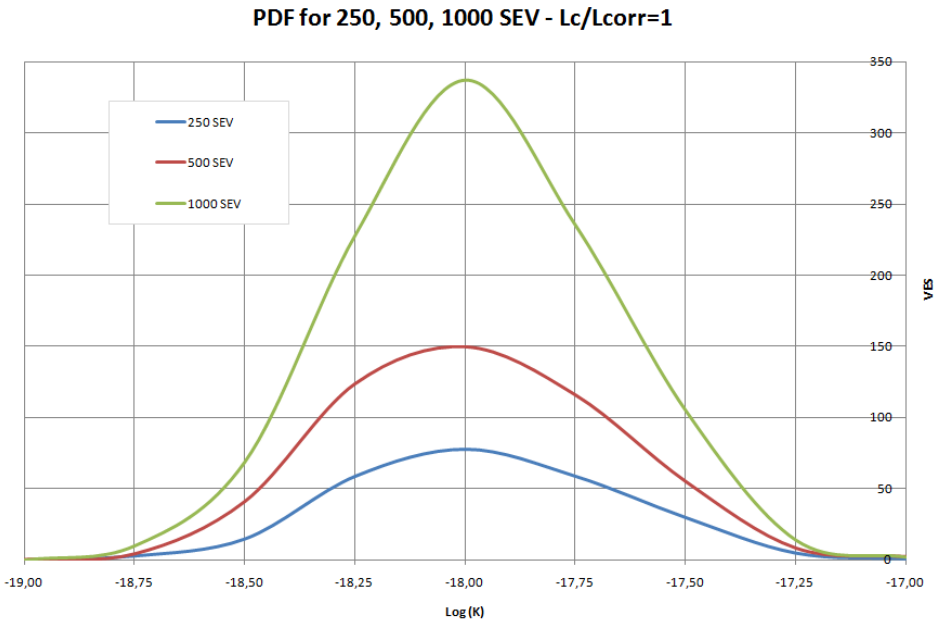

Figure 40 - Log-normal PDF of the random intrinsic permeability K [m^2] for 250, 500, 1000 SEV in the case Lc/Lcorr = 1

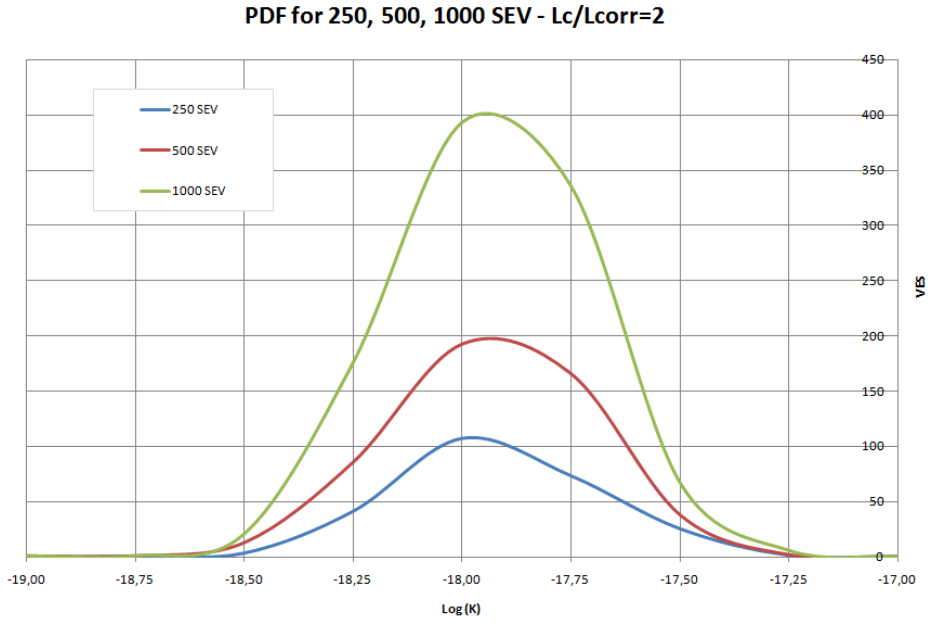

Figure 41 - Log-normal PDF of the random intrinsic permeability K [m^2] for 250, 500, 1000 SEV in the case Lc/Lcorr = 2

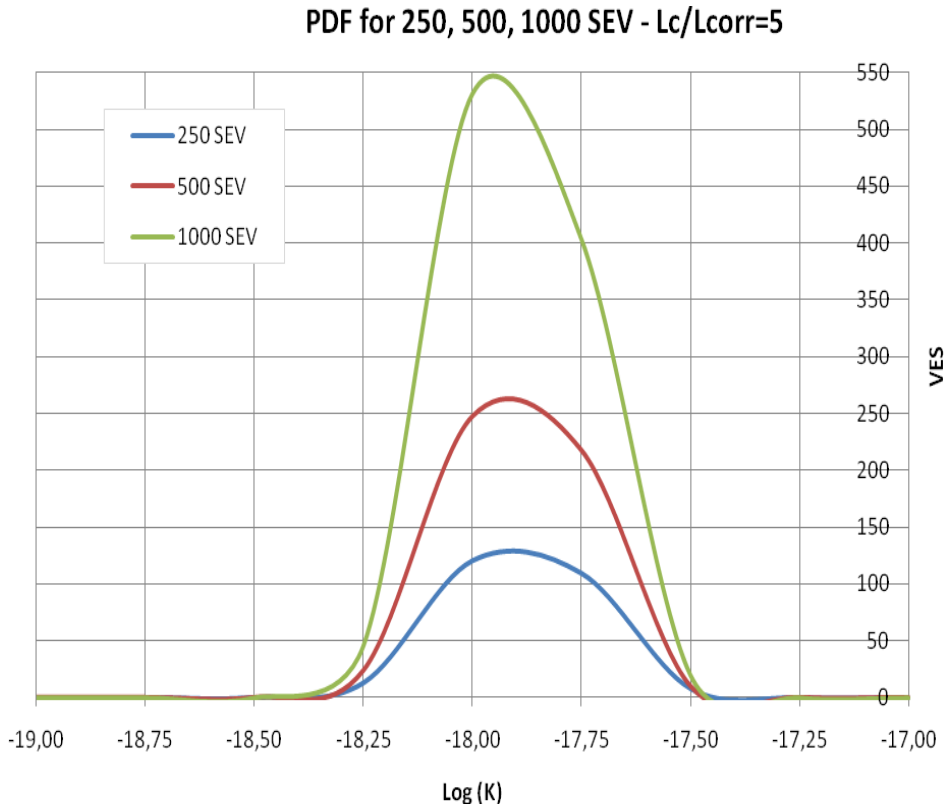

Figure 42 - Log-normal PDF of the random intrinsic permeability K [m^2] for 250, 500, 1000 SEV in the case Lc/Lcorr = 5

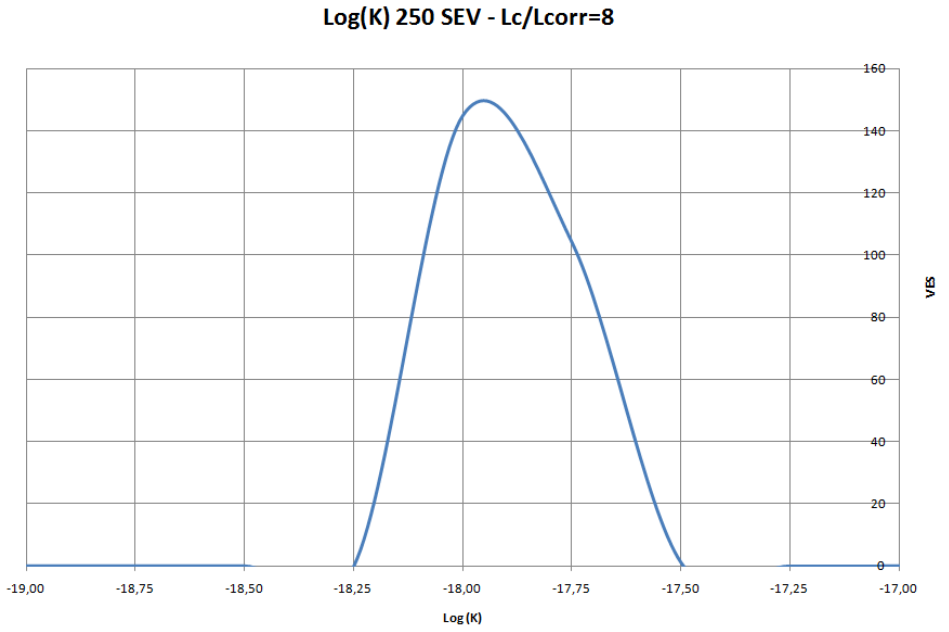

Figure 43 - Log-normal PDF of the random intrinsic permeability K [m^2] for 250 SEV in the case Lc/Lcorr = 8

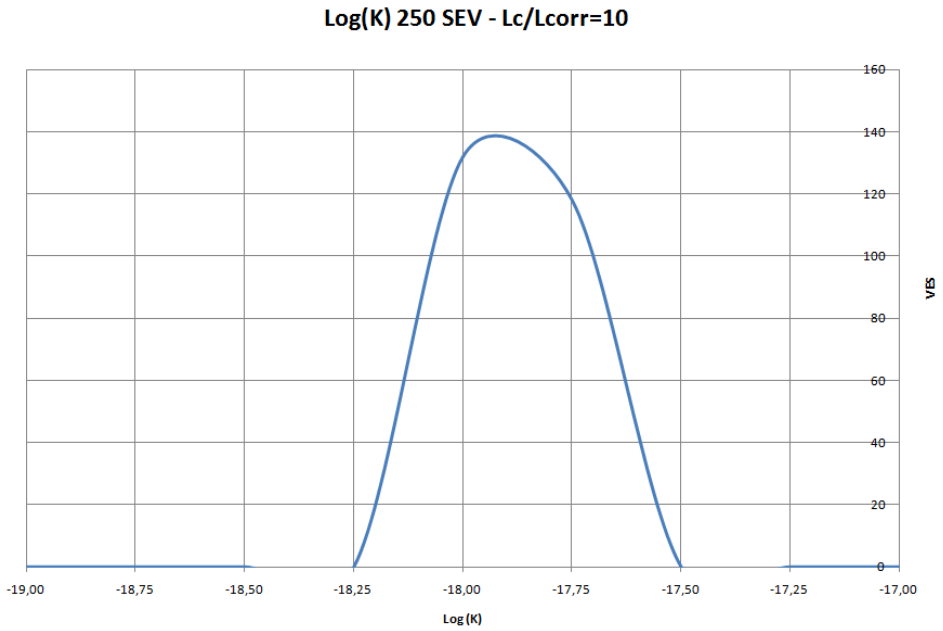

Figure 44 - Log-normal PDF of the random intrinsic permeability K [m^2] for 250 SEV in the case Lc/Lcorr = 10

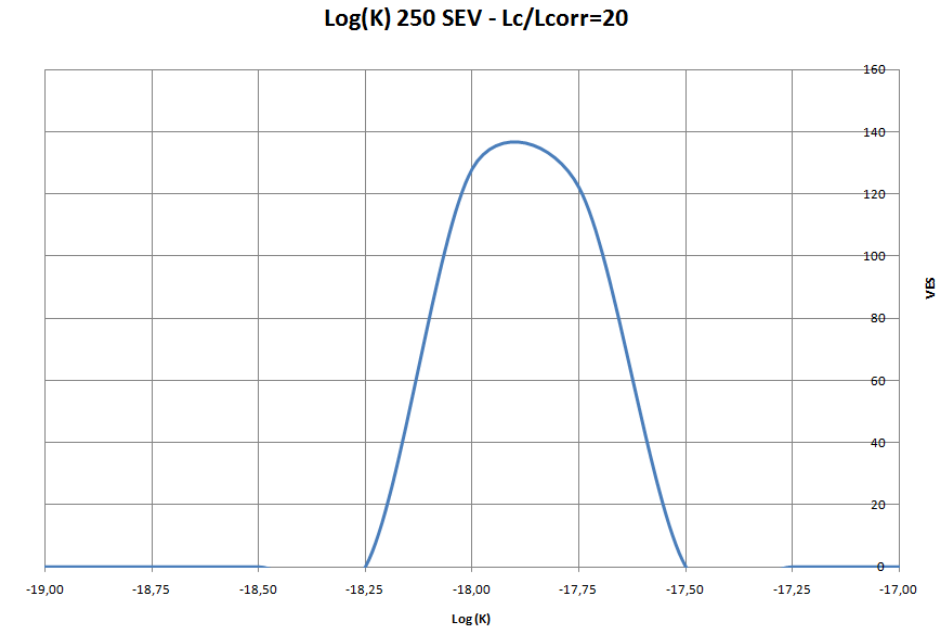

Figure 45 - Log-normal PDF of the random intrinsic permeability K [m^2] for 250 SEV in the case Lc/Lcorr = 20

III.2 - CORRELATION LENGTH

Recent studies were carried out for spatially non-correlated fields; this means the random value at any material point x does not depend on values drawn at its neighborhood, this latter being defined by the correlation length (equal zero in the field is not-correlated). Hence, if the intrinsic permeability is, for instance, assumed to be a log-normally distributed value, represented by the parameters $\overline{K}_G$ and σ_n**,** then the random field is given by:

$$K(\boldsymbol{x}) = \exp\ (\ln(\overline{K}_G) + \sigma_n \Psi(\boldsymbol{x})) \tag{118}$$

where Ψ(x) is a non-correlated normally distributed random field, with zero mean and unit variance, that can be obtained using the spectral representation method **[50].** In this case the spatial average value $\langle K(\boldsymbol{x})\rangle$ of the random intrinsic permeability field must coincide with the statistical mean $\overline{K}_M$ **:**

$$\langle K(\boldsymbol{x})\rangle = \frac{1}{|\Omega|}\int_{\Omega} K(\boldsymbol{x})\, d\Omega \approx \overline{K}_M \tag{119}$$

with an error not exceeding 5%. In the above equation $|\Omega|$ stands for the volume of the discretized domain Ω.

In our study we analyzed the evolution of permeability with regard to correlation length and to the size of the specimen.

$$L_{corr} = L_{spec} \ / \ n \tag{121}$$

and $L_{spec} = \sqrt{|\Sigma|} = L \ in\ 2D \quad and \quad L_{\text{spec}} = \sqrt[3]{|\Omega|} = \sqrt[3]{V} \ in\ 3D$.

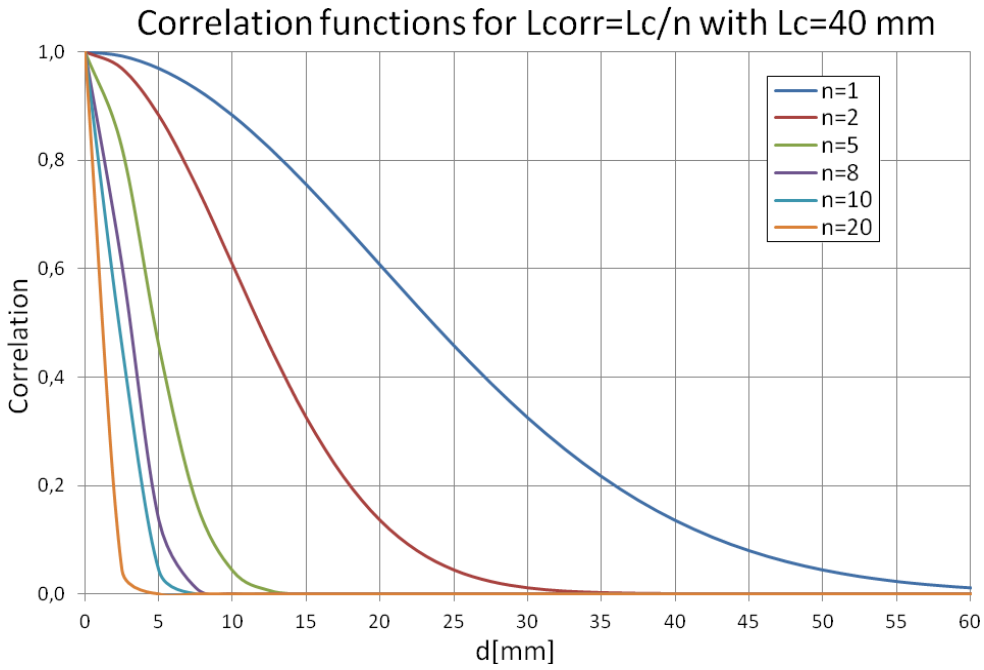

Figure 46 - Correlation functions

If $n \to \infty$, $L_{corr} \to 0$ and we are in the case of non correlated fields. In this case we can speak about *white noise (bruit blanc)* and it indicates random values with no correlation. If there is correlation we can consider a spacial correlation function. It is the correlation between random variables at two different points in space, usually as a function of the spatial distance between the points. If one considers the correlation function between random variables representing the same quantity measured at two different points then this is often referred to as an autocorrelation function being made up of autocorrelations. Correlation functions of different random variables are sometimes called cross correlation functions to emphasize that different variables are being considered and because they are made up of cross correlations.

Spatial correlation functions are a useful indicator of dependencies as a function of distance in space, and they can be used to assess the distance required between sample points for the values to be effectively uncorrelated. In addition, they can form the basis of rules for interpolating values at points for which there are observations.

Different expression indicates the influence of the random value at one point on its neighborhood decreases with the distance with the expressions (Su et al. (2010); Srivastava et al. (2010)):

$$K\left(\left|\vec{x}_1 - \vec{x}_2\right|\right) = \exp\left(-\frac{\pi\left|\vec{x}_1 - \vec{x}_2\right|^2}{L_{corr}^2}\right) \tag{122}$$

$$K\left(\left|\vec{x}_1 - \vec{x}_2\right|\right) = \exp\left(-\frac{2\left|\vec{x}_1 - \vec{x}_2\right|^2}{L_{corr}^2}\right) \tag{123}$$

Which are exponentially decaying functions of separation distance.

III.2.1 - 2D mesh

In our study we considered 2D specimens with $S = l_x \cdot l_y = 4\ x\ 4\ cm^2$, using a non-uniform mesh (refined at the exposed faces) of 100 x 100 QUAD4 elements, that change their size linearly from the boundary of the specimen to the center from $(0{,}0005)^2$ cm^2 to $(0{,}001)^2$ cm^2. Computations are performed for a drying test duration of 5 hours. We carried out some results for the different correlation lengths:

$$L_{corr} = L_{spec} / n$$
$$with\ n = 1, 2, 5, 8, 10, 20 \tag{121}$$

Input data of M30 concrete mix	
Initial water content [% of mass]	3.9
Initial saturation S_l [%]	63
Initial porosity ϕ_0 [%]	10.1
Initial ambient temperature T_0 [^oC]	20
Surrounding gas pressure p_g [Pa]	p_{atm}

Please note in the following figures that the visible mesh is not the real one, that is refined on the boundary as mentioned above.

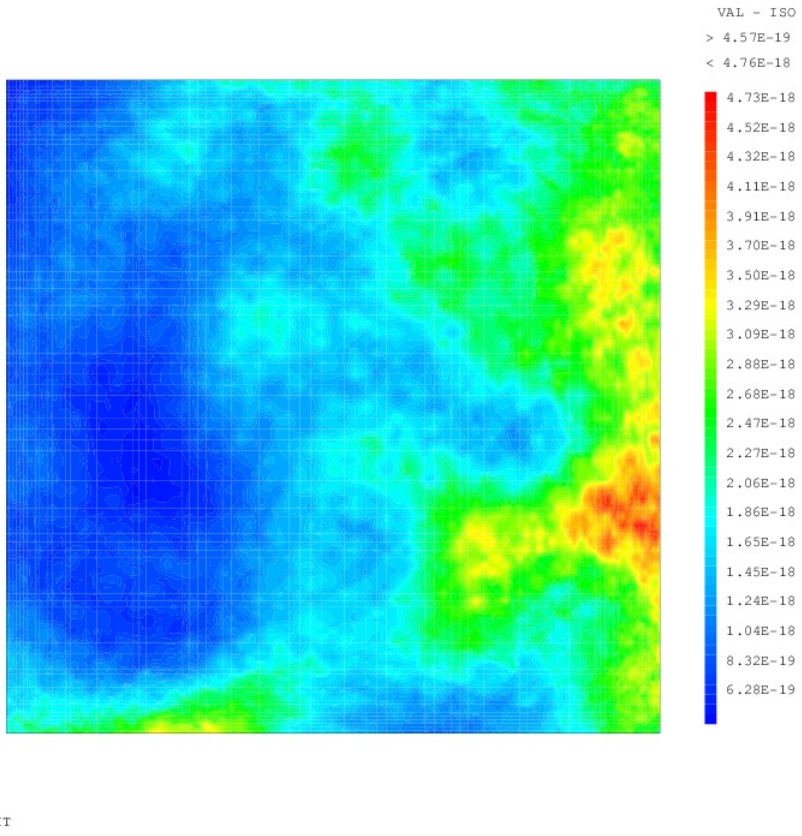

Figure 47 - 2D mesh showing intrinsic permeability evolution for Lc/Lcorr = 1

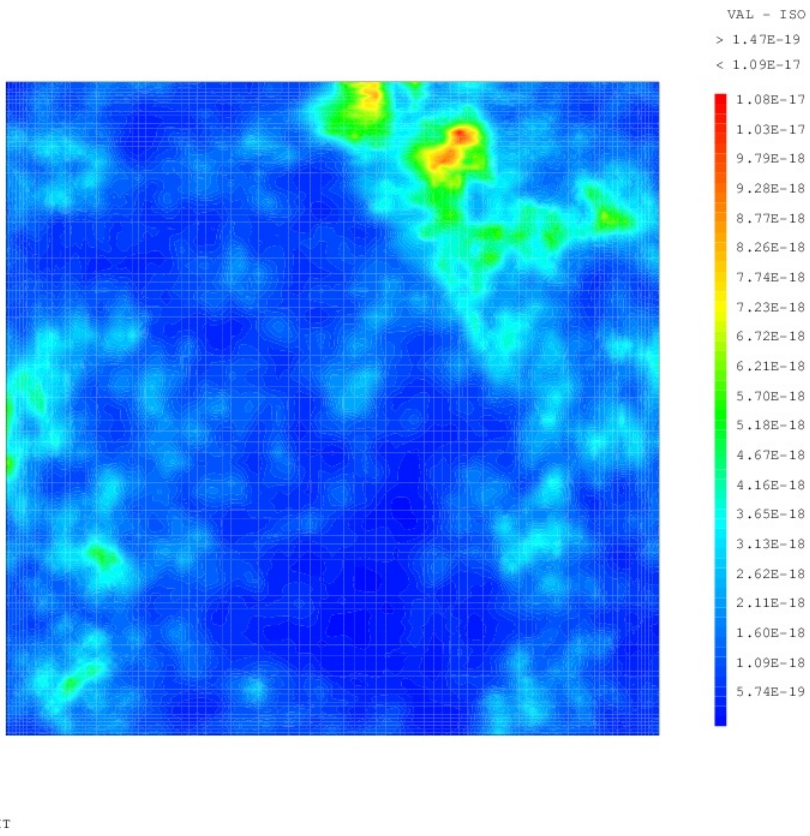

Figure 48 - 2D mesh showing intrinsic permeability evolution for Lc/Lcorr = 5

III.2.2 - Convergence of the SEV towards the REV for different correlation lengths

In this part of the work we will show the results of the statistical analysis for a certain number of realized specimens with regard to different correlation lengths.
We firstly realized 250, 500 and 1000 specimens for each correlation length.

$$\text{Target mean : } \overline{K}_M = 1,34 \cdot 10^{-18} \; and \; \sigma = 1,20 \cdot 10^{-18} m^2$$

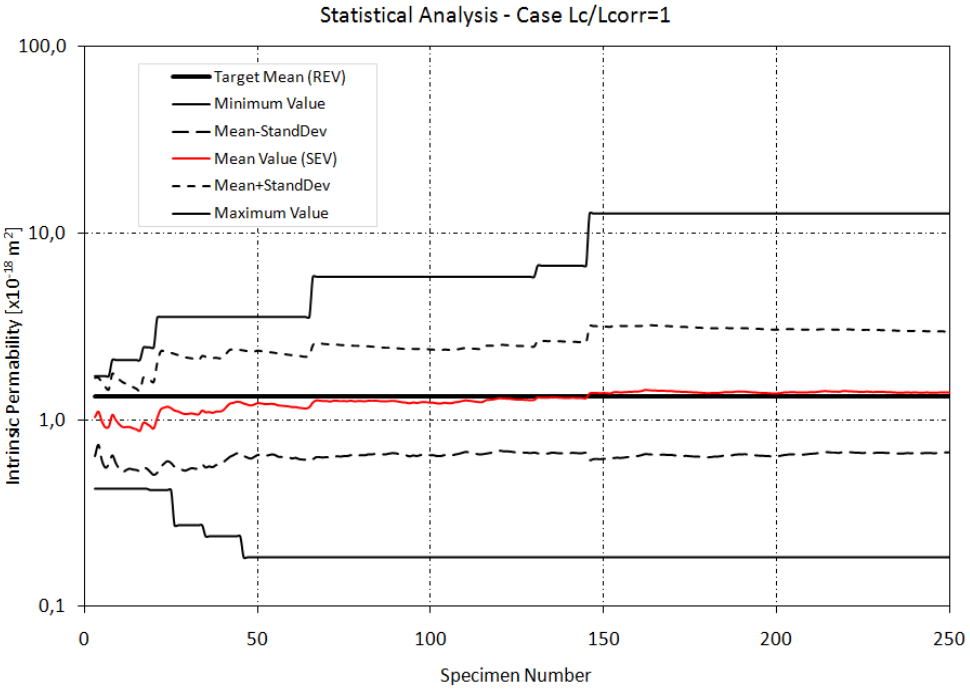

Figure 49 - Statistical analysis on intrinsic permeability for 250 SEV in the case Lc/Lcorr = 1

From the figure we can note that in the first case we analyzed (Lc/Lcorr = 1), the value of the mean value for the SEV cross the target mean (statistically invariant) of the REV for a number of specimens next to 150. That's why we reduced the analysis we began also for 500 SEV and 1000 SEV to 250 SEV.

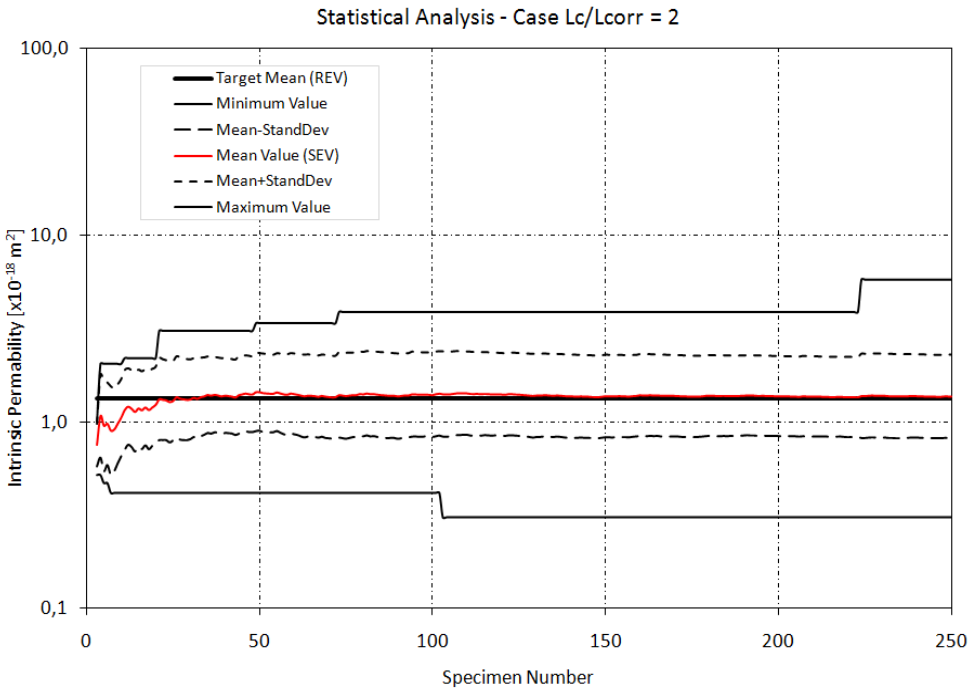

Figure 50 - Statistical analysis on intrinsic permeability for 250 SEV in the case Lc/Lcorr = 2

In this case, where the correlation is weaker than the previous case the mean value of the SEV cross the target mean at about 30 specimens and the two values are really closed each other for the following realizations.

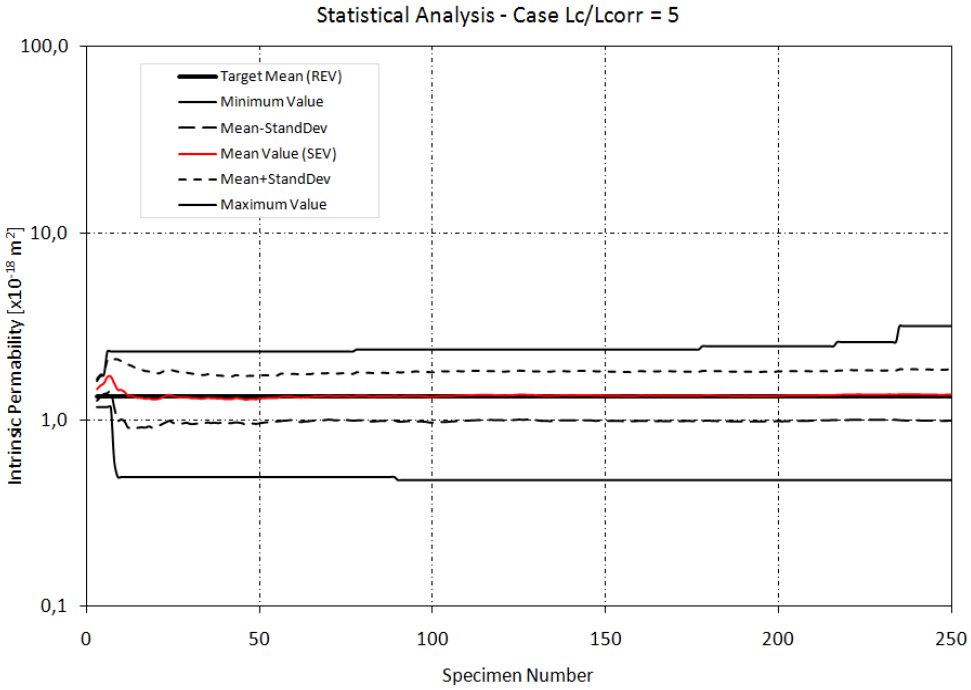

Figure 51 - Statistical analysis on intrinsic permeability for 250 SEV in the case Lc/Lcorr = 5

For this third case the convergence of the SEV towards the REV is obtained before 20 realizations.

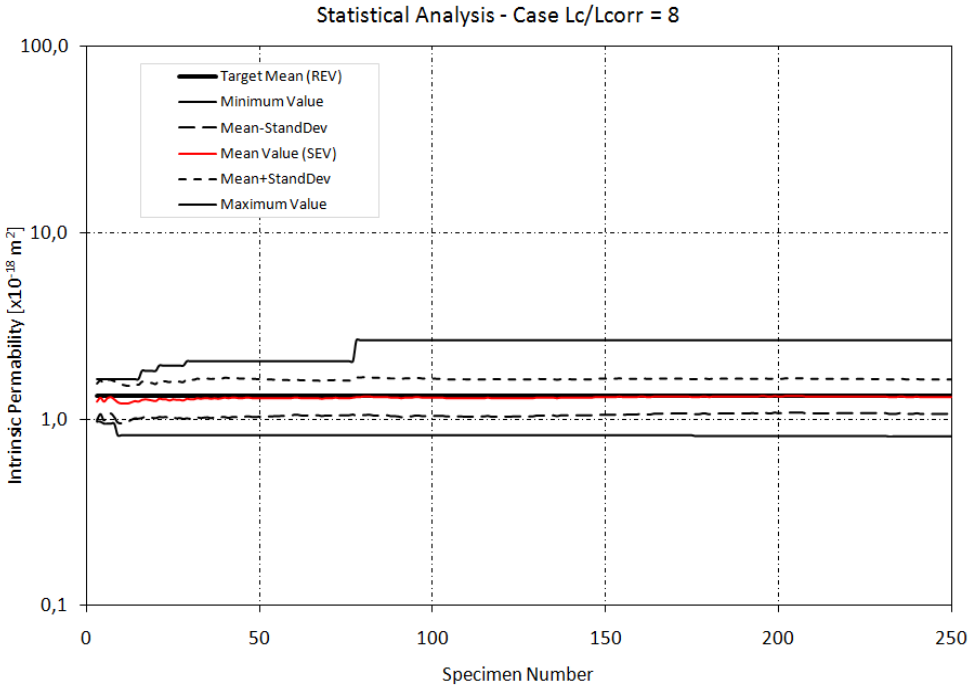

Figure 52 - Statistical analysis on intrinsic permeability for 250 SEV in the case Lc/Lcorr = 8

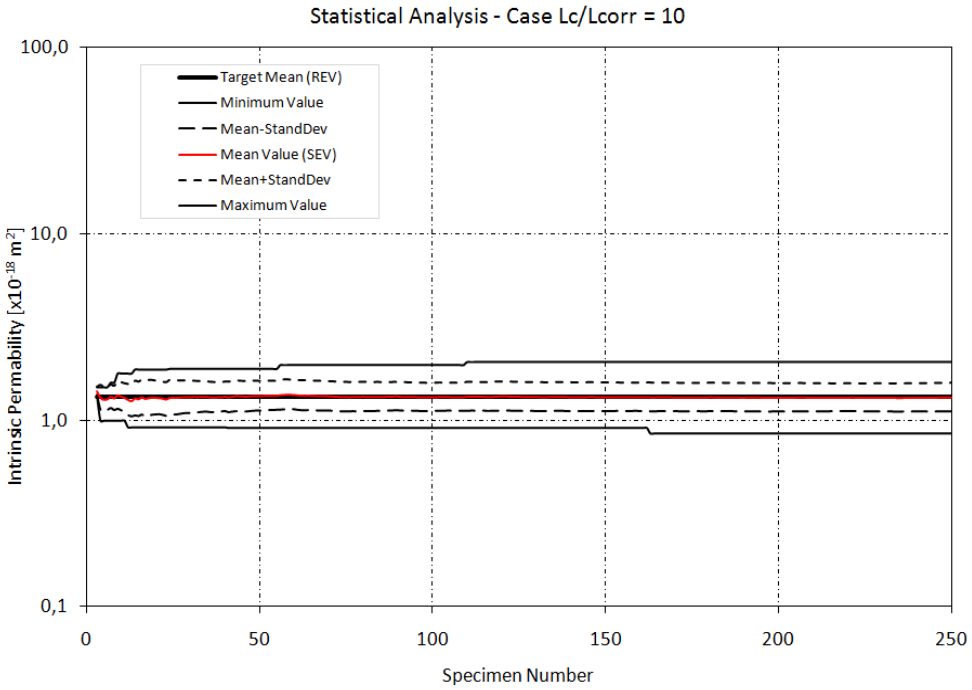

Figure 53 - Statistical analysis on intrinsic permeability for 250 SEV in the case Lc/Lcorr = 10

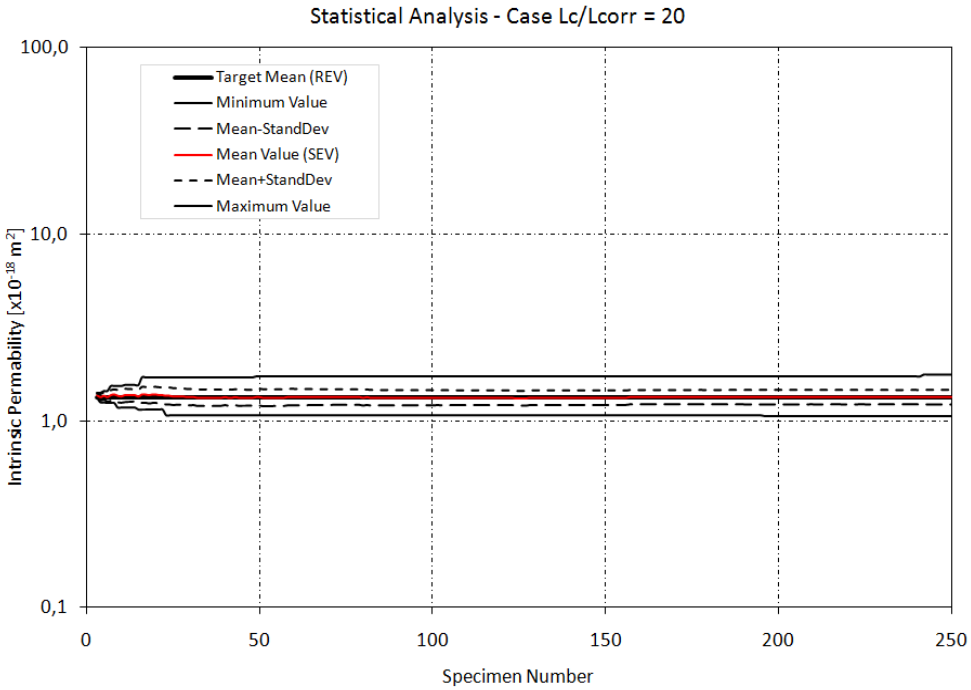

Figure 54 - Statistical analysis on intrinsic permeability for 250 SEV in the case Lc/Lcorr = 20

For the last three analyzed cases the convergence of the SEV towards the REV is nearly from the beginning, and they tend to the solution of not-correlated random fields.

III.3 - WEIGHT LOSS CURVES

We carried out the T-H model for all the analyzed cases of spatial correlation lengths until 5 h and at a temperature of 80°C. In the following part there are the output of the program for the % weight loss for all the cases.

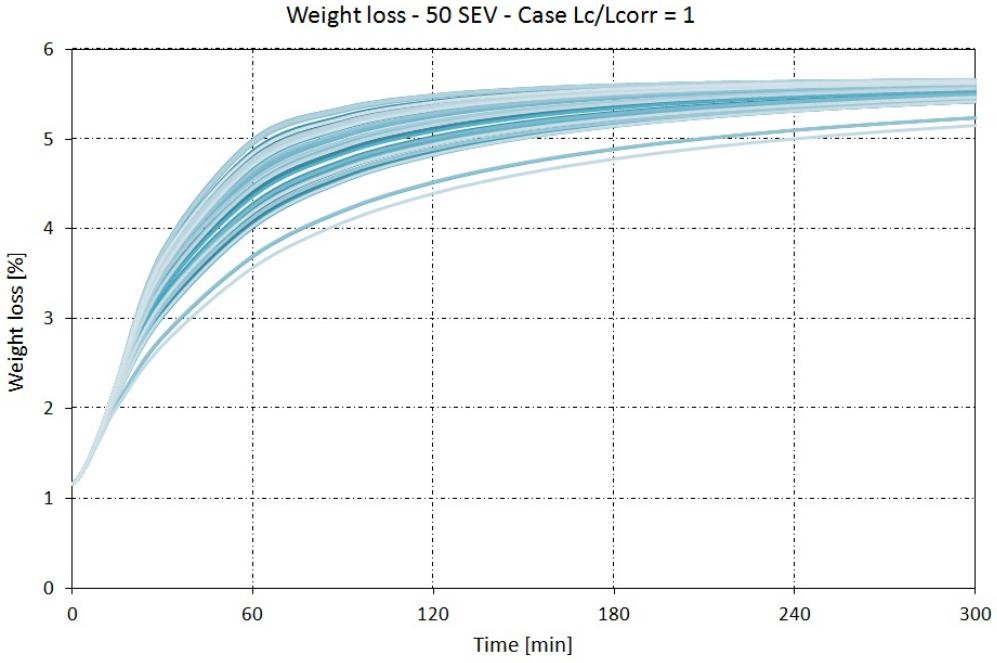

Figure 55 - Weight loss curves for 50 SEV up to 5 h in the case Lc/Lcorr = 1

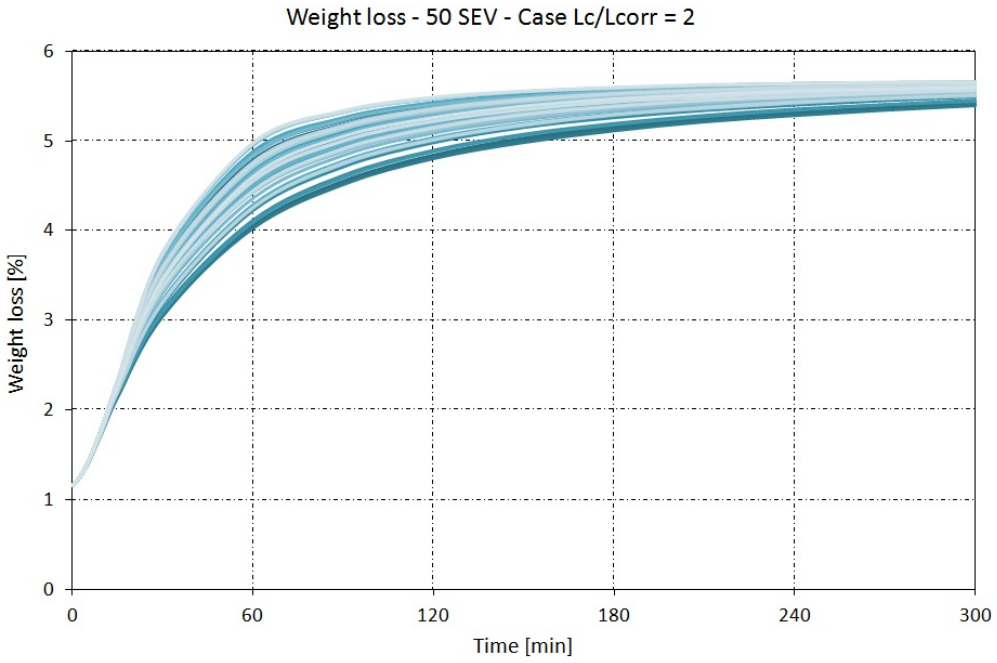

Figure 56 - Weight loss curves for 50 SEV up to 5 h in the case Lc/Lcorr = 2

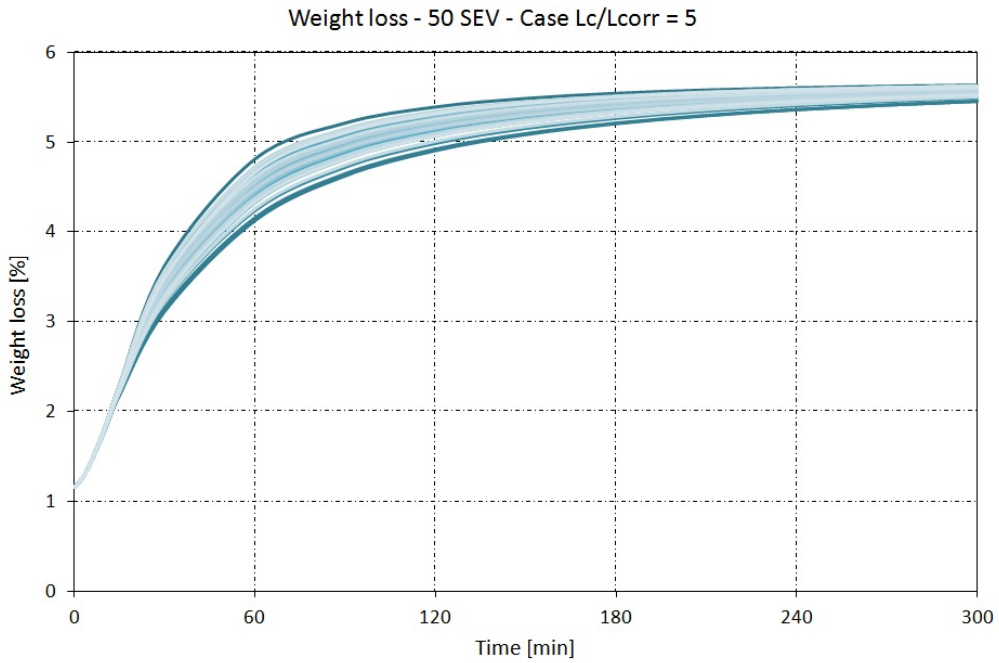

Figure 57 - Weight loss curves for 50 SEV up to 5 h in the case Lc/Lcorr = 5

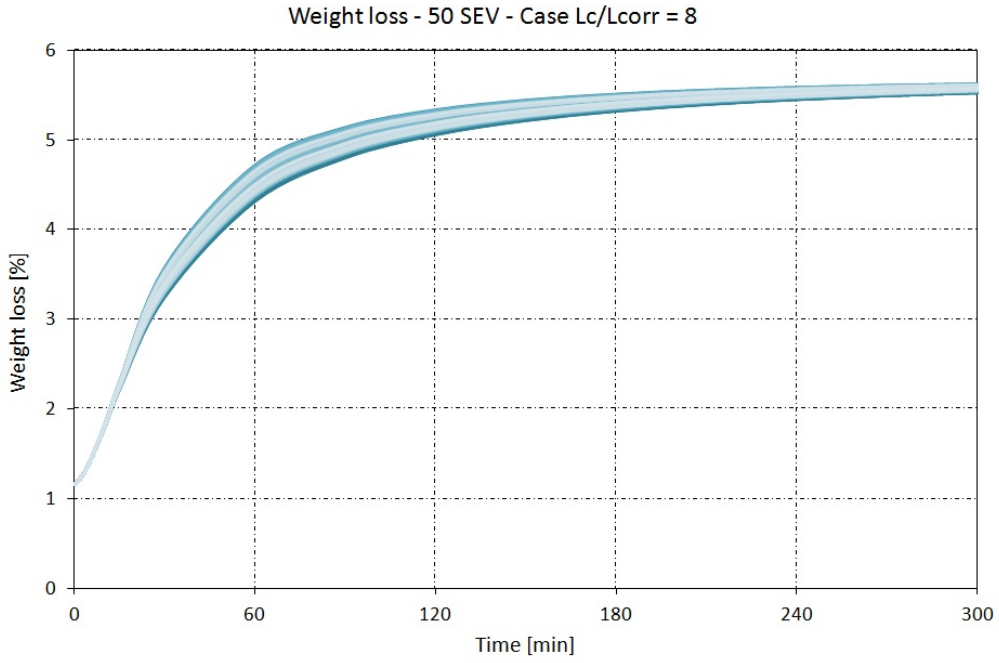

Figure 58 - Weight loss curves for 50 SEV up to 5 h in the case Lc/Lcorr = 8

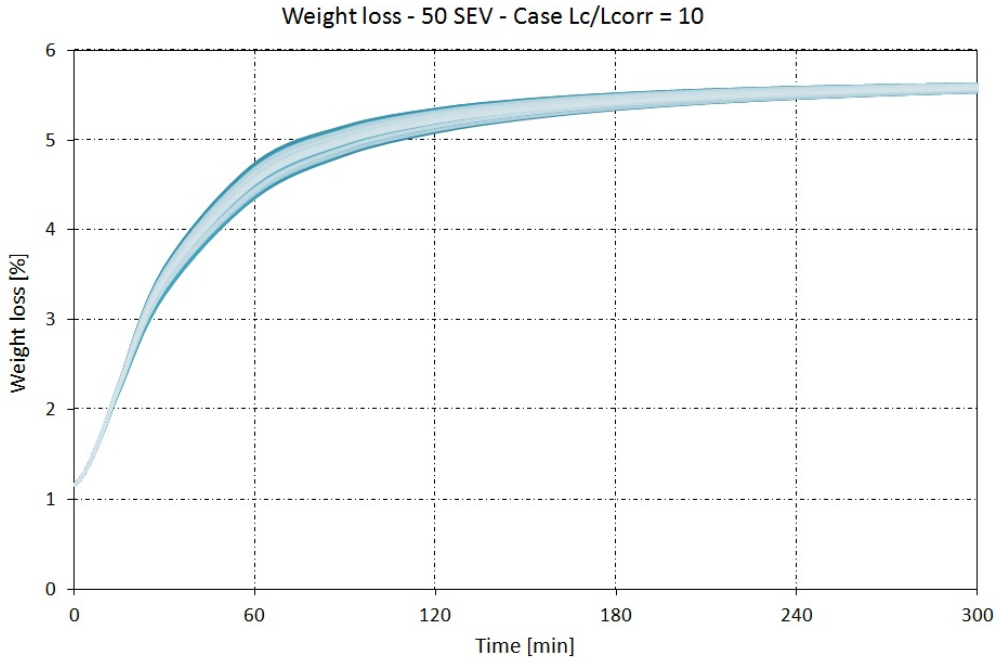

Figure 59 - Weight loss curves for 50 SEV up to 5 h in the case Lc/Lcorr = 10

III.3.1 - Dispersion Analysis for the case Lc/Lcorr = 1

In this part we will show the results of the dispersion analysis for the first case, at different time steps; it is visible how the random values are distributed from the first one up to the 50th one.

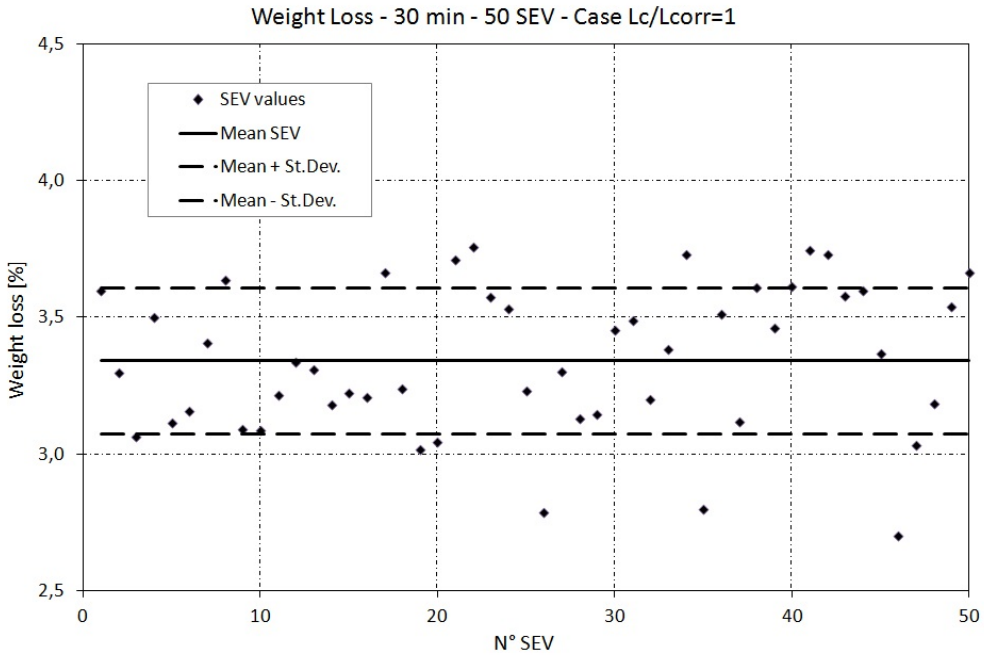

Figure 60 - Weight loss at 30 min in the case Lc/Lcorr = 1

Mean value: 3,340 Standard deviation: 0,268

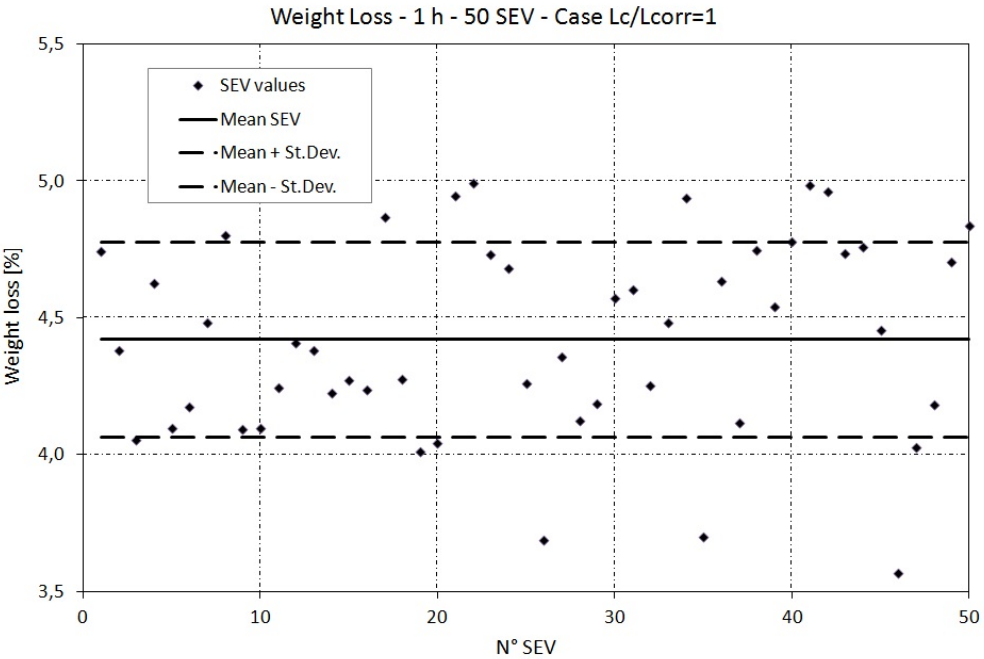

Figure 61 - Weight loss at 1 h in the case Lc/Lcorr = 1

Mean value: 4,421 Standard deviation: 0,357

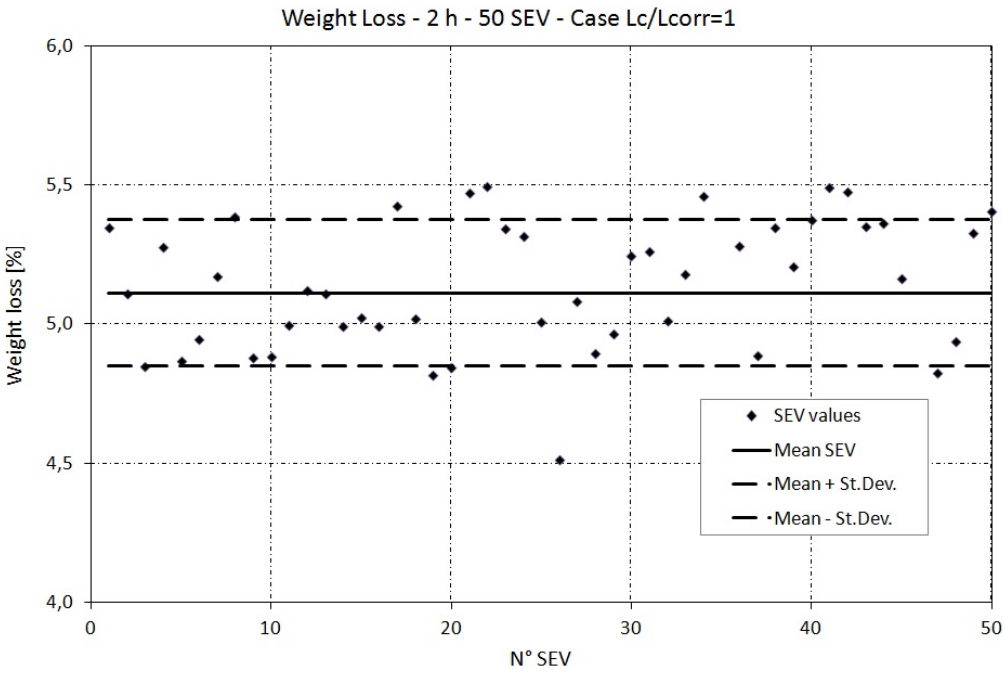

Figure 62 - Weight loss at 2 h in the case Lc/Lcorr = 1

Mean value: 5,112 Standard deviation: 0,265

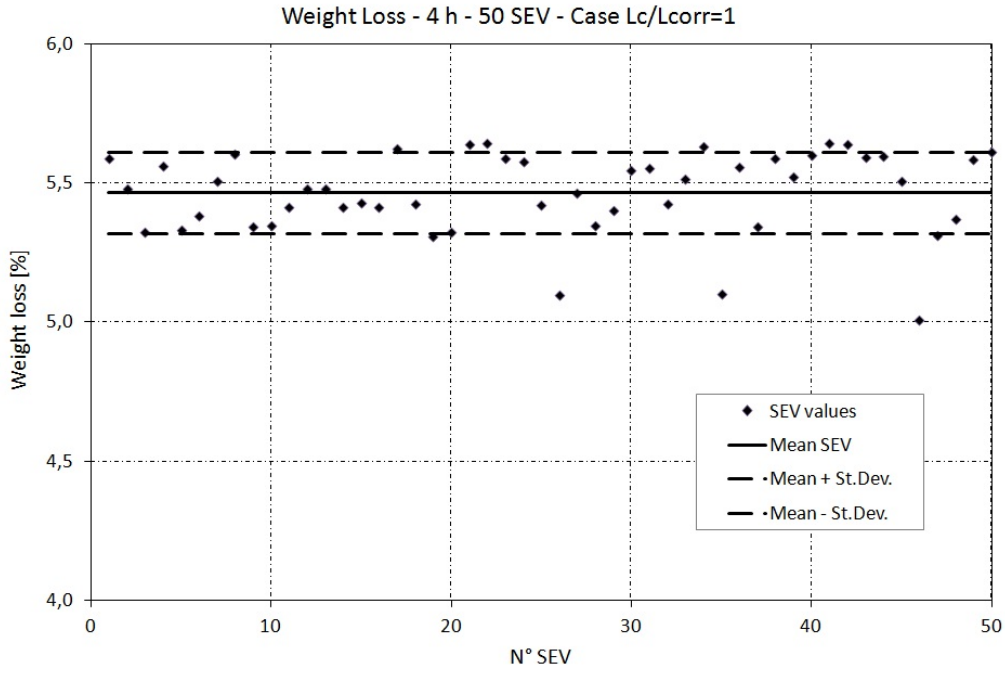

Figure 63 - Weight loss at 4 h in the case Lc/Lcorr = 1

Mean value: 5,464 Standard deviation: 0,147

III.3.2 - Dispersion Analysis for the case Lc/Lcorr = 2

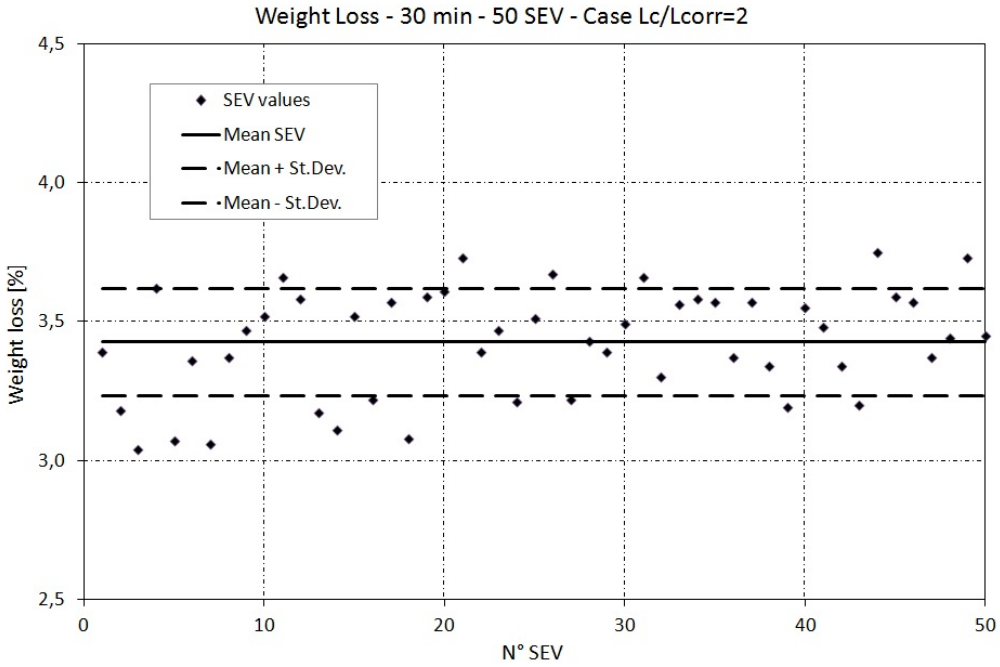

Figure 64 - Weight loss at 30 min in the case Lc/Lcorr = 2

Mean value: 3,426 Standard deviation: 0,193

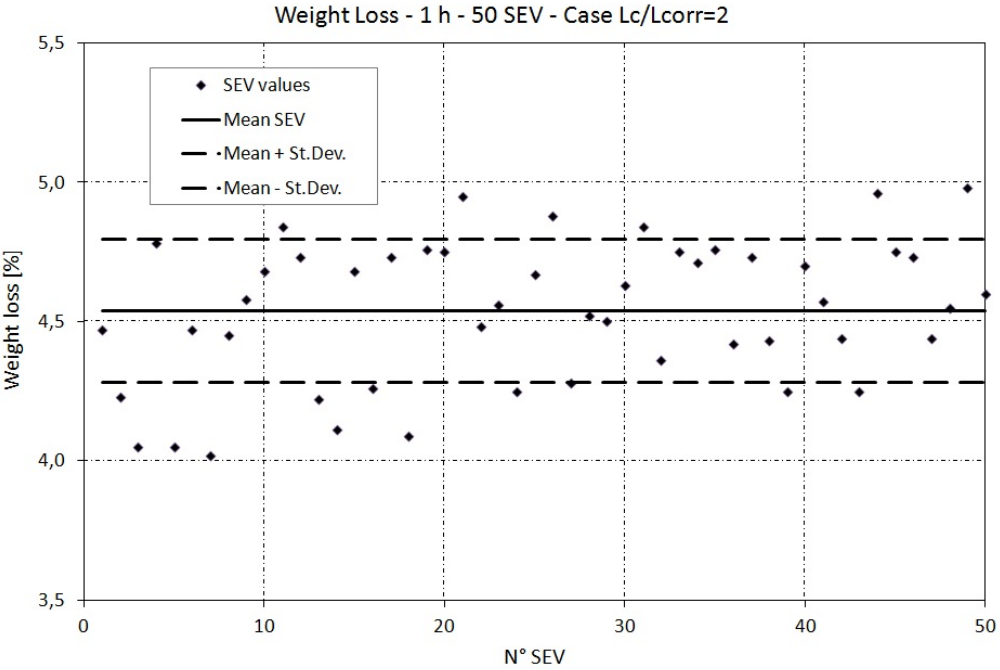

Figure 65 - Weight loss at 1 h in the case Lc/Lcorr = 2

Mean value: 4,538 Standard deviation: 0,257

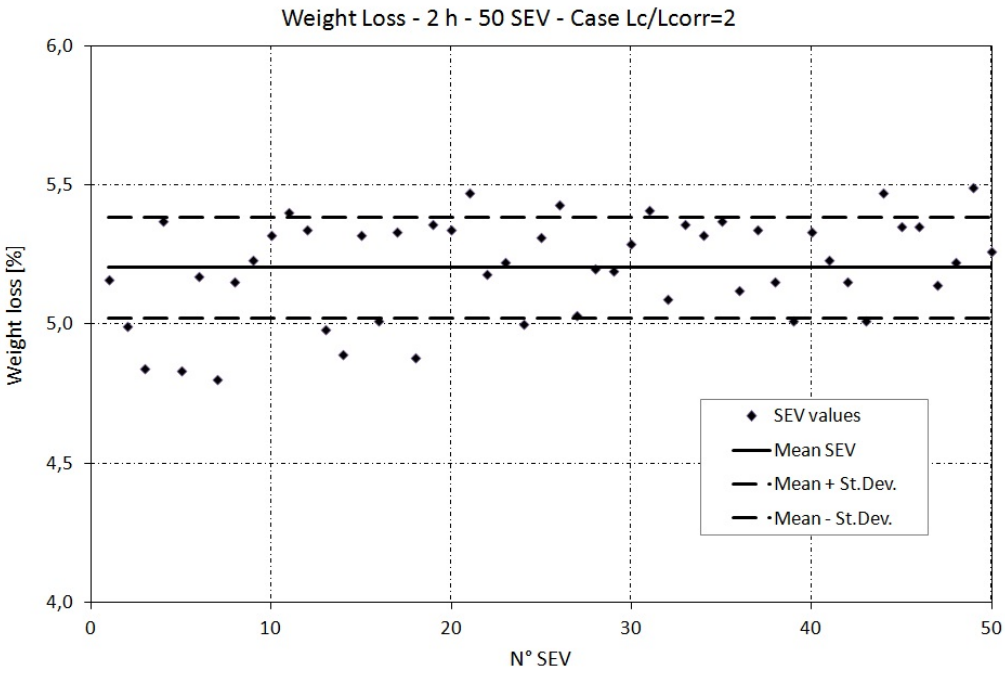

Figure 66 - Weight loss at 2 h in the case Lc/Lcorr = 2

Mean value: 5,204 Standard deviation: 0,181

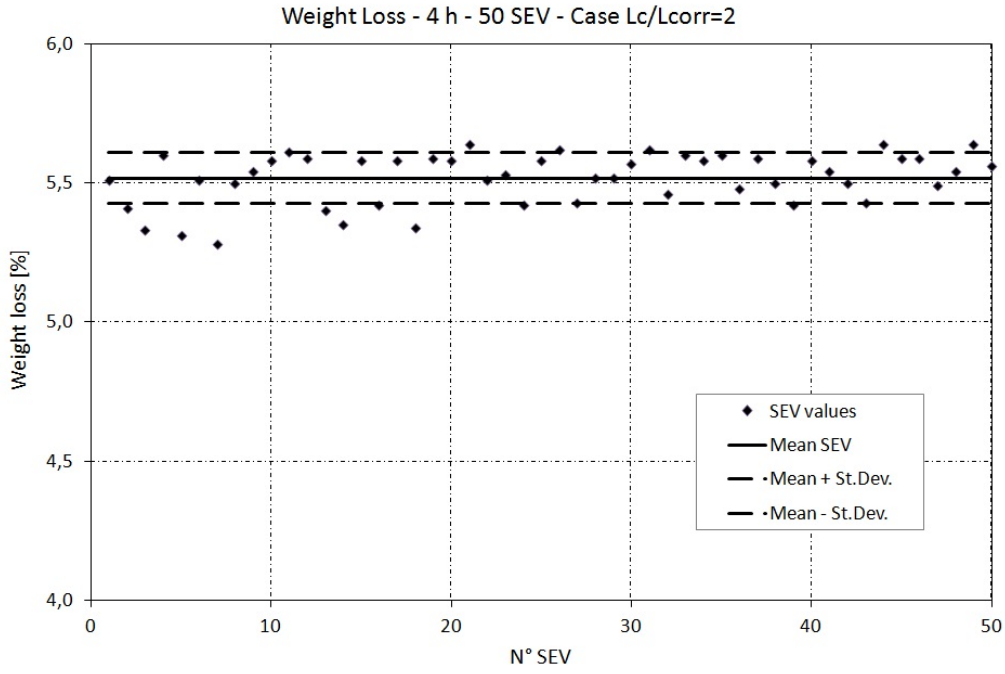

Figure 67 - Weight loss at 4 h in the case Lc/Lcorr = 2

Mean value: 5,518 Standard deviation: 0,093

III.3.3 - Dispersion Analysis for the case Lc/Lcorr = 5

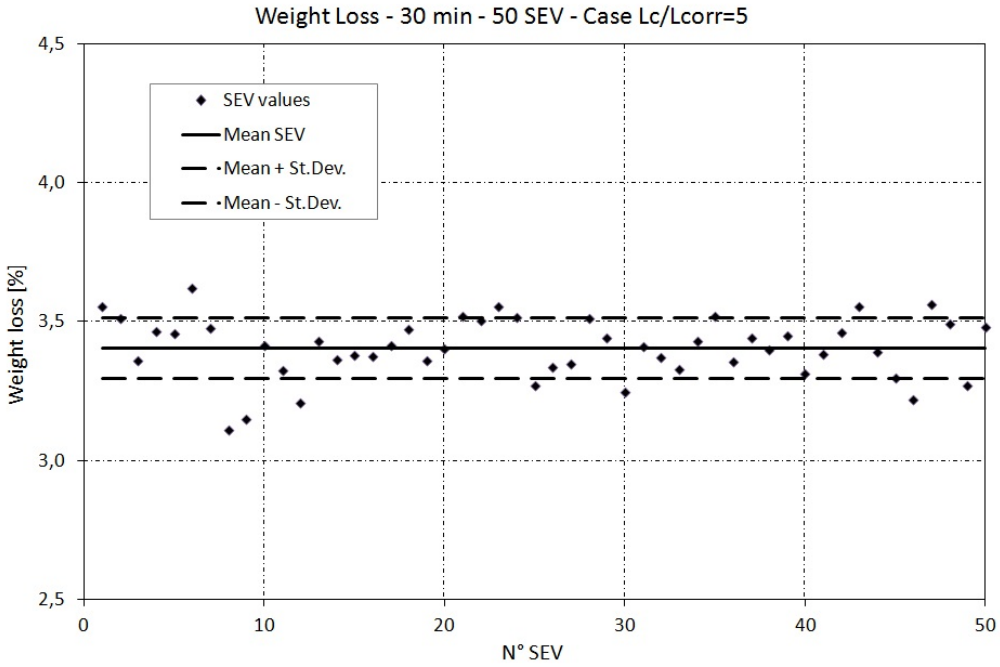

Figure 68 - Weight loss at 30 min in the case Lc/Lcorr = 5

Mean value: 3,404 Standard deviation: 0,110

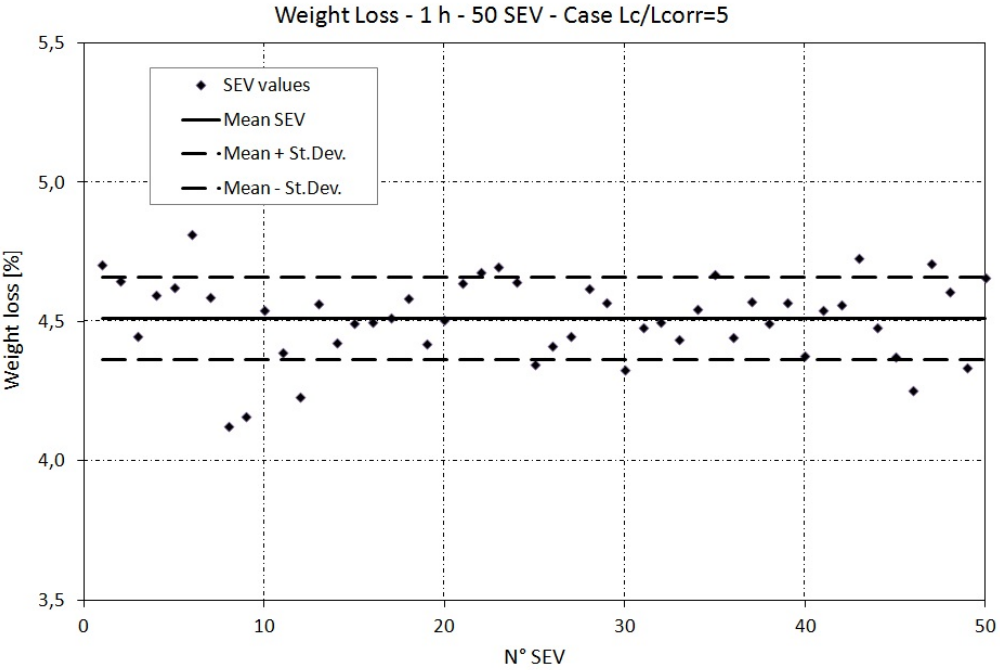

Figure 69 - Weight loss at 1 h in the case Lc/Lcorr = 5

Mean value: 4,510 Standard deviation: 0,147

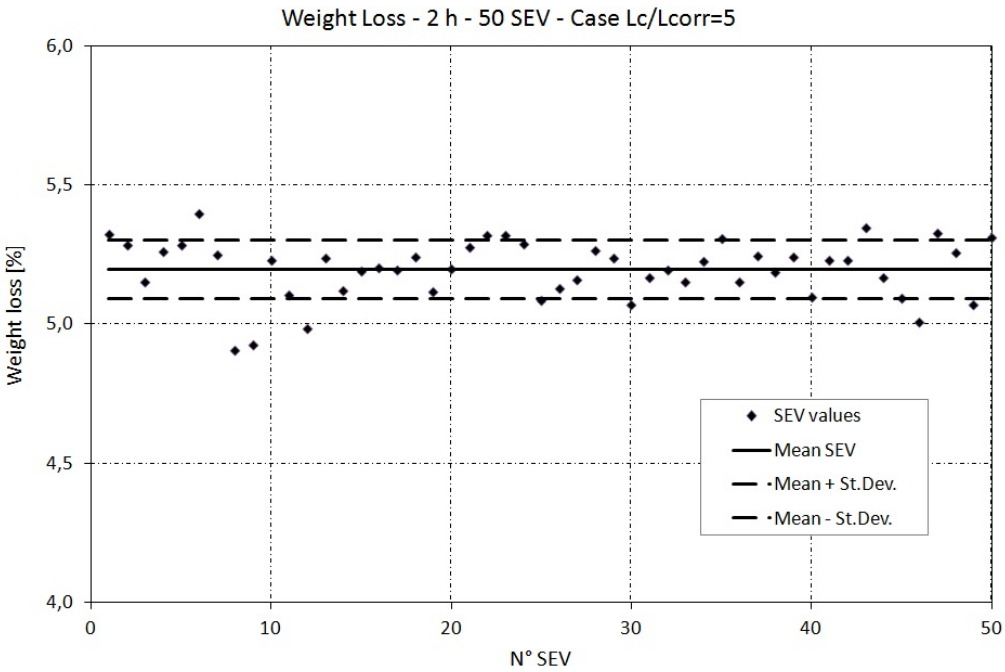

Figure 70 - Weight loss at 2 h in the case Lc/Lcorr = 5

Mean value: 5,195 Standard deviation: 0,106

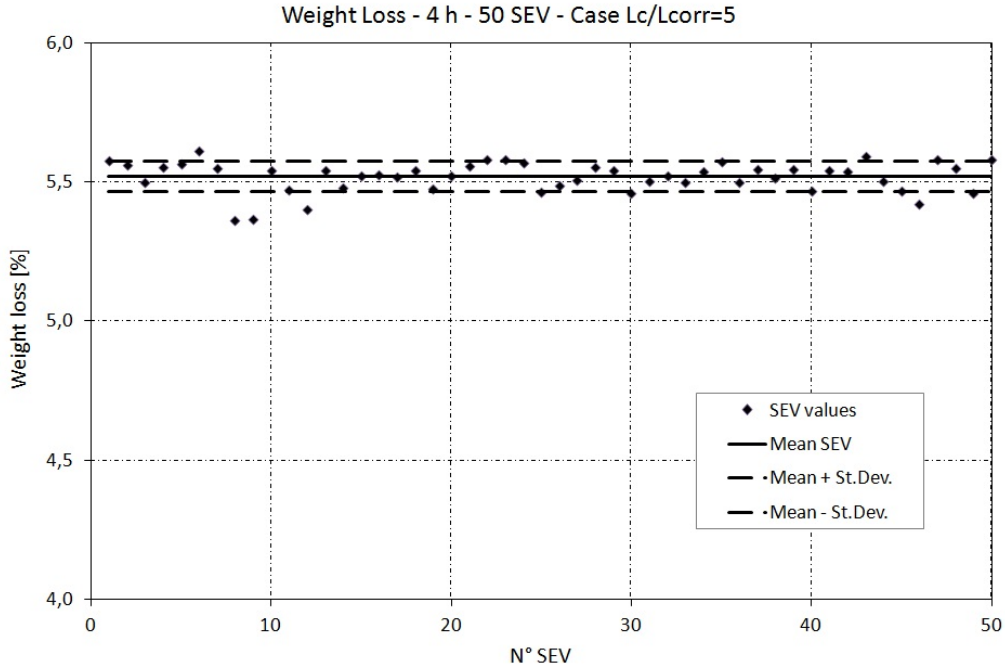

Figure 71 - Weight loss at 4 h in the case Lc/Lcorr = 5

Mean value: 5,519 Standard deviation: 0,055

III.3.4 - Dispersion Analysis for the case Lc/Lcorr = 8

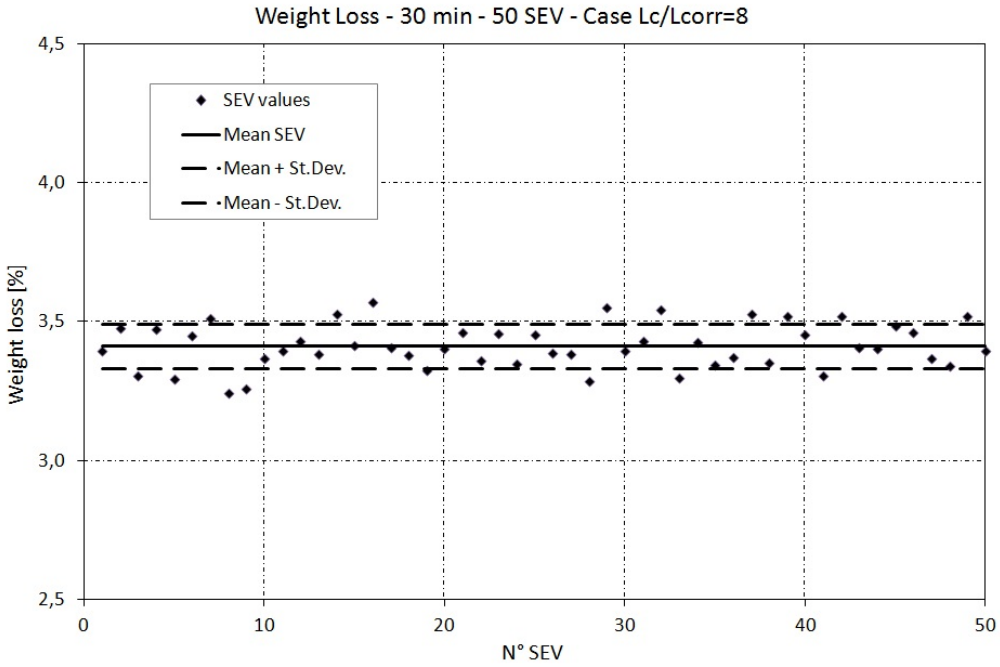

Figure 72 - Weight loss at 30 min in the case Lc/Lcorr = 8

Mean value: 3,411 Standard deviation: 0,080

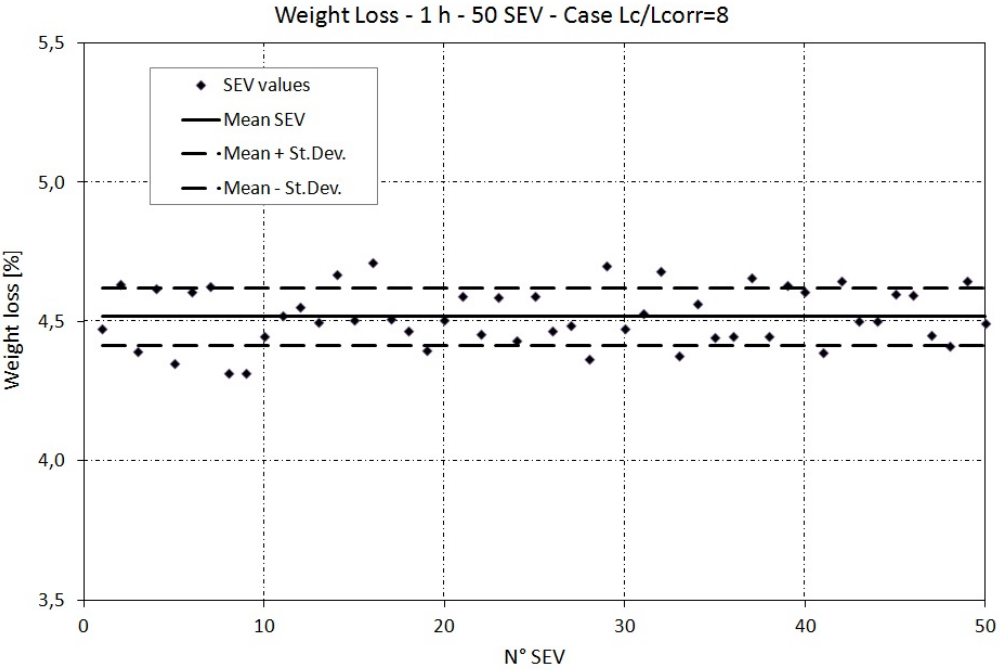

Figure 73 - Weight loss at 1 h in the case Lc/Lcorr = 8

Mean value: 4,517 Standard deviation: 0,104

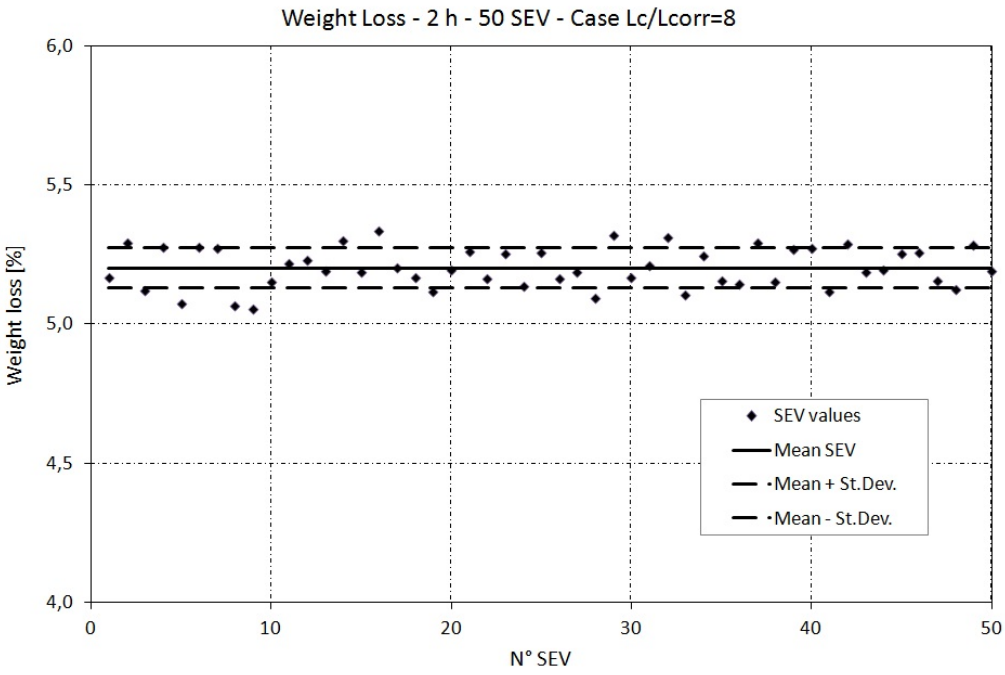

Figure 74 - Weight loss at 2 h in the case Lc/Lcorr = 8

Mean value: 5,202 Standard deviation: 0,072

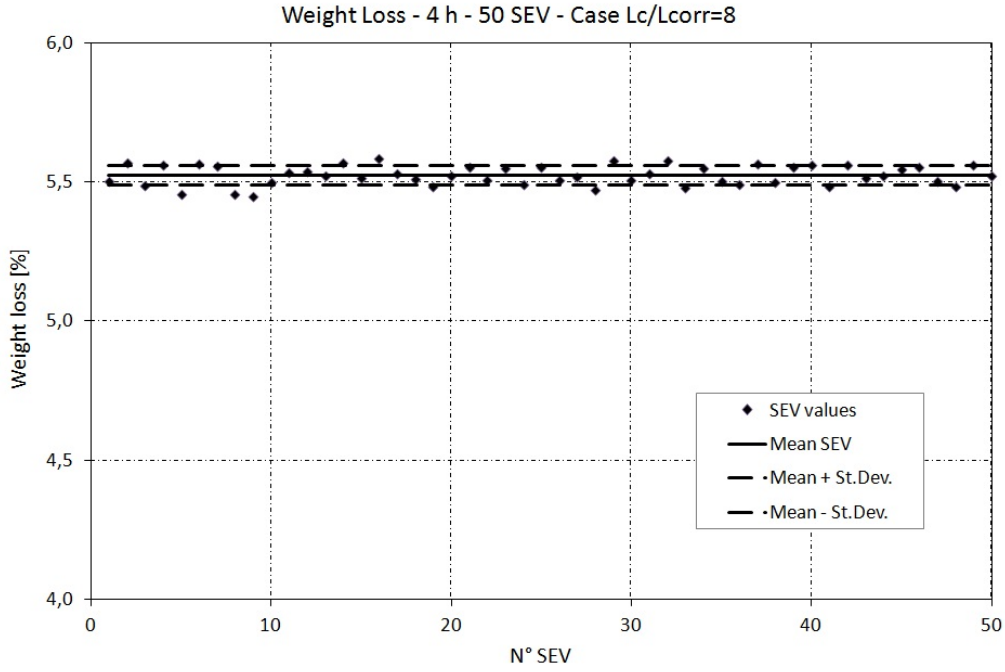

Figure 75 - Weight loss at 4 h in the case Lc/Lcorr = 8

Mean value: 5,524 Standard deviation: 0,036

III.3.5 - Dispersion Analysis for the case Lc/Lcorr = 10

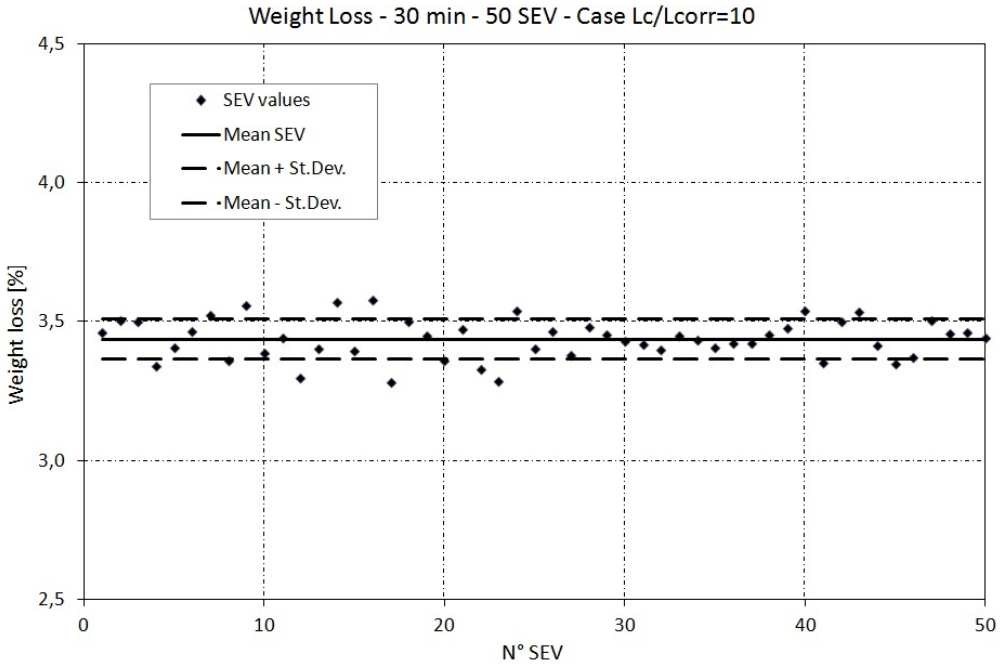

Figure 76 - Weight loss at 30 min in the case Lc/Lcorr = 10

Mean value: 3,436 Standard deviation: 0,072

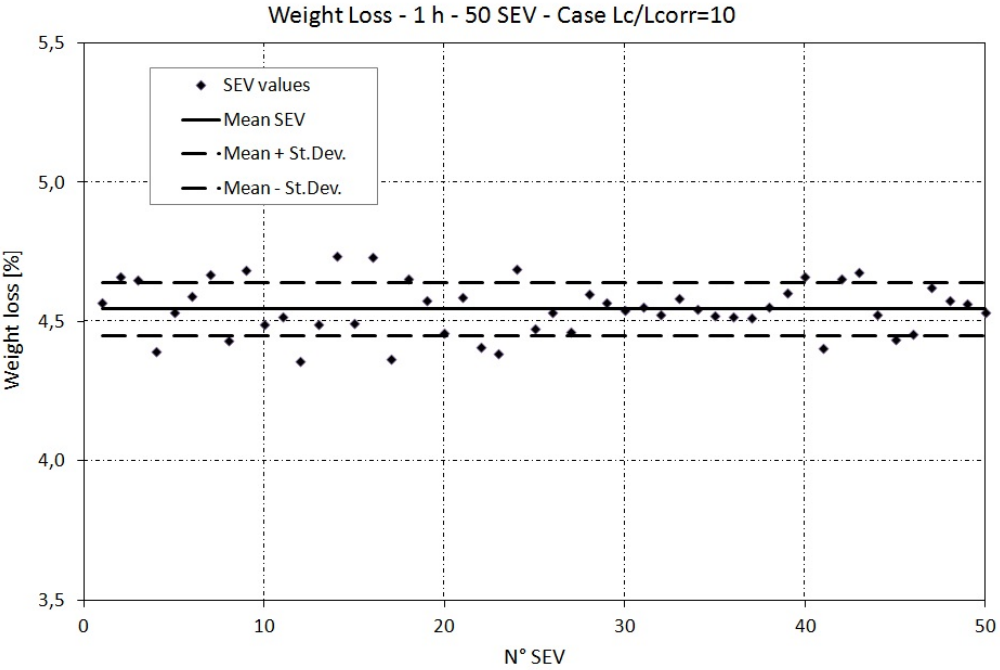

Figure 77 - Weight loss at 1 h in the case Lc/Lcorr = 10

Mean value: 4,546 Standard deviation: 0,095

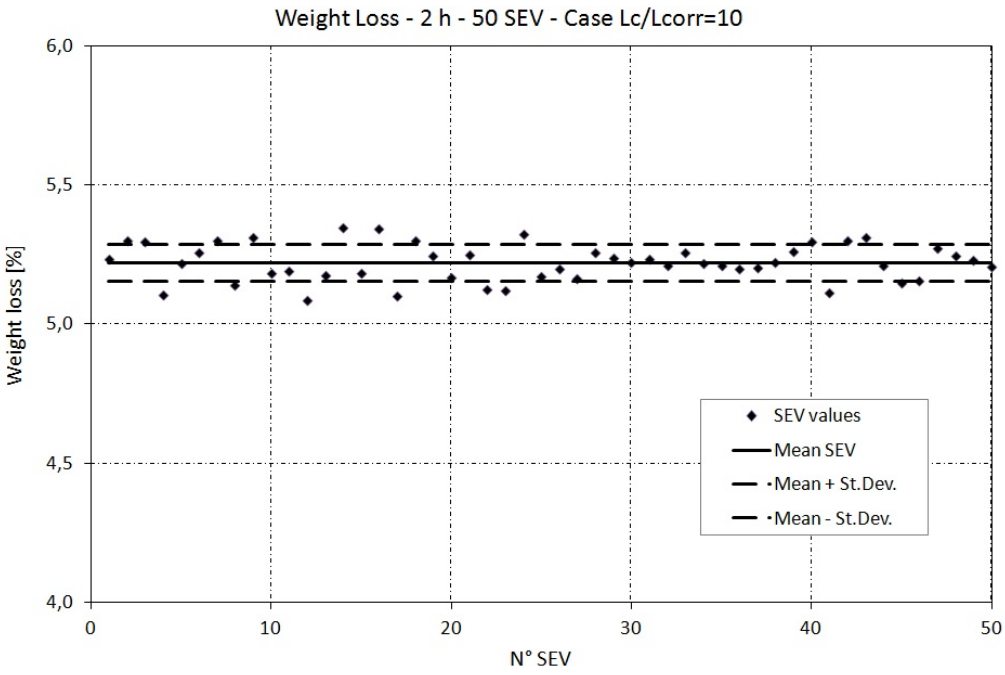

Figure 78 - Weight loss at 2 h in the case Lc/Lcorr = 10

Mean value: 5,221 Standard deviation: 0,066

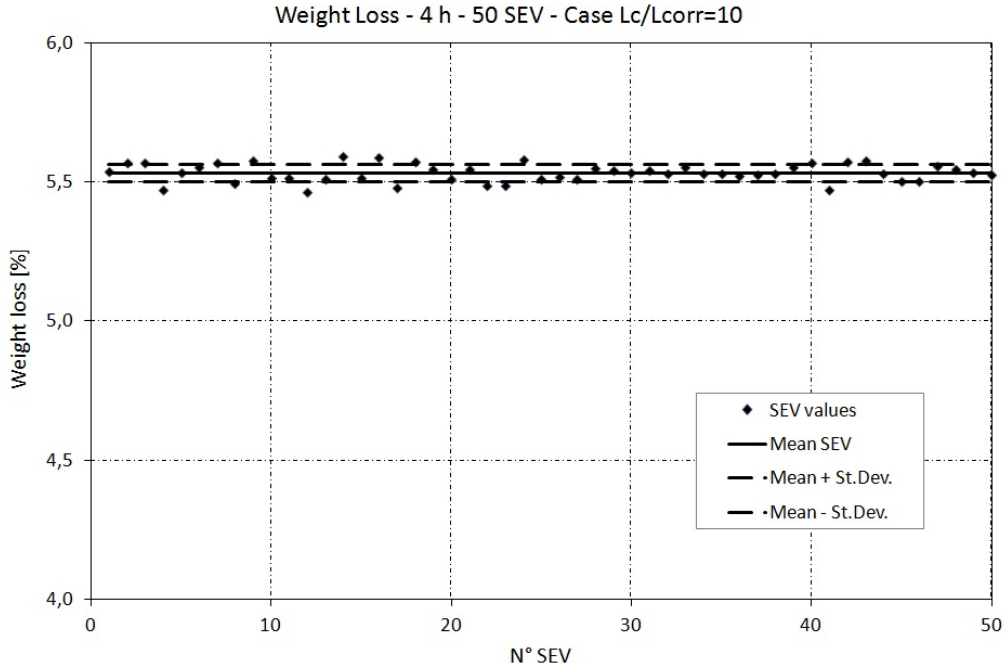

Figure 79 - Weight loss at 4 h in the case Lc/Lcorr = 10

Mean value: 5,533 Standard deviation: 0,032

Data Resume - % Weight loss for 50 SEV

	Lc/Lcorr = 1		Lc/Lcorr = 2		Lc/Lcorr = 5	
Time [min]	Mean	St.Dev.	Mean	St.Dev.	Mean	St.Dev.
30	3,340	0,268	3,426	0,193	3,404	0,110
60	4,421	0,357	4,538	0,257	4,510	0,147
120	5,112	0,265	5,204	0,181	5,195	0,106
240	5,464	0,147	5,518	0,093	5,519	0,055

	Lc/Lcorr = 8		Lc/Lcorr = 10	
Time [min]	Mean	St.Dev.	Mean	St.Dev.
30	3,411	0,080	3,436	0,072
60	4,517	0,104	4,546	0,095
120	5,202	0,072	5,221	0,066
240	5,524	0,036	5,533	0,032

The higher dispersion in all the cases is at 60 min.

III.4 – Conclusion

In the case of intrinsic permeability the mean value tend to the target mean following a log-normal distribution. For all the studied correlated cases the SEV tend to the log-normal distribution. For Lc/Lcorr = 1, the value of the mean value for the SEV crosses the target mean (statistically invariant) of the REV for a number of specimens next to 150. For the second case the cross is about after 30 SEV. For weak correlation (Lc/Lcorr = 20) the distribution tend to the non-correlated normally distributed random field.

Concerning the weight loss analysis we can see that the higher dispersion in all the cases is at 60 min.

GENERAL CONCLUSION AND PERSPECTIVES

Transfers processes (mass and energy) in partially saturated open porous media is a research topic that permit to obtain tools to evaluate the pathology and durability of materials and structures during service situation (aging) or in accidental situation (fire).

The first part of this thesis has been dedicated to a bibliographical study related to the principal physical parameters (hydrous and thermal) that govern the thermo-hygral behavior (TH) of concrete in temperature. During the bibliographic study, it was found that it is hard to determine the thermo-hygral properties of the concrete at a high temperature because of the numerous phenomena occuring simultaneously within the microstructures and they cannot be separated easily. As a result, the relationships of these properties should take into account the different phenomena which take place in the porous medium.

The second part of this work explained in a synthetic way the framework of the adopted TH model, based on a three fluids approach (liquid water, vapor and dry air) in a partially saturated porous medium. The presentation of the model relates to the conservation equations and their discretization with finite elements. For heat and mass transport equations, Fourier's, Darcy's and Fick's constitutive equations were used to connect the fluxes of the conserved quantities with the gradients of state variables.

The purpose is to implement model tools that allow to better take into account the random structural risk impacting the lifespan of the works.

The following part of the work consisted in carrying out probabilistic analyses regarding the influence of the spacial correlation of the parameters on the convergence of statistic elementary volumes (SEV: achievements obtained by random realizations) towards representative elementary volumes (REV) which are statistically invariant. The effect of the spacial correlation has been studied by considering the length of correlation of the probabilistic parameter with regard to the size of the SEV (smaller than that of the REV). Regarding intrinsic permeability, for all the studied correlated cases the SEV tend to the log-normal distribution. For the stronger correlation length we studied (Lc/Lcorr = 1), the value of the mean value for the SEV crosses the target mean (statistically invariant) of the REV for a number of specimens next to 150 on 250 realizations. For the second case the cross is about after 30 SEV. For weak correlation (Lc/Lcorr = 20) the distribution tend to the non-correlated normally distributed random field.

Concerning the weight loss analysis we lanced the T-H model for different correlation lengths (Lc/Lcorr = 1, 2, 5, 8, 10) up to 50 SEV for each case.

We could see that for the values of means and standard deviations indicate a smaller dispersions of data at all the analyzed times for the second case. The higher dispersion in both the two cases is at 60 min.

It would be surely interesting for future researches to add to the T-H model the mechanical part too and extend the 2D approach to a 3D one, to take into account some local effects that may impact the structural behaviour.

This random approach to intrinsic permeability could also be oriented to other properties such as diffusivity and thermal conductivity.

.

ANNEX CHAPTER II

The operators **C** et **K** and the vectors **f** that derive from the weak-form of conservation equations **(95)-(97)** read:

$$\mathbf{C}_{cc} = \int_{\Omega} \varphi \left(\left(1 - S_l\right) \frac{\partial \rho_v}{\partial p_c} + \left(\rho_l - \rho_v\right) \frac{\partial S_l}{\partial p_c} \right) \mathbf{N}^T \mathbf{N} d\Omega \tag{II.1}$$

$$\mathbf{C}_{cg} = \int_{\Omega} \left(1 - S_l\right) \varphi \frac{\partial \rho_v}{\partial p_g} \mathbf{N}^T \mathbf{N} d\Omega \tag{II.2}$$

$$\begin{aligned} \mathbf{C}_{cT} = \int_{\Omega} \Bigg(& \left(1-\varphi\right) \left(S_l \frac{\rho_l}{\rho_s} + \left(1 - S_l\right) \frac{\rho_v}{\rho_s} \right) \frac{\partial \rho_s}{\partial T} + \left(1 - S_l\right) \varphi \frac{\partial \rho_v}{\partial T} \\ & + S_l \varphi \frac{\partial \rho_l}{\partial T} - \left(S_l \frac{\rho_l}{\rho_s} + \left(1 - S_l\right) \frac{\rho_v}{\rho_s} - 1 \right) \frac{\partial m_{dehyd}}{\partial T} \\ & + \varphi \left(\rho_l - \rho_v\right) \frac{\partial S_l}{\partial T} \Bigg) \mathbf{N}^T \mathbf{N} d\Omega \end{aligned} \tag{II.3}$$

$$\mathbf{K}_{cc} = -\int_{\Omega} \left(K \frac{\rho_l k_{rl}}{\mu_l} + D \frac{M_v M_a}{M_g RT} \frac{\rho_v}{\rho_l} \right) \mathbf{B}^T \mathbf{B} d\Omega \tag{II.4}$$

$$\mathbf{K}_{cg} = \int_{\Omega} \left(K \left(\frac{\rho_l k_{rl}}{\mu_l} + \frac{\rho_v k_{rg}}{\mu_g} \right) + D \frac{M_v M_a}{M_g RT} \left(\frac{\rho_v}{\rho_l} - \frac{p_v}{p_g} \right) \right) \mathbf{B}^T \mathbf{B} d\Omega \tag{II.5}$$

$$\mathbf{K}_{cT} = \int_{\Omega} D \frac{M_v M_a}{M_g RT} \frac{\partial p_v}{\partial T} \mathbf{B}^T \mathbf{B} d\Omega \tag{II.6}$$

$$\mathbf{C}_{gg} = \int_{\Omega} \left(1 - S_l\right) \varphi \frac{\partial \rho_a}{\partial p_g} \mathbf{N}^T \mathbf{N} d\Omega \tag{II.7}$$

$$\mathbf{C}_{gc} = \int_{\Omega} \left(\left(1 - S_l\right) \varphi \frac{\partial \rho_a}{\partial p_c} - \rho_a \varphi \frac{\partial S_l}{\partial p_c} \right) \mathbf{N}^T \mathbf{N} d\Omega \tag{II.8}$$

$$\mathbf{C}_{gT} = \int_{\Omega} \left((1-S_l)(1-\varphi)\frac{\rho_a}{\rho_s}\frac{\partial \rho_s}{\partial T} - \rho_a \varphi \frac{\partial S_l}{\partial T} + (1-S_l)\varphi \frac{\partial \rho_a}{\partial T} - (1-S_l)\frac{\rho_a}{\rho_s}\frac{\partial m_{dehyd}}{\partial T} \right) \mathbf{N}^T \mathbf{N} d\Omega \tag{II.9}$$

$$\mathbf{K}_{gg} = \int_{\Omega} \left(K \frac{\rho_a k_{rg}}{\mu_g} - D \frac{M_v M_a}{M_g RT} \left(\frac{\rho_v}{\rho_l} - \frac{p_v}{p_g} \right) \right) \mathbf{B}^T \mathbf{B} d\Omega \tag{II.10}$$

$$\mathbf{K}_{gc} = \int_{\Omega} D \frac{M_v M_a}{M_g RT} \frac{\rho_v}{\rho_l} \mathbf{B}^T \mathbf{B} d\Omega \tag{II.11}$$

$$\mathbf{K}_{gT} = -\int_{\Omega} D \frac{M_v M_a}{M_g RT} \frac{\partial p_v}{\partial T} \mathbf{B}^T \mathbf{B} d\Omega \tag{II.12}$$

$$\mathbf{C}_{TT} = \int_{\Omega} \left(\rho C_p - H_{vap} \left((1-\varphi) S_l \frac{\rho_l}{\rho_s}\frac{\partial \rho_s}{\partial T} + S_l \varphi \frac{\partial \rho_l}{\partial T} \right) - \left(H_{vap} \left(1 - S_l \frac{\rho_l}{\rho_s} \right) + H_{dehyd} \right) \frac{\partial m_{dehyd}}{\partial T} - H_{vap} \rho_l \varphi \frac{\partial S_l}{\partial T} \right) \mathbf{N}^T \mathbf{N} d\Omega \tag{II.13}$$

$$\mathbf{C}_{Tc} = -\int_{\Omega} H_{vap} \rho_l \varphi \frac{\partial S_l}{\partial p_c} \mathbf{N}^T \mathbf{N} d\Omega \tag{II.14}$$

$$\mathbf{C}_{Tg} = \mathbf{0} \tag{II.15}$$

$$\mathbf{K}_{TT} = \int_{\Omega} \left(\lambda - K \left(\left(C_l + \frac{\partial H_{vap}}{\partial T} \right) \frac{\rho_l k_{rl}}{\mu_l} + C_g \frac{\rho_g k_{rg}}{\mu_g} \right) \mathbf{N}^T \mathbf{p}_g^T + \left(C_l + \frac{\partial H_{vap}}{\partial T} \right) K \frac{\rho_l k_{rl}}{\mu_l} \mathbf{N}^T \mathbf{p}_c^T \right) \mathbf{B}^T \mathbf{B} d\Omega \tag{II.16}$$

$$\mathbf{K}_{Tc} = \int_{\Omega} H_{vap} K \frac{\rho_l k_{rl}}{\mu_l} \mathbf{B}^T \mathbf{B} d\Omega \tag{II.17}$$

$$\mathbf{K}_{Tg} = -\int_{\Omega} H_{vap} K \frac{\rho_l k_{rl}}{\mu_l} \mathbf{B}^T \mathbf{B} d\Omega \tag{II.18}$$

$$\mathbf{f}_c = \int_{\bar{\Sigma}_p} \mathbf{N}^T \left(\bar{q}_l + \bar{q}_v - h_g \left(\rho_v - \rho_v^{\infty} \right) \right) d\Sigma \tag{II.19}$$

$$\mathbf{f}_g = \int_{\bar{\Sigma}_p} \mathbf{N}^T \left(\bar{q}_a - h_g \left(\rho_a - \rho_a^{\infty} \right) \right) d\Sigma \tag{II.20}$$

$$\mathbf{f}_T = \int_{\bar{\Sigma}_T} \mathbf{N}^T \left(\bar{q}_T - h_T \left(T - T_{\infty} \right) - \varepsilon\sigma \left(T^4 - T_{\infty}^4 \right) \right) d\Sigma \tag{II.21}$$

REFERENCES

Adenekan A.E., Patzek T. & Pruess K. (1993) *Modeling of multiphase transport of multicomponent organic contaminants and heat in the subsurface: Numerical model formulation,* Water Resour. Res., 29(11), 3727-3740.

Aldea C.-M. & al. (2000) *Estimation of water flow through cracked concrete under load,* ACI Mater. J., 97(5), 567-575.

Alnajim A. (2004) *Modelisation et simulation du comportement du beton sous hautes temperatures par une approche thermo-hygro-mecaniique couplee application a des situations accidentelles,* Ph.D. thesis, Univ. Marne la Vallée.

Alnajim A., Meftah F. & Mebarki A. (2003) *A non-saturated porous medium approach for the modelling of concrete behaviour submitted to high temperatures,* Euro-C Computational Modeling of Concrete Structures, Pongau, Autriche, 17-20 Mars.

Anderberg Y. (2003) *Course on effect of heat on concrete,* International Center for Mechanical Sciences (CISM), 9-13 June 2003, Udine, Italy.

Andrade C., Alonso C. & Khoury G.A. (2003) *Course on effect of heat on concrete,* International Center for Mechanical Sciences (CISM), 9-13 June 2003, Udine, Italy.

Auriault J.L., Boutin C. & Geindreau C. (2009) *Homogenization of Coupled Phenomena in Heterogenous Media.* Wiley-ISTE.

Baggio P., Bonacina C. & Strada M. (1993) *Trasporto di calore e di massa nel calcestruzzo cellulare.* La Termotecnica, 47(12):53-60.

Bal G. et al. (2008) *Random integrals and correctors in homogenization.* Asymptot. Anal., 59(1-2):1-26.

Bamforth P.B. (1987) *The relationship between permeability coefficients for concrete obtained using liquid and gas.* Magazine of Concrete Research, 39(138):3-11.

Baroghel-Bouny V. (1994) *Caractérisation microstructurale et hydrique des pâtes de ciment et des bétons ordinaires et à très hautes performances.* PhD thesis, ENPC, Paris.

Baroghel-Bouny V. & al. (1999) *Characterization and identification of equilibrium and transfer moisture properties for ordinary and high-performance cementitious materials,* Cement and Concrete Research, 29, p. 1225-1238.

Batycky P.R. & Brenne H. (1997) *Thermal macro-transport processes in porous media. A review.* Advances in Water Resources, 20(2-3):95-110.

Bažant Z.P. & Najjar L.J. (1972) *Non linear water diffusion in non saturated concrete, Matériaux Constructions,* Paris, 5(25):3-20.

Bažant Z. P. & Thonguthai W. (1978), *Pore pressure and drying of concrete at high temperature,* In J. Eng. Mech. Div. ASCE. 104: 1059-1079.

Bažant Z. P. & Thonguthai W. (1979) *Pore pressure in heated concrete walls: theoretical prediction,* In Mag. of Concr. Res. 31(107): 67-76.

Bažant Z.P. & Kaplan M.F. (1996) *Concrete at High Temperatures: Material Properties and Mathematical Models,* Harlow: Longman.

Bear J. (1979) *Dynamics in fluids in porous media.* Dover, New York.

Bear J. & Bachmat Y. (1990) *Introduction to modeling of transport in porous media.* Kluwer.

Bear J. & Buchlin J.M (1991) *Modelling and application of transport phenomena in porous media.* Kluwer, Academic Publisher.

Benboudjema F., Meftah F., and Torrenti J.M. (2005) *On the structural effect of drying shrinkage.* ASCE Journal of Engineering Mechanics, 131:1195-1199.

Benboudjema F., Meftah F., and Torrenti J.M. (2005) *Interaction between drying, shrinkage, creep and cracking phenomena in concrete.* Engineering Structures, 27:239-250.

Benboudjema F., Meftah F., and Torrenti J.M. (2007) *A visco-elastic approach for the assessment of the drying shrinkage behaviour of concrete.* Materials and Structures, 40(2):163-174.

Bendar T. (2002) *Approximation of liquid moisture transport coefficient of porous building materials by suction and drying experiment. Demands on determination of drying curve.* Trondheim, Norway, 17-19 June 2002. 6th Symposium on Building Physics in the Nordic Countries.

Blundell R., Diamond C. & Browne R.G. (1976) *The properties of concrete subjected to elevated temperatures,* Technical Note No. 9, June, CIRIA Underwater Engineering Group, London.

Bouddour A. et al. (1998) *Heat and mass transfer in wet porous media in presence of evaporation-condensation.* Int. J. Heat Mass Transfer, 41(15):2263-2277.

CAST3M, *Code de Calcul aux Eléments Finis CAST3M,* Commissariat à l'Energie Atomique, CEA - DRN/DMT/SEMT.

Collet Y. (1977) *Etude des propriétés du béton soumis a des températures élevées entre 200 et 900°C,* Annales des Travaux Publics Beiges, no 4, p 332-338.

Couture F., Jomaa W. & Puiggali J.-R. (1996) *Relative permeability relations: a key factor for a drying model,* Transp. Porous Media, 23, 303–335.

Daian J.F. (1989) *Condensation and isothermal water transfer in cement mortar, Part II–transient condensation of water vapour,* Transp. Porous Media, 44, 1–16.

Dal Pont S. and Ehrlacher A. (2003) *Numerical and experimental analysis of chemical dehydration, heat and mass transfers in a concrete hollow cylinder submitted to high temperatures,* Int. J. Heat and Mass Transfer, in press.

Dal Pont S. (2004) *Lien entre la permeabilité et l'endommagement dans les betons a haute temperature.* PhD thesis, ENPC, Paris.

Dal Pont S. & Ehrlacher A. (2004) *Numerical and experimental analysis of chemical dehydration, heat and mass transfer in a concrete hollow cylinder submitted to high temperatures.* Int.J.Heat and Mass transfer, 1(47):135-147.

Dal Pont S., Schrefler B.A. & Ehrlacher A. (2005) *Intrinsic permeability evolution in*
high temperature concrete: an experimental and numerical analysis. Transport in Porous Media, 60(1):43-74.

Dal Pont S., Durand S. & Schrefler B.A. (2007) *A multiphase thermo-hydro-mechanical model for concrete at high temperatures - finite element implementation and validation under local load.* Nuclear Engineering and Design, 237(22):2137-2150.

Dayan A. & Gluekler E. L. (1982) *Heat and Mass Transfer within an Intensely Heated Concrete Slab,* Int. J. Heat Mass Transfer, vol. 25, pp. 1461-1467.

Deseur B. (1999) *Modélisation du comportement du béton à hautes températures,* Mémoire de DEA, ENPC, France.

Dougill J.W. (1968) *Some effects of thermal volume changes on the properties and behaviour of concrete, The Structure of Concrete.* Cement and Concrete Association, London, pp. 499-513.

Duval F., Fichot F. & Quintard M. (2004) *A local thermal non-equilibrium model for two-phase flows with phase-change in porous media.* Int. J. Heat Mass Transfer., 47:613639.

Feldman R.F., Sereda P.J. (1968) *The model for hydrated Portland cement as deduced from sorption-length change and mechanical properties.* Materials and Construction, 1, p. 509-520.

Fenton G.A. & Griffiths D.V. (1995) *Flow through earth dams with spatially random permeability.* Proceedings of the 10th ASCE Engineering Mechanics Conference, Boulder, Colorado, May 1995.

Feraille A. (2000) *Le rôle de l'eau dans le comportement a haute température des bétons,* Thèse de doctorat, ENPC, France, 186 p.

Forsyth P.A. & Simspon R.B. (1991) *A two phase, two component model for natural convection in a porous medium.* International Journal for Numerical Methods in Fluids, 12(7):655-682.

Franssen J.M. (1987) *Etude du comportement au feu des structures mixtes acier-béton.* Thèse de Doctorat, Université de liège, Belgique, 276p.

Gawin D., Majorana C.E. & Schrefler B.A. (1999) *Numerical analysis of hygro-thermal behaviour and damage of concrete at high temperature.* Mech. Cohes. Frict. Mater., 4:37-74.

Gawin D. et al. (2001) *Modelling thermo-mechanical behaviour of High Performance Concrete in high temperature environments,* Fracture mechanics.

Gawin D., Schrefler B.A. & Pesavento F. (2002) *Modelling of hygro-thermal behavior and damage of concrete at temperature above the critical point of water.* International Journal for Numerical and Analytical Methods in Geomechanics, 26(6):537-562.

Gawin D., Pesavento F. & Schrefler B.A. (2003) *Modelling of hygro-thermal behaviour of concrete at high temperature with thermo-chemical and mechanical material degradation.* Computer Methods in Applied Mechanics and Engineering, 192(13-14):1731-1771.

Gens A. & Olivella S. (2001) *THM phenomena in saturated and unsaturated porous media,* RFGC, 5(6), Environmental Geomechanics, pp. 693-717.

Gérard B. & al. (1996) *Cracking and permeability of concrete under tension,* Mater. Struct. 29, pp. 141–151.

Gray W.G. & Hassanizadeh S.M. (1979) *General conservation equations for multiphase systems: 1. averaging technique.* Adv.Water.Res, 2:131-144.

Gray W.G. & Hassanizadeh S.M. (1979) *General conservation equations for multiphase systems: 2. mass, momenta, energy and entropy transfer.* Adv.Water.Res, 2:191-203.

Gray W.G. & Hassanizadeh S.M. (1980) *General conservation equations for multiphase systems: 3. constitutive theory for porous media.* Adv.Water.Res, 3(1):25-40.

Griffiths D.V. & Fenton G.A. (2007) *Probabilistic Methods in Geotechnical Engineering.* Springer.

Grigoriu M. (1993) *On the spectral representation method in simulation. Probabilistic* Engineering Mechanics, 8(2):75-90.

Gross H. (1973) *On high temperature creep of concrete,* International Conference on Structural Mechanics in Reactor Technology 2, SMIRT vol. 3, Berlin : Edited by T.A. Jaeger, Paper H6/5.

Halamickova P. et al. (1995) *Water permeability and chloride ion diffusion in portland cement mortars: Relationship to sand content and critical pore diameter.* Cement and Concrete Research, 25(4):790-802.

Harmathy T. Z. (1965) *Effect of moisture on the fire endurance of building materials,* ASTM No. 385, Philadelphia, pp. 74-95, 1965.

Harmathy T.Z. (1970) *Thermal properties of concrete at elevated temperatures.* ASTM Journal of Materials, 5(1):47-74.

Harmathy T.Z & Allen L.W. (1973) *Thermal properties of selected masonry unit concretes,* Journal of American Concrete Institute, vol. 70, no 2, p 132-142.

Hicks M.A. & Samy K. (2002) *Influence of heterogeneity on undrained clay slope stability.* Quarterly J. Eng. Geology Hydrogeology, 35(1):41-49.

Huang J.S., Griffiths D.V. & Fenton G.A. (2010) *Probabilistic settlement analysis by stochastic and random finite-element methods.* J. Geotech. Geoenv. Eng., 136(3):417-430.

Incropera F.P. & de Witt D.P. (1990) *Fundamentals of Heat and Mass transfer,* 3rd ed., Wiley, New York.

Ju J.W. & Zhang Y. (1998) *Axisymmetric thermo-mechanical constitutive and damage modeling for air field concrete pavement under transient high temperature,* Mechanics of Materials, 29, 307-323.

Kalifa P. (2000) *Annual report, CSTB, reporting on pore pressure measurements at high temperatures.*

Kalifa P., Tsimbrovska M. & Baroghel-Bouny V. (1998) *High performance concrete at elevated temperature – An extensive experimental investigation on thermal, hydral and microstructure properties.* Proc. of Int. Symp. On high-performance and reactive powder concrete. Aug. 16-20, Sherbrooke Canada.

Kalifa P., Menneteau F.D. & Quenard D. (2000) *Spalling and pore pressure in HPC at high temperatures.* Cement and Concrete Research, 30(12):1915-1927.

Khoury G.A., Grainger B.N. & Sullivan, P. J. E. (1985) *Strain of concrete during first heating to 600 °C under load,* Magazine of Concrete-Research, 37(133) December, pp. 195-215.

Khoury G. & Majorana C. (2003) *Course on effect of heat on concrete,* International Center for Mechanical Sciences (CISM), 9-13 June 2003, Udine, Italy.

Kuiken G.D.C. (1994) *Themodynamics of irreversible processes. Applications to diffusion and rheology.* J. Wiley & Sons.

Lankard D. et al. (1971) *Effects of moisture content on the structural properties of Portland cement concrete exposed to temperatures up to 500°F,* ACI special edition Publication, paper SP25-3, p 59-102.

Le Neindre B. (1993) *Tensions superficielles des composés inorganiques et des mélanges,* volume K476 of Traite Constantes Physico-Chimiques. Techniques de l'Ingenieur.

Lee C.K. & Mei C.C. (1997) *Thermal consolidation in porous media by homogenization theory - i. derivation of macroscale equations.* Advances in Water Resources, 20(2-3):127-144.

Lewis R. W. & Schrefler B. A. (1998) *The Finite Element Method in the Static and Dynamic Deformation and Consolidation of Porous Media.* Chichester, J. Wiley & Sons.

Lydon F.D. (1995) *Effect of coarse aggregate and water/cement ratio on intrinsic permeability of concrete subject to drying.* Cement and Concrete Research, 25(8):1737-1746.

Luckner L., van Genuchten M.T. & Nielsen D.R. (1989) *A consistent set of parametric models for the two-phase-flow of immiscible fluids in the subsurface,* Water Res., 25(10), 2225-2245.

Mainguy M., Coussy O. & Baroghel-Bouny V. (2001) *Role of air pressure in drying of weakly permeable materials,* J. Eng. Mech., 127(6), 582–592.

Marechal J.C. (1972) *Creep of concrete as a function of temperature, In International Seminar on Concrete for Nuclear Reactors.* ACI Special Publication No. 34, Vol. 1.

Mason E.A. and Monchik L. (1965) *Survey of the equation of state and transport properties of moist gases,* Humidity Moisture Measurement Control Science, 3, 257–272.

Meftah F. & Sabeur H. (2006) *A thermo-hydro damage model for the dehydration creep of concrete subjected to high temperature.* Lisbon, Portugal, 5-8 Junem 2006. ECCOMAS / ECCM 3. DOI: 10.1007/1-4020-5370-3 356.

Meftah F. & Dal Pont S. (2010) *Staggered finite volume modeling of transport phenomena in porous materials with convective boundary conditions. Transport in Porous Media,* 82(2):275-298.

Meftah F., Dal Pont S. & Schrefler B.A. (2011) *A three-dimensional staggered finite element approach for random parametric modeling of thermo-hygral coupled phenomena in porous media.* J. Wiley & Sons.

Mehta K. & Monteiro P.J.M. (2001) *Concrete Microstructure, Properties and Materials.*

Meschke G. & Grasberger S. (2003) *Numerical modeling of coupled hygro-mechanical degradation of cementitious materials,* J. Eng. Mech., 129(4), 383–392.

Millington R.J. (1959) *Gas diffusion in porous media,* Science, 130, 100-102.

Monteith J.L. & Unsworth M.H. (1990) *Principles of environmental physics.* Edward Arnold, London.

Mualem Y. (1976) *A new model for predicting the hydraulic conductivity of unsaturated porous media.* Water Resour. Res., 12, 513-522.

Nasrallah S. B. & Perre P. (1988) *Detailed study of a model of heat and mass transfer during convective drying of porous media,* Int. J. Heat Mass Transfer, 31(5), 957–967.

Neville A.M. (1973) *Properties of Concretes.* A Halsted Press Book, J. Wiley & Sons, New York, N.Y.

Noumowé A. (1995) *Effet de hautes températures (20-600°C) sur le béton - Cas particulier du béton à hautes performances.* Thèse de Génie Civil: Institut National des Sciences Appliquées de Lyon et Univ. Lyon I, 1995.

Nyame B.K. & Illston J.M. (1981) *Relationships between permeability and pore structure of hardened cement paste,* Magazine of Concrete Research, 33(116):139–146.

Ohigishi S., Miyasaka S. & Chida J. (1972) *On properties of magnetite and serpentine concrete at elevated temperatures for nuclear reactor shielding,* In International Seminar on Concrete for Nuclear Reactors, AC1 Special Publication No. 34, Vol. 3, Paper PS34-57, American Concrete Institute, Detroit, pp. 1243-53.

Oshita H. & Tanabe T. (2000) *Water migration phenomenon model in cracked concrete, II: Calibration,* J. Eng. Mech., 126(5), 544-549.

Pearce C.J., Nielsen C.V. & Bicanic N. (2003) *A transient thermal creep model for concrete,* Computational Modelling of Concrete Structures, Bicanic et al. (eds).

Perre P. (1987) *Measurements of softwoods' permeability to air: importance upon the drying model,* Int. Comm. Heat Mass Transfer, 14, 519–529.

Perre P. & Degiovanni A. (1990) *Simulation par volumes finis des transfers couples en milieux poreux anisotropes: sechage du bois a basse et a haute temperature.* International Journal of Heat and Mass Transfer, 33(11):2463-2478.

Pesavento F. (2000) *Non linear modelling of concrete as multiphase material in high temperature conditions.* PhD thesis, Università degli Studi di Padova.

Pezzani P. (1988) *Propriétés thermodynamiques de l'eau* (K585), Techniques de l'ingénieur, traité constantes phisico-chimiques.

Philajavaara S.E. (1974) *A review of some of the main results of a research on the aging phenomena of concrete: effect of moisture conditions on strength, shrinkage and creep of mature concrete,* Cement and Concrete Research, 4 (5), p. 761-771.

Picandet V., Khelidj A. & Bastian G. (2001) *Effect of axial compressive damage on gas permeability of ordinary and high-performance concrete,* Cement and Concrete Research, 31, 1525-1532.

Powers T.C. & Brownyard T.L. (1948) *Studies of the physical properties of hardened cement paste.* Research Department Bulletin No. 22. Portland Cement Association, Chicago.

Quintard M. & Whitaker S. (1995) *Local thermal equilibrium for transient heat conduction: theory and comparison with numerical experiments.* Int. J. Heat Mass Transfer., 38(15):2779-2796.

Ranc G., Sercombe J. & Rodrigues S. (2003) *Comportement a haute temperature du beton de structure - impact de la fissuration sur le transferts hydriques.* Revue francaise de genie civil, 7(4):397-423.

Raznjevic K. (1970) *Tables et diagrammes thermodynamiques,* Editions Eyrolles.

Reid R.C., Praunsnitz J.M. & Bruce E.P. (1987) *The properties of gases and liquids.* McGraw Hill, New York.

Sabeur H. & al. (2008) *Correlation between transient creep of concrete and its dehydration.* Magazine of Concrete Research, 60(3):157-163.

Sabeur H. & Meftah F. (2008) *Dehydration creep of concrete at high temperatures. Materials and Structures,* 41(1):17-30.

Savage B.M. & Janssen D.J. (1997) *Soil physics principles validated for use in predicting unsaturated moisture movement in Portland cement concrete,* ACI Mat J., 94(1), 63-70.

Schneider U. (1982) *Behaviour of concrete at high temperatures.* Paris: RILEM, 72p. Report to Committee no 44-PHT.

Schneider U. (1988) *Concrete at high temperatures: A general review,* Fire safety Journal, vol. 13, p 55-68.

Schneider U. & Herbst H.J. (1989) *Permeabilitaet und Porositaet von Beton bei hohen Temperaturen (in German),* Deutscher Ausschuss Stahlbeton, 403, 23–52.

Schrefler B.A., (1995), *F.E. in environmental engineering: coupled thermo-hydro-mechanical processes in porous media including pollutant transport,* Archive of Computational Methods in Engineering, vol. 2, pp 1-54.

Schrefler B.A. (2002) *Mechanics and thermodynamics of saturated/unsaturated porous materials and quantitative solutions.* Appl.Mech.Rev., 4:351-388.

Schrefler B.A. (2004) *Multiphase flow in deforming porous material.* Int. J. Numer. Meth. Engn., 60:27-50.

Sleep B.E. & Sykes J.F. (1993) *Compositional simulation of groundwater contamination by organic compounds, 1. Model development and verification,* Water Resour. Res., 29(6), 1697-1708.

Srivastava A., Babu G.L.S. & Haldar S. (2010) *Influence of spatial variability of permeability property on steady state seepage flow and slope stability analysis.* Engineering Geology, 110(3-4):93-101.

Staicu D.M. et al. (2001) *Effective thermal conductivity of heterogeneous materials: calculation methods and application to different microstructures.* High Temperatures-High Pressures, 33(3):253-344.

Su X.T., Yang Z.J. & Liu G.H. (2010) *Monte Carlo simulation of complex cohesive fracture in random heterogeneous quasi-brittle materials: A 3D study.* International Journal of Solids and Structures 47 (2010) 2336–2345.

Tenchev R.T., Li L.Y. & Purkiss J.A. (2001) *Finite element analysis of coupled heat and moisture transfer in concrete subjected to fire,* Numer. Heat Transfer, 2001, 39(7), 685-710.

Thomas H.R. & Sansom M.R. (1995) *Fully coupled analysis of heat, moisture and air transfer in unsaturated soil,* J. Eng. Mech., 121(3), 392–405.

Torrenti J.-M. et al. (1999) *La dégradation des bétons,* Hermès (Eds.), Paris.

Trangenstein A.J. (2002) *Multi-scale iterative techniques and adaptive mesh refinement for flow in porous media.* Advances in Water Resources, 25:11751213.

Turska E. & Schrefler B.A. (1993) *On convergence conditions of partitioned solution procedures for consolidations problems.* Computer Methods in Applied Mechanics and Engineering, 106(1-2):51-63.

Van Genuchten M. Th. (1980) *A closed-form equation for predicting the hydraulic conductivity of unsaturated soils,* Soil Science Society of America, 44, 892-898.

Verpeaux P., Charras T. & Millard A. (1998) *Castem2000: Une approche modern du calcul des structures. Calcul des Structures et Intelligence Artificielle.* Pluralis.

Wang K., Jansen D.C. & Shah S.P. (1997) *Permeability study of cracked concrete,* Cem. Concr. Res. 27 3, pp. 381–393.

Whitaker S. (1977) *Simultaneous heat mass and momentum transfer in porous media: a theory of drying. In Advances in heat transfer 13.* New York: Academic Press.

Zienckiewicz O.C., Paul D.K., Chan A.H.C. (1988) *Unconditionally stable staggered solution procedure for soil-pore fluid interaction problems,* Int. J. for Num. Meth. In Eng., vol. 26, p. 1039-1055.